



HAL
open science

Influence of volatiles transport in disks on giant planets composition

Mohamad Ali Dib

► **To cite this version:**

Mohamad Ali Dib. Influence of volatiles transport in disks on giant planets composition. Astrophysics [astro-ph]. Université de Franche-Comté, 2015. English. NNT : 2015BESA2051 . tel-01682878

HAL Id: tel-01682878

<https://theses.hal.science/tel-01682878v1>

Submitted on 12 Jan 2018

HAL is a multi-disciplinary open access archive for the deposit and dissemination of scientific research documents, whether they are published or not. The documents may come from teaching and research institutions in France or abroad, or from public or private research centers.

L'archive ouverte pluridisciplinaire **HAL**, est destinée au dépôt et à la diffusion de documents scientifiques de niveau recherche, publiés ou non, émanant des établissements d'enseignement et de recherche français ou étrangers, des laboratoires publics ou privés.

N° d'ordre:

THÈSE DE DOCTORAT
UNIVERSITÉ DE FRANCHE-COMTÉ

École Doctorale Carnot-Pasteur

Pour obtenir le grade de:
Docteur en Astrophysique

Présentée et soutenue par
Mohamad ALI DIB

**Influence of volatiles transport in disks on giant planets
composition**

**L'influence du transport des volatils dans les disques sur la
composition des planètes géantes**

Soutenue le 21 Septembre 2015
devant le jury composé de :

Magali Deleuil	Professeur à Aix-Marseille Université	Présidente
Tristan Guillot	Directeur de recherche à l'OCA/Nice	Rapporteur
Anders Johansen	Senior Lecturer à L'Observatoire de Lund	Rapporteur
Emmanuel Lellouch	Astronome au LESIA/Paris-Meudon	Examineur
Jonathan I. Lunine	Professeur à l'Université de Cornell	Examineur
Pierre Vernazza	Chargé de recherche au LAM/Marseille	Examineur
Olivier Mousis	Professeur à Aix-Marseille Université	Directeur de thèse
Jean-Marc Petit	Directeur de recherche à l'institut UTINAM	Directeur de thèse
Philippe Rousselot	Professeur à l'Université de Franche-Comté	Invité

Thèse préparée à l'OSU THETA - Besançon
Institut UTINAM, CNRS/INSU (UMR 6213)

Remerciements

Il y a cinq ans, je suis arrivé pour la première fois en France. Un étranger dans un pays étrange. Beaucoup des rêves, sans garanties. Beaucoup de monde, sans amis. Je savais que l'astronomie m'intéressait, mais rien de plus. Tout ce que je voulais c'était une expérience fluide. Aboutir dans mes études était ma seule priorité, rater n'était pas une option. Ce n'est jamais une option quand tu es à des milliers de kilomètres de "chez toi". Tout le reste n'était qu'un petit détail. Je n'aurais jamais imaginé les souvenirs que j'aurai un jour de ce pays, ni les émotions que je lui attacherai un jour. Maintenant qu'il faut se dire au revoir, c'est le temps pour exprimer mes sincères reconnaissances pour la France et ses citoyens: le peu que j'ai rencontré, et les autres que j'en ai pas.

En 2012, toujours en stage de Master 2 au LESIA, j'ai reçu un email m'informant d'une position de thèse ouverte dans un endroit mystérieux connu sous le nom de Besançon. Le sujet me paraît intéressant, et j'ai bien aimé l'idée de déménager dans une petite ville après quelques mois d'enfer à Paris. J'ai donc postulé pour ce poste et finis par l'avoir. J'ai alors visité plus tard l'Observatoire de Besançon à fin de rencontrer mes future directeurs de thèse pour la toute première fois: Jean-Marc et Olivier. Mes trois années avec Olivier et Jean-Marc étaient au-delà de mes attentes. Travailler avec eux était tout sauf évident, mais ça valait le coup. C'est pas un secret qu'ils ont des caractères très différents, ce qui m'a déstabilisé à des moments, et m'a permis de bien m'en sortir à d'autres. Olivier est un directeur de thèse jeune (jusqu'au ce jour), cool, très pragmatique et plein d'idées et d'énergie. Il m'a appris comment voir les choses de loin, de rester à jour en bibliographie, et des anecdotes intéressantes sur la communauté scientifique. Jean-Marc, en revanche, est le directeur de thèse très relax et rigoureux. Il a essayé de m'apprendre l'importance de travailler plus lentement mais avec plus de rigueur, d'entrer dans les détails fins, et quelque mots sur l'escalade. Travailler avec Olivier et Jean-Marc était stimulant, même si ce fût frustrant de temps en temps, et, avec le recul, je ne choisirais pas un autre chemin. Les connaissances diverses divers que j'ai appris de tout les deux est la force principale qui ma permit de finir ma thèse avec succès, et je j'exprime donc mes sincères remerciements pour eux. J'oublierai jamais nos discussions bien animées, nos cris, nos rires, et nos batailles.

Je remercie la ville de Besançon pour le financement de ma thèse, et surtout le maire Jean-Louis Fousseret pour son encouragement et support.

Je tiens à remercier aussi l'artiste doué Jean-Michel Mourey pour avoir réaliser la page de couverture de cette thèse.

Durant ces années de recherche en thèse, j'ai eu la chance de discuter et collaborer avec un grand nombre de scientifiques qui m'ont guidé et nourri mes idées. Je suis reconnaissant envers Jonathan Lunine qui était présent dans plusieurs de mes projets et m'a permis de lui rendre visite à Cornell. J'aimerais également remercier Dominique Bockelée-Morvan, Thibault Cavalié, Sebastien Charnoz, Emmanuel Lellouch, Nikku Madhusudhan, Rebecca G. Martin, Gül Sevin Pekmezci, Pierre Vernazza et beaucoup d'autres pour leur assistance et les discussions utiles. Je tiens à remercier aussi Daniel Cordier, Aurelie Guilbert-Lepoutre et Philippe Rousselot pour les discussions très intéressantes qu'on a eu à Besançon au propos du science et autres sujets innocents. Mes remerciements s'étendent au membres de mon jury de thèse comprenant Magali Deleuil, et surtout à Tristan Guillot et Anders Johansen pour avoir accepté de rapporter ce manuscrit.

L'Observatoire de Besançon est un petit labo où tout le monde est comme une petite famille. Je tiens à remercier, sans nommer, tout les personnels administratifs, techniques et scientifiques pour leurs aide, support, et les moments magiques qu'on a passé ensemble. Durant ma deuxième année j'ai profité d'un avenant d'enseignement à l'université. J'aimerais remercier Vincent Ballenegger et Ludovic Martin-Gondre pour m'avoir donner cette chance et aider à réussir mes taches d'enseignements.

Durant ma troisième année, j'ai eu l'opportunité fantastique de faire partie du service de diffusion culture scientifique à l'université. J'aimerais adresser mes remerciements à Claire, Jérémy, Johanna, et tout l'équipe de la Fabrikà sciences et du service Sciences, arts et culture avec qui j'ai partagé des moments magnifiques.

Un coté complètement inattendu de mon séjour à Besançon était le développement de deux nouveaux loisirs dont je n'aurais jamais imaginé qu'ils m'intéresserait: la salsa et l'escalade. J'offre mes remerciements pour les deux communautés: surtout pour m'avoir permis de conquérir des peurs profondes, pour les nombreuses heures plaisantes, et pour les beaux souvenirs. je suis particulièrement reconnaissant envers Ange, Flo, Fabien et Mehdi pour m'avoir appris à danser, pour Claude & (les deux) Nicolas pour m'avoir appris à grimper, et pour tout le monde avec qui j'ai grimpé/dansé.

Un aspect très particulier à la vie comme doctorant dans un labo c'est le flux constant des amis, vu qu'il y a toujours du monde qui arrive ou départ. C'est une verre à moitié rempli, et chacun peut choisir de voir une partie ou l'autre. Durant le temps que j'ai passé à Besançon j'ai rencontré des nombreux amis. Je remercie Alexis, André, Cory, Eric, Gaël, José, Khaoula, Leila, Mohammed, et (les deux) Timothée pour tout les moments inoubliable qu'on a partagé ensemble. Je remercie aussi (les deux) Alexis, Augustin, Gül Sevin, Bastien, et Quentin dont j'ai eu la chance de partager le bureau. Mes remerciements s'étendent pour mes amis hors du labo: Bader, Claire, Elise, Hassan, Indiana, Laureline, Marlene, Sarah, et Vincent, en plus de mes amis d'enfance Bilal, Hani et Mehio.

Finalement, arriver ici aurait été impossible sans ma famille, pour laquelle je dédie cette thèse et j'offre mes remerciements éternels.

Acknowledgments

Five years ago I arrived for the first time to France. A stranger in a strange land. Lots of dreams, no expectations. Lots of people, no friends. I knew I kinda liked astronomy, but this was pretty much it. All what I could hope for was a smooth experience. To get my diplomas was my only priority, since failure was not an option. It never is when you are thousands of kilometers away from “home”. Everything beside that was a mere detail. I never imagined the memories I would one day have in this country, I never imagined the emotions I would one day attach to it. Now that I must say farewell, it is time to express my sincere gratitude for France and her citizens: the few I met, and the many I didn’t.

In 2012, while I was still preparing my Masters degree thesis at LESIA/Meudon, I received an email informing me of an open PhD position at this mysterious place called Besançon. The subject seemed interesting, and I liked the idea of moving to a small city after the few months I spent lost in the Paris subways, so I applied for the job and got it. I then visited the Besançon observatory for the first time, to meet my to be advisers: Jean-Marc and Olivier. My three years with Olivier and Jean-Marc were better than anything I expected. Working with them was anything but trivial, but totally worth it. It is not a secret that they have very different personalities, confusing me some times, and allowing me ways out of problems at others. Olivier is the young (to date), cool, very pragmatic adviser full of ideas and energy. He taught me to see the big picture, to stay very up to date on the literature, and some interesting anecdotes on the scientific community. Jean-Marc on the other hand is the more relaxed, very rigorous adviser. He (tried to) teach me the importance of working more slowly but rigorously, to dive deep into details, and some interesting facts on climbing. Working with both Olivier and Jean-Marc was challenging, even frustrating at times, but now I wouldn’t have chosen any other way. All the different knowledge and experiences I acquired from both is the main reason I was able to finish this PhD successfully, and for both I am very grateful. I will never forget our heated discussions, screaming, laughs, and battles.

I would like also to thank the city of Besançon for funding my PhD. Special thanks go to the mayor Jean-Louis Fousseret for his encouragement and support.

I would like to wholeheartedly thank the talented artist Jean-Michel Mourey for designing my PhD manuscript cover.

During my PhD research I had the opportunity to work and interact with many scientists who taught me a lot and allowed my ideas to develop and nurture. I am grateful

to Jonathan Lunine for collaborating on many projects and allowing me to visit him at Cornell. I would like also to thank Dominique Bockelée-Morvan, Thibault Cavalié, Sébastien Charnoz, Emmanuel Lellouch, Nikku Madhusudhan, Rebecca Martin, Gül Sevin Pekmezci, Pierre Vernazza, and many others for their assistance and useful discussions. Special thanks go also to Daniel Cordier, Aurelie Guilbert-Lepoutre and Philippe Roussetot for the very interesting discussions we had in Besançon on science and other fundamental life issues. A double thanks goes for the members of my thesis committee including Magali Deleuil, and specially to Tristan Guillot and Anders Johansen for accepting to review this work.

The Besançon observatory is a small place indeed, and everyone feels like family. I would like to thank all of the administrative, technical and scientific staff for their help, support, and the great times we spent together.

During my second year I had a Professor assistant contract at the university. I would like to thank Vincent Ballenegger and Ludovic Martin-Gondre for giving me this opportunity and helping me succeed my teaching duties. During my third year, I had the wonderful chance of being part of the scientific culture service at the university. I would like to thank Claire, Jérémy, Johanna, and the rest of the Fabrikà sciences and the Sciences, arts et culture teams with whom I shared great moments.

A completely unexpected result of my three years in Besançon is the development of 2 new hobbies I would never have guessed existed in me: Salsa and rock climbing. I would like to thank both communities first and foremost for allowing me to conquer fears I once thought insurmountable, for the endless hours of fun, and for all of the unforgivable memories. I am specially thankful for Ange, Flo, Fabien, and Mehdi for teaching me to dance, for Claude and (both) Nicolas who taught me to climb, and for everyone I danced/climbed with.

A very particular aspect to being a PhD student is the constant flux of friends, since new people arrive to and leave the lab all the time. This is a half full cup you can choose to see either sides of. During my time in the lab I got to meet a bunch of great friends. I would like to thank Alexis, André, Cory, Eric, Gaël, José, Khaoula, Leila, Mohammed, and (both) Timothée for all the special moments we shared together. I would also like to thank (both) Alexis, Augustin, Gül Sevin, Bastien, and Quentin with whom I enjoyed sharing the office. My thanks are extended to my out-of-the lab friends: Bader, Claire, Elise, Hassan, Indiana, Laureline, Marlene, Sarah, and Vincent, and to my childhood friends Bilal, Hani and Mehio.

Finally, I could have never made it this far in life without my family, to whom I dedicate this thesis and offer my eternal gratitude.

Beforehand

Planets formation theory is an infant scientific field that originated in the sixties by Victor Safronov and George Wetherill in the context of the large stellar astrophysics. Their “nebular hypothesis”, based on the Kant-Laplace theory of the 18th century, proposed that planets form in protosolar nebulas surrounding the stars in their early stages of life. These nebulas are the early version of what is called today “the protoplanetary disks” of gas and dust, observed unambiguously around many *T Tauri* stars, and thought to be the birth place of planets. In the seventies and eighties of last century, the planets formation field dealt mainly with the solar system: how did Earth and the rest of the solar system form and why do we have a giant - telluric planets dichotomy ? What is the origin of comets and asteroids and what can they tell us about our own ? What is the origin of the moon ? and many other questions. The only informations available back then were the solar system bodies mass and orbital distribution.

The formation of planets in a disk-like structure can be intuitively concluded from the flatness of the solar system: all of the 8 planets orbit the sun in the ecliptic plane. Moreover, all of them revolve around the sun in the prograde direction, and so is their rotational movement (except Venus and Uranus, due to their later evolution). This indicates further that they formed along with the sun in a one big rotating disk. Additionally, since the solar system’s mass is completely dominated by the sun, the disk’s global chemical composition should be solar-like with 98% in mass as hydrogen and helium, and only a small fraction as heavier metals. This can be seen further in the composition of the solar system’s most massive planet: Jupiter. Even non trivial deductions can be made from simple observations. In our solar system, all of the 4 telluric planets are packed together in the inner solar system, in contrast with the 4 giant gaseous planets that dominates the outer solar system, hinting to location dependent formation processes as we will see throughout this manuscript.

Next came Earth and space bound spectroscopy starting from the *Voyager* program with the first informations about the planets and small bodies chemical compositions, adding new parameters to the puzzle and opening new questions such as: How did each of the 8 planets acquire its unique chemical composition ? Why is Jupiter and the other giants enriched in volatile elements with respect to the solar value ? How did the solar system’s small bodies (asteroids, comets and satellites) acquire their chemical compositions and why do several dynamical and chemical families of each exist ? Finally, in the last two decades, the exoplanets breakthrough brought a wealth of new data on planets along with new problems for formation models. Our solar system was revealed to be anything but

typical, with new planetary types (hot-Jupiters & super-Earths) found to be common in the galaxy but absent from our own solar system. It became clear that systems with unimaginable architecture and properties can exist, forcing us to stretch our imagination in order to understand their formation mechanisms and what can they tell us about our home.

The current picture we have consists of bottom-up formation of the solar system bodies from micrometric dust all the way to the large bodies we see today through chemical sticking and gravitational attraction. More massive bodies will form farther out from the sun due to the presence of ices, unavailable in the inner hot nebula. In these regions, planetary bodies ten times heavier than Earth will then gravitationally capture the surrounding gas and transform into giant gaseous planets. The solar system's small bodies are the remaining debris once planets formation has ceased. However, the devil is in the detail, since measurements showed a large discrepancy in the chemical compositions of giant planets. This necessitate invoking additional mechanisms and formation steps to explain the unique chemical composition of individual bodies. Jupiter for example was visited in 1995 by the space probe *Galileo*, who revealed the planet to be more rich in volatiles elements (such as carbon, nitrogen, noble gases and others) than expected. This motivated a lot of research on the origin of giant planets, considering Jupiter as a benchmark and test lab for the theories. Another surprise came recently with the inference of a near unity Carbon-to-Oxygen (C/O) ratio in the hot Jupiter *WASP 12b*, indicating a chemical composition different than its host star. This discovery lead me to the first question I tried answering during my PhD thesis:

How do the C/O ratio vary in disks and can we form a planet with a superstellar value?

Another observation that motivated part of my work is the inference of the Deuterium-to-hydrogen (D/H) ratio in the atmospheres of Uranus and Neptune. The lower than cometary values found were surprising since these icy giant planets are thought to have been formed from cometary-like building blocks. The second question I tried answering then was:

Why do Uranus and Neptune have a sub-cometary D/H value and what can this tell us about their formation?

Then, motivated by yet another recent observation (the Earth-like D/H ratio in comet 103P/Hartley), my interest changed towards much smaller bodies: chondritic meteorites, while remaining in the general D/H ratio context where I tried offering a new opinion for an old question:

Why do different chondritic families have different D/H ratios?

Tentative answers to these questions and many others will be presented in this manuscript.

A wise man told me once about my work:

Wrong, like any model.. but hopefully less than the others..

Abstract

In this manuscript I present multiple original works on planets formation theory. The main goal is to connect the chemical composition of giant planets and small bodies to the physical and chemical processes taking place in the protoplanetary disk.

1. In **chapter 1** I introduce the fundamental properties of disks and the basics of planets formation theory.
2. In **chapter 2** I tackle the supersolar C/O and subsolar C/H ratios measured recently in WASP 12b. I elaborate a model that tracks water and CO vapors and ices evolution through diffusion, condensation, coagulation, gas drag and sublimation in order to quantify the variation of the C/O ratio as a function of distance and time. My model shows that, over time, vapors will get permanently depleted inside of their respective snowlines with CO getting depleted much slower than water. This will increase the C/O ratio inside of the water snowline from the solar value of 0.55 to near unity, allowing the formation of giant planets with C/O ~ 1 , such as WASP 12b. I end this chapter by discussing the observational proofs for the existence of such vapor depletions inside the icelines
3. In **chapter 3** I use the same model to interpret the chemical composition of Uranus and Neptune. I show how the formation of both planets on the CO snowline's ices overdensity predicted by this model can explain why both planets are rich in carbon, poor in nitrogen and have subcometary D/H ratios.
4. In **chapter 4** I shift the discussion to the chemical properties of chondritic meteorites, mainly their D/H ratios. I use a snapshot from a layered (active + dead) zones disk model with a D/H ratio evolution code to check if the non monotonic thermal profiles in these disks can explain the wide range of D/H ratios measured in the different chondritic families. I end this chapter by discussing the implications of the dead zone disk models for the formation of Jupiter.
5. I finally summarize my results in **Conclusions & perspectives**, and finish by pointing out several relevant open questions to be hopefully resolved soon.

Résumé

Ce manuscrit présente des travaux originaux sur la théorie de la formation des planètes. Le but fondamental est de connecter la composition chimique des planètes géantes et des petits corps avec les processus physiques et chimiques prenant lieu dans le disque protoplanétaire.

1. Dans le **chapitre 1** j'introduis les propriétés fondamentales des disques protoplanétaires ainsi que les bases de la théorie de formation des planètes.
2. Dans le **chapitre 2** j'attaque le problème du rapport C/O supersolaire mesuré récemment dans WASP 12b. J'élabore un modèle qui suit la distribution et transport de l'eau et du CO gazeux et solides à travers leurs diffusion, condensation, coagulation, gaz drag et sublimation afin de quantifier la variation du rapport C/O dans le disque en fonction du temps et de la distance. Mon modèle montre que, au fur et à mesure du temps, les vapeurs vont être enlevé de l'intérieur de leur lignes de glaces respectives, avec le vapeur CO enlevé beaucoup plus lentement que la vapeur d'eau. Cette effet va augmenter le rapport C/O à l'intérieur de la ligne de glace de l'eau d'une valeur initiale solaire (0.55) vers une valeur au voisinage de l'unité, permettant de former des planètes géantes avec des rapports C/O ~ 1 , comme WASP 12b. Je finis ce chapitre en discutant les preuves observationnelles de cette enlèvement des vapeurs à l'intérieur des lignes de glaces.
3. Dans le **chapitre 3** j'utilise la même modèle pour interpréter la composition chimique d'Uranus et Neptune. Je montre comment la formation de ces deux planètes sur la sur-densité de glaces prédite par mon modèle sur la ligne de glace de CO peut expliquer pourquoi ces planètes sont à la fois riches en carbone, pauvres en azote et avec des valeurs D/H sous-cométaires.
4. Dans le **chapitre 4** je change de sujet vers les propriétés chimiques des météorites chondritiques, surtout leurs rapports D/H. J'utilise un modèle de disques à 2 couches (actif et morte) avec une code d'évolution D/H pour vérifier si les profils thermiques non monotone trouvés dans ces disques peuvent expliquer la large gamme des valeurs D/H trouvé entre les différents familles chondritiques. Je finis ce chapitre en discutant les implications de ce modèle des disques contenant des zones mortes sur la formation de Jupiter

5. Finalement je résume nos résultats dans **Conclusions & perspectives**, et finis en posant des questions que j'espère voir résolus prochainement.

Contents

Remerciements	i
Acknowledgments	iii
Beforehand	v
Abstract	vii
Résumé	ix
Table of contents	xv
1 Introduction to planets formation	1
1.1 Protoplanetary disks	2
1.1.1 Physics of PPDs	2
1.1.2 Chemistry of PPDs	8
1.2 Basics of planets formation	16
1.2.1 Gravitational instability model	17
1.2.2 Core accretion model	17
1.3 Chemical composition of planets and small bodies	23
1.3.1 Giant planets	23
1.3.2 The solar system's small bodies	27
2 A new volatile distribution model and application to WASP 12b	35
2.1 An introduction to exoplanets	35
2.1.1 Overview	35
2.1.2 WASP-12b's atmospheric composition	36
2.2 The problematic of WASP 12b's formation	37
2.3 The formation of WASP 12b in the literature	38
2.3.1 Clathrates formation models	38
2.3.2 Static formation models	38
2.4 Water distribution models	39
2.4.1 The cold finger effect	39
2.4.2 vapor replenishment	40

2.4.3	Modern models	41
2.5	Published article summary	42
2.6	Published article	43
2.7	Methods & Caveats	51
2.7.1	The protoplanetary disk	51
2.7.2	Gas drag & dust diffusion	53
2.7.3	On the validity of WASP 12b's measurements	53
2.7.4	The cold finger effect vs observations	54
3	The formation of Uranus and Neptune on the CO iceline	61
3.1	On pebbles growth via vapor condensation	61
3.2	Published article summary	62
3.3	Published article	63
3.4	Methods & Caveats	71
3.4.1	On the main C and N bearing species in disks	71
3.4.2	The width of the ices over-density beyond the icelines	72
3.4.3	On the tropospheric CO in Uranus and Neptune	72
4	Nebular dead zone effects on the D/H ratio in chondrites and comets	77
4.1	A brief history of comets	77
4.2	An introduction to dead zones	79
4.3	A few words on chondrites	80
4.4	Published article summary	81
4.5	Published article	83
4.6	Perspectives: Dead zones and the formation of Jupiter	93
4.6.1	A pressure trap on the snowline ?	93
4.6.2	Jupiter's formation region initial chemical composition	94
4.6.3	The role of water	96
4.6.4	Caveats & Discussions	97
	Conclusions & perspectives	107
	Other contributions	113
	Appendices	115
A	Chapter 2: numerical methods	117
A.1	Vapor diffusion	117
A.2	Gas drag	119
A.3	Pebbles sublimation	120
A.4	Putting the pieces together	120
A.4.1	The model's flowchart	120
A.4.2	On the diffusion timescale	121

B Chapter 4: numerical methods	123
B.1 Solving the global equation	123
B.2 Numerical convergence	125

The whole problem with the world is that fools and fanatics are always so certain of themselves, and wiser people so full of doubts. - Bertrand Russell

Chapter 1

Introduction to planets formation

In the beginning the Universe was created. This has made a lot of people very angry and been widely regarded as a bad move.

Douglas Adams

In this first chapter I introduce the basics of planet formation theory. The objective is by no mean a comprehensive review of the theory and relevant observations, but rather a semi-qualitative overview of how do planets form in disks and what are the main effects influencing their final properties. Since the work presented in this manuscript consists of connecting the dots between how does a planet form and its chemical composition, this chapter will cover a large number of relevant topics but without going into more details than needed.

Our own solar system is by far the most studied planetary system to date, and most of our current knowledge on planetary formation originated from observing its bodies. Jupiter for example is the benchmark of giant planets formation models, and it contributed along the other planets, the main asteroids belt and the trans Neptunian objects in shedding light on the formation, composition and dynamics of planetary systems. The coplanar, circular and uniform orbits, along with the almost entirely prograde rotation of planets were the first indications that planets form in disk-like environments. Since the Sun by far dominates the solar system mass, the planetary formation environment should have had a solar composition (98% hydrogen and Helium and 2% heavier elements, by mass), explaining also the presence of giant gaseous planets. The solar system's angular momentum however is dominated almost entirely by the giant planets, indicating that the planetary formation environment was very efficient in angular momentum transport. These are some of the main solar system properties indicating that planets form in what are called today protoplanetary disks (PPDs)¹. The formation of planets, along with their

¹PPD, disk, and the (proto)solar nebula are used interchangeably throughout this manuscript.

final chemical compositions and properties depend almost entirely on the processes taking place in these disks.

1.1 Protoplanetary disks

1.1.1 Physics of PPDs

From clouds to PPDs

Stars form in the cold interstellar medium, where a molecular cloud will collapse on itself if its gas pressure is unable to counteract its gravitational attraction. The conservation of angular momentum will then increase its rotational velocity and result in a central proto-star surrounded by a disk. Magnetic fields and turbulence are also thought to play a significant role in this process. The Virial theorem states that, for a cloud at equilibrium, the gravitational energy is twice the kinetic energy:

$$|E_{grav}| = 2E_{kin} \quad (1.1)$$

where $E_{grav} = -\frac{3}{5}\frac{GM_c^2}{R}$ (for a spherical cloud) and $E_{kin} = \frac{M_c}{m_H}\frac{5}{2}k_bT$, with G the gravitational constant, M_c the cloud mass, R its radius, m_H the hydrogen atom mass, k_b the Boltzmann constant and T the cloud's temperature. The cloud will collapse if E_{grav} is larger than $2E_{kin}$, leading to the following condition:

$$R \geq R_J \equiv \sqrt{\frac{25}{4\pi} \frac{k_b T}{G m_H^2 n_H}} \quad (1.2)$$

where R_J is called the Jeans radius and n_H the hydrogen's number density. Typical values are $n_H \sim 100 \text{ cm}^{-3}$ and $T \sim 20 \text{ K}$ giving R_J in the order of 0.3-1.2 pc².

During a collapse, the system's angular momentum $\vec{L} \equiv M\vec{r} \times \vec{v} = M\vec{r}^2 \times \vec{\omega}$ is conserved. The cloud's radial size decrease will be compensated by an increase in its rotational velocity. A collapsing particle will feel 2 forces in the radial direction: the centripetal acceleration $g = -\frac{GM_c m_p}{r^2}$ and the radial component of the centrifugal force $a_r = r^2 \omega \sin \phi$ resulting from the angular momentum conservation. A particle at the poles ($\phi = 0^\circ$) will then feel a total radial force $a_t = g$ and collapse to the center, while a particle at the equator ($\phi = 90^\circ$) will feel $a_t = g + a_r$ (the collapse is opposed by a_r), resulting in the formation of a disk surrounding the central star.

²A Parsec (pc) is equal to 3.26 light-years, or around 2×10^5 AU. 1 AU is defined as the Earth-Sun distance, equal to 1.49×10^8 km.

Disks structure

A gas particle in the disk orbiting the central star will mainly feel gravity as the main force in the azimuthal direction, and thus will orbit with a keplerian velocity:

$$\vec{v}_\phi \equiv r\Omega_k\vec{u}_\phi = \sqrt{\frac{GM_*}{r}}\vec{u}_\phi \quad (1.3)$$

In more realistic situations though, the gas particle's orbital velocity will also be affected by the gas radial pressure gradient:

$$\frac{v_\phi^2}{r} = \frac{GM_*}{r^2} + \frac{1}{\rho} \frac{\partial P}{\partial r} \quad (1.4)$$

Assuming that pressure is a decreasing function with distance from the sun, the second term will decrease the gas orbital velocity to sub-Keplerian values by a factor of $\sim 0.25\%$. This effect is negligible for all gas related processes, but is crucial for solids as discussed later.

Let's now define the disk's centrifugal radius R_c as the radial point where the angular momentum in the cloud becomes equal to the angular momentum in the disk:

$$R_c(t) = \frac{l(t)^4\omega(l)^2}{GM(t)} \quad (1.5)$$

where l_i is the cloud's radius at t , $\omega(l)$ its associated angular velocity and M the total system mass. R_c can be roughly interpreted as the disk characteristic size, with typical values in the order of 100-1000 AU.

Now let's consider the simplest possible disk:

- Axisymmetric, geometrically thin and flat
- In hydrostatic and thermal equilibrium
- Heated only from the central star (no accretion "viscous" heating)
- Mass very low compared to the central star

Hydrostatic equilibrium implies that the pressure is governed by:

$$\frac{\partial P}{\partial z} = -\rho g_z \quad (1.6)$$

where z is the disk's vertical axis. We furthermore assume an ideal diatomic gas described by the equation of state:

$$P = \rho c_s^2 \quad (1.7)$$

where $c_s = \sqrt{\frac{7}{5} \frac{RT}{\mu}}$ is the speed of sound (R is the ideal gas constant, μ its molar mass and T its temperature). Equations 1.6 and 1.7, in the $z \ll r$ limit, give the vertical density profile:

$$\rho(z) = \rho_0 \exp[-z^2/2H^2] \quad (1.8)$$

where H is defined as the disk scale height:

$$H = \frac{c_s}{\Omega_k} \quad (1.9)$$

and is usually assumed to be around $\sim 0.01 - 0.1 \times r$ in the planets forming region.

We can finally define the vertically isothermal disk's surface density as:

$$\Sigma \equiv \int \rho(z) dz = \sqrt{2\pi} \rho H \quad (1.10)$$

Typical orders of magnitude at 1 AU for our simple disk with a total mass of $M_d \sim 0.01 M_\odot$ are: $\Sigma \sim 1000 \text{ g cm}^{-2}$, $\rho_0 \sim 10^9 \text{ g cm}^{-3}$ and $c_s \sim 10^5 \text{ cm s}^{-1}$.

For “passive” disks (heated only by the central star), the temperature is governed by the stellar radiation absorption-emission equilibrium. The stellar photons ($\lambda \sim 1 \mu\text{m}$) will heat up the dust. Dust will then radiate as a black body in the infrared (IR) wavelengths, exchanging energy with the gas and heating it up. The nebular gas will then cool down by lines emission. Quantitatively, the stellar flux reaching the disk at a distance r from a star with a radius R_* and brightness I_* is given by:

$$F_+ = I_* \left[\sin^{-1} \left(\frac{R_*}{r} \right) - \left(\frac{R_*}{r} \right) \sqrt{1 - \left(\frac{R_*}{r} \right)^2} \right] \quad (1.11)$$

On the other hand, assuming the disk is optically thick and $T_{gas} = T_{dust}$, its black body emission rate is given by a Stefan-Boltzmann law:

$$F_- = \sigma T_{irr}^4 \quad (1.12)$$

where σ is the Stefan-Boltzmann constant and T_{irr} is the passive disk's temperature. For $I_* = (1/\pi)\sigma T_*^4$, the equilibrium of these two equations gives the passive disk's radial temperature profile:

$$\left(\frac{T_{irr}}{T_*} \right)^4 = \frac{1}{\pi} \left[\sin^{-1} \left(\frac{R_*}{r} \right) - \left(\frac{R_*}{r} \right) \sqrt{1 - \left(\frac{R_*}{r} \right)^2} \right] \quad (1.13)$$

For $r \gg R_*$, we finally get $T_{irr} \propto r^{-3/4}$.

Disks evolution

A fundamental property of PPDs is their accretion onto the central star. This is an unambiguous behavior found in most T Tauri systems via observations of the hot continuum radiation generated when accreted gas impacts the star's surface. However, for a gas parcel to be accreted into the central star, it needs to lose angular momentum. The fundamental angular momentum transport mechanism in disks is a major unknown in disks theory. For this reason, it is common to parameterize this effect by introducing a "turbulent viscosity" into the system. This (kinematic) viscosity is different from the molecular level disk viscosity (which is too low to be relevant), and is a consequence of a turbulence generated from an unknown mechanism. Shakura & Sunyaev (1973) and Lynden-Bell & Pringle (1974) introduced the widely used model where the turbulent viscosity is defined as:

$$\nu = \alpha c_s H \quad (1.14)$$

where α is a free dimensionless turbulence encoding parameter, usually assumed in simple models to be constant throughout the disk and its lifetime. This prescription assumes that the turbulent eddies have a characteristic scale comparable to the disk scale height H , and a characteristic speed c_s . The presence of viscosity will allow the disk's surface density $\Sigma(r, t)$ to evolve with time and radial distance. We consider the continuity equation:

$$r \frac{\partial \Sigma}{\partial t} + \frac{\partial}{\partial r} (r \Sigma v_r) = 0 \quad (1.15)$$

where v_r is the gas radial velocity, and the angular momentum conservation equation:

$$r \frac{\partial}{\partial t} (r^2 \Omega \Sigma) + \frac{\partial}{\partial r} (r^2 \Omega \times r \Sigma v_r) = \frac{1}{2\pi} \frac{\partial \tau_G}{\partial r} \quad (1.16)$$

where τ_G is the local torque:

$$\tau_G = 2\pi r \times \nu \Sigma r \frac{\partial \Omega}{\partial r} \times r \quad (1.17)$$

Equation 1.17 introduces the viscosity into the system. By considering these 3 equations together, we get the disk's surface density evolution equation:

$$\frac{\partial \Sigma}{\partial t} = \frac{3}{r} \frac{\partial}{\partial r} \left[r^{1/2} \frac{\partial}{\partial r} (\nu \Sigma r^{1/2}) \right] \quad (1.18)$$

This is partial differential equation with a diffusive term (second order derivative with respect to r) governing the evolution of the disk's materials. Fig. 1.1 shows that, as a response to an impulse (green's function solution), the system's material flows toward the central star (accretion), but its angular momentum is carried outward by a tail of mass to infinity (angular momentum conservation) and thus spreading the disk. This equation also allows us to obtain the radial density and pressure profiles of the disk.

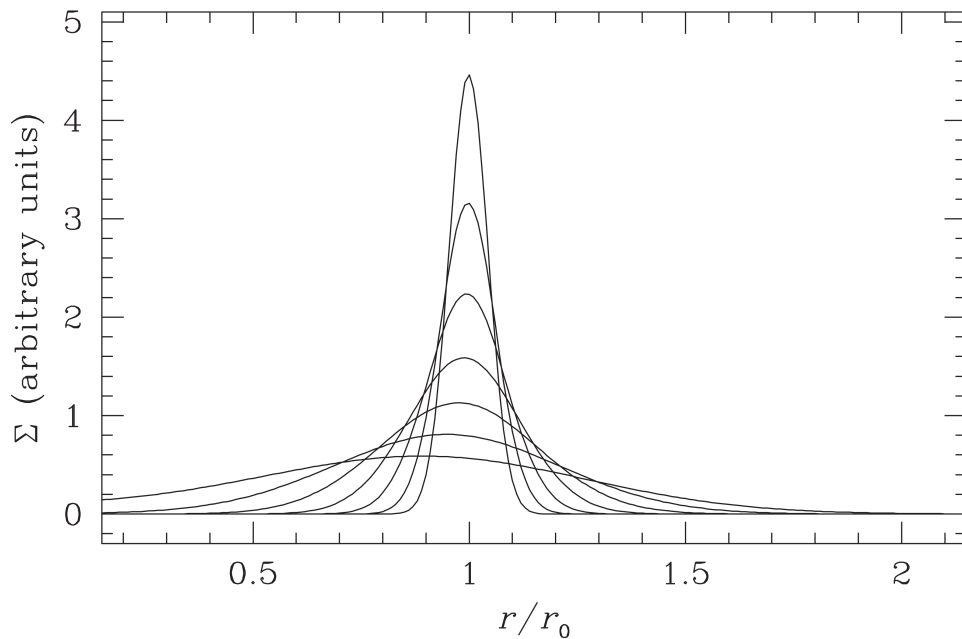


Figure 1.1: The disk's response to a Green's function source, from Armitage (2010). Mass is accreted inward, but angular momentum is transported outward.

Now, from the steady state solution to equation 1.18, we can define the disk's accretion rate as:

$$\dot{M} \equiv \frac{\Sigma}{3\pi\nu} = \frac{\Sigma}{3\pi\alpha c_s H} \quad (1.19)$$

α values around $10^{-2} - 10^{-3}$ reproduce well the observed disks accretion rates of $\dot{M} \sim 10^{-7} - 10^{-6} M_\odot \text{yr}^{-1}$. This implies viscosity ν values in the order of $10^{15} \text{ cm}^2 \text{ s}^{-1}$.

Another consequence of the presence of a kinematic viscosity is viscous (accretional) heating, that adds up in the disk to the stellar irradiation heating discussed above. We define the accretion luminosity as:

$$L_{acc} = \frac{1}{2} \frac{GM_* \dot{M}}{R_*} \quad (1.20)$$

this luminosity will result in a viscous temperature for the surface layer given by (Armitage, 2010):

$$T_{visc}^4 = \frac{3GM_* \dot{M}}{8\pi\sigma^3} \left(1 - \sqrt{\frac{R_*}{r}}\right) \quad (1.21)$$

For $z_{disk} = 0$, where planets formation takes place, one should take into account also the optical depth to the disk's midplane:

$$\tau = \frac{1}{2} \kappa_R \Sigma \quad (1.22)$$

where κ_R is the Rosseland mean opacity. Assuming finally that all energy dissipation occurs in the midplane, and that $\tau \gg 1$, we get the central temperature of the disk:

$$T_c^4 \simeq \frac{3}{4}\tau T_{visc}^4 + T_{irr}^4 \quad (1.23)$$

Disks models meet observations

Several disk models have been developed over the years in an effort to fit the disks measurements. In this work, we used extensively the disk model of Hueso & Guillot (2005) (HG05). This is a relatively recent 1-D classical disk model that incorporates the basic physics discussed above, in addition to:

- The ongoing cloud collapse as a source function of surface density.
- The disk's autogravitation (for M_{disk} non negligible with respect to M_*).
- The disk's geometry via the introduction of disk flaring effects on T_{irr} .
- Photoevaporation due to the central star's UV.
- The disk's local gravitational stability against axisymmetric perturbations.

This model was used in order to fit two typical protoplanetary disks: DM Tau and GM Aur (main observed properties presented in Table 2.1).

The age of the central star (hence the disk) can be estimated by comparing its measured luminosity to evolutionary tracks from pre-main sequence phase models. Fig. 1.2 shows the disks frequency as a function of stellar age. This frequency drops below 50% around 3 Myr, implying that most disks are already dispersed (through a currently unknown mechanism) by this time. This is a firm limit on the formation timescale of giant planets, since they need to accrete their gaseous envelope before the disk's dispersal.

The disk's size R_{out} is observationally defined as the outermost radius where gaseous CO (through its isotopes ^{12}CO and ^{13}CO) and/or the continuum dust emission are detected via radio-interferometric observations. The surface densities in the outer disk (beyond 100 AU) can be measured either directly via ^{12}CO , ^{13}CO and ^{18}CO (through assumptions on CO abundance), or also from continuum dust emission (though assumptions on the gas/dust ratio and opacities). Finally, accretion rates can be inferred by measuring the star's accretion luminosity L_{acc} estimated from UV excess, H α emissions with large equivalent width or U bands excess emission.

Figure 1.3 shows typical surface density profiles from the HG05 disk model, with DM Tau observations. Figure 1.4 shown the midplane temperature profiles corresponding to the same model parameters. This example is only to show how observations compare to disk models. The exact disk parameters used in this work will be presented later.

System:	DM Tau	GM Aur
Distance:	140 pc \pm 10%	140 pc \pm 10%
Age:	1.5–7 Myr	1–10 Myr
Spectral type:	M 1	K7
Star mass:	0.4–0.6 M_{\odot}	0.5–1.0 M_{\odot}
Luminosity:	0.25 L_{\odot}	0.74 L_{\odot}
Temperature:	3720 K	4060 K
Star radius:	0.0065 AU	0.0085 AU
Constraints from CO emission lines:		
R_{out}	\sim 850 \pm 20 AU	525 \pm 20 AU
$\Sigma_{(100 \text{ AU})}$	$>$ 0.05 g cm $^{-2}$	–
$\Sigma_{(R_{\text{out}})}$	$>$ 1.6 $\times 10^{-3}$ g cm $^{-2}$	3.0 $\times 10^{-3}$ g cm $^{-2}$
Constraints from continuum dust emission:		
R_{out}	$>$ 500 AU	280 AU
$\Sigma_{(100 \text{ AU})}$	$<$ 4.3 g cm $^{-2}$	23.0 g cm $^{-2}$
$\Sigma_{(100 \text{ AU})}$	$>$ 0.23 g cm $^{-2}$	1.4 g cm $^{-2}$
$\tilde{\beta}$	0.48–1.03	1.11–1.34
Accretion rate:		
Log \dot{M}	= -7.95 ± 0.54	-8.02 ± 0.54
$[M_{\odot} \text{ yr}^{-1}]$		

Table 2.1: The observed properties of protoplanetary disks DM Tau and GM Aur, from Hueso & Guillot (2005).

1.1.2 Chemistry of PPDs

Disks are born from the same molecular cloud as the central star. we therefore expect the average bulk chemical composition of the disk to be stellar-like. However, small scale inhomogeneities can arise due to temperature and phase dependent chemical reactions and fractionation mechanisms. Planets forming in different regions of the disk can therefore acquire different chemical compositions. In this work, the chemical elements I am most interested in are Oxygen O, Carbon C, and Nitrogen N. These elements can be found in two forms: volatiles that condense at relatively low temperatures (10s to 100s K) and refractories (rocks and metals condensing for $T > 1000$ K). Volatiles, depending to the temperature, can be present either in vapor or ice phase. We define a snowline³ as the region where the temperature becomes low enough for a vapor to condense into ice. Different volatiles have different snowlines locations in different regions in the disk (due

³Used interchangeably with iceline and condensation front throughout this manuscript.

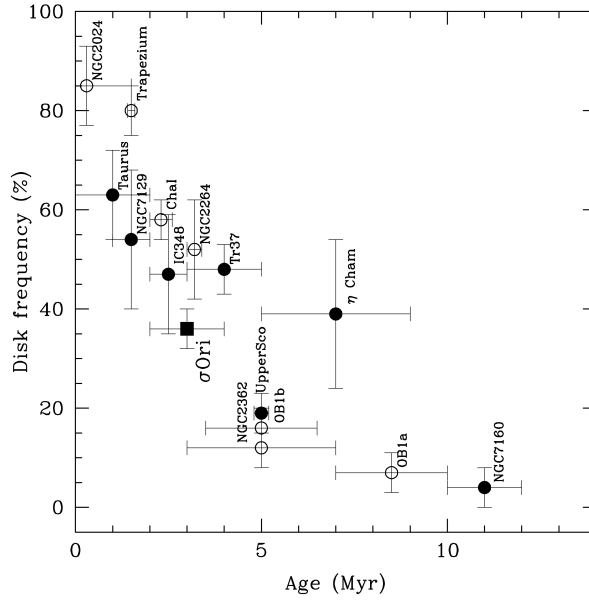


Figure 1.2: The observed disks frequency as a function of their age, from Hernández et al. (2007). An average disk lifetime around 3 Myr can be inferred from this plot.

to the decreasing temperature profile). The water, CO and N₂ icelines for example are present roughly around 3, 30 and 32 AU respectively, as discussed later in more details.

Disks chemistry models

One of the most simple methods to infer the chemical composition of a system at equilibrium starting from a known initial condition in a fixed thermodynamic environment is through the Gibbs energy minimization technique, originally developed by White et al. (1958). In this method, the equilibrium state is obtained by minimizing the Gibbs free energy (G_E) of the system, at constant temperature T and pressure P , with respect to the number of moles of each component in each phase n_i^k . For a system with NP phases and NC components, we have

$$G_E = \sum_{k=1}^{NP} \sum_{i=1}^{NC} n_i^k \mu_i^k, \quad (1.24)$$

where n_i^k and μ_i^k are the number of moles and the chemical potential of component i in phase k , respectively. The chemical potential is a function of the composition of phase k at temperature T and pressure P (Rossi et al., 2009). This method being extensively used in various domains, several computing codes have been developed to perform the heavy numerical calculations. The most known are SOLGASMIX (Sharp & Huebner, 1990),

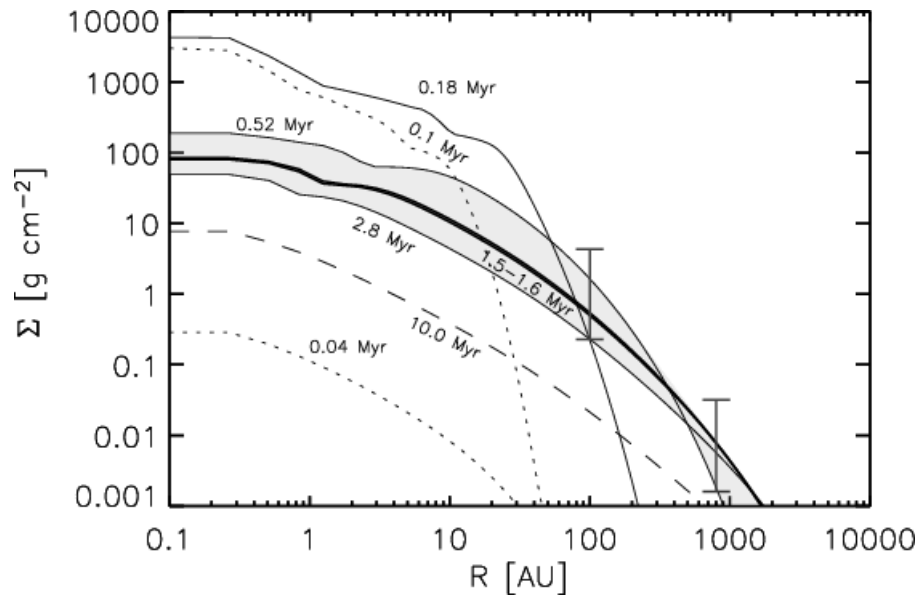


Figure 1.3: DM Tau surface density observations (the two vertical error bars) along with best fit time and distance profiles issued from the Hueso & Guillot (2005) model.

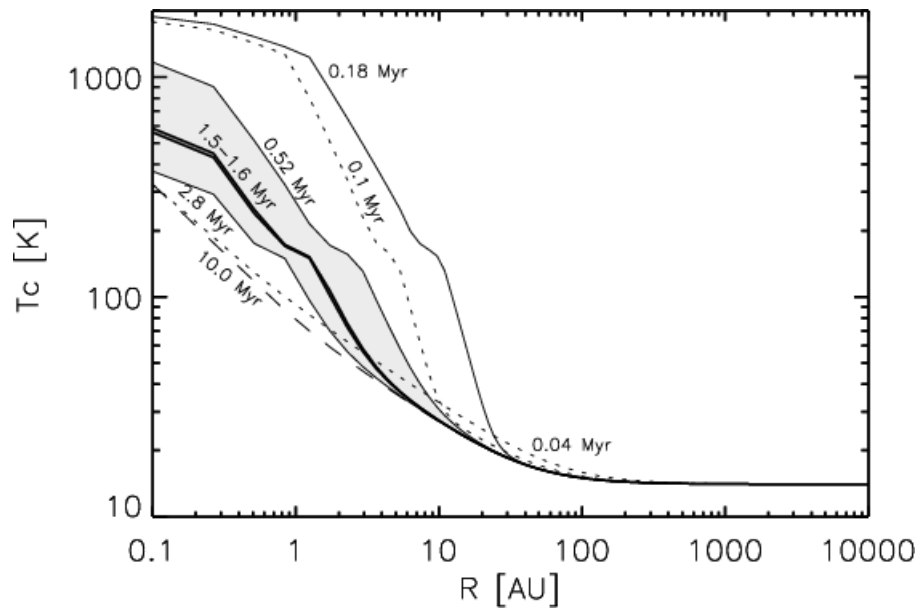


Figure 1.4: The temperature profiles corresponding to the models fitting the DM tau observations, from Hueso & Guillot (2005).

NASA's CEA⁴ and the HSC Chemistry package developed by Outotec Research⁵.

⁴<http://www.grc.nasa.gov/WWW/CEAWeb/ceaHistory.htm>

⁵<http://www.outotec.com/en/Products-services/HSC-Chemistry>

Practically in the case of a PPD, we need to input the initial gas phase elemental composition of the system, in addition to the pressure and temperature of the equilibrium state. The algorithm will then find the lowest energy state of the system with the corresponding molecules and their abundances. A large database of molecules is thus required for accuracy.

The output of such calculations is very dependent on the initial relative elemental abundances. The C/O ratio for example controls the final C and O bearing species relative abundances. Figs. 1.5 and 1.6 shows the volatiles and refractories equilibrium composition for a system of solar composition (C/O \sim 0.55, Asplund et al. (2009)). On the volatiles side, H₂O is always very abundant. CO and N₂ dominates C and N chemistry at high enough temperatures, while CH₄ and NH₃ become the major C and N bearing species once temperature drops below a certain point. CO₂ on the other hand is a minor element under all conditions. Fig. 1.7 shows the volatiles dominant at equilibrium for different temperatures and a wide range of C/O ratios. We notice how for high temperatures and a C/O ratio near unity, most oxygen goes into CO instead of water.

However, this is but equilibrium chemistry. Several non-equilibrium processes can affect the disk's composition. Chemical quenching due to the low temperatures in the outer nebula and the rapid turbulent mixing can have a profound effect on the carbon and nitrogen volatile chemistries (Lewis & Prinn, 1980; Prinn & Fegley, 1981; Prinn, 1993). Turbulent transport will diffuse vapor N₂ out from the inner hot regions where it dominates, to the outward cold zones where NH₃ should be the main nitrogen bearing specie at equilibrium. At these low temperatures however, due to the long chemical reaction timescales, N₂ conversion to NH₃ will be inhibited. N₂ can thus dominate the entire disk as long as the diffusive mixing timescales are shorter than the chemical conversion timescales. The same process applies for CO - CH₄ chemistry. In these models, CO and N₂ are the main C and N bearing species throughout the disk at all temperatures. Qualitatively, we define the turbulent mixing timescale τ_{mix} as:

$$\tau_{mix} \sim \frac{L_{mix}^2}{k_{rr}} \quad (1.25)$$

where L_{mix} is the radial mixing characteristic length scale and k_{rr} the radial eddy diffusion coefficient. Lewis & Prinn (1980) estimated $L_{mix} \sim 3 \times 10^{12}$ cm and $k_{rr} \sim 2 \times 10^{16}$ cm² s⁻¹, giving:

$$\tau_{mix}^{CO} \sim 5 \times 10^8 \text{ s}$$

The chemical conversion timescale τ_{chem} on the other hand depend on the chemical species equilibrium concentrations in addition to the chemical reaction rate constant. The reaction governing CO and N₂ conversion to respectively methane and ammonia at low temperatures are:



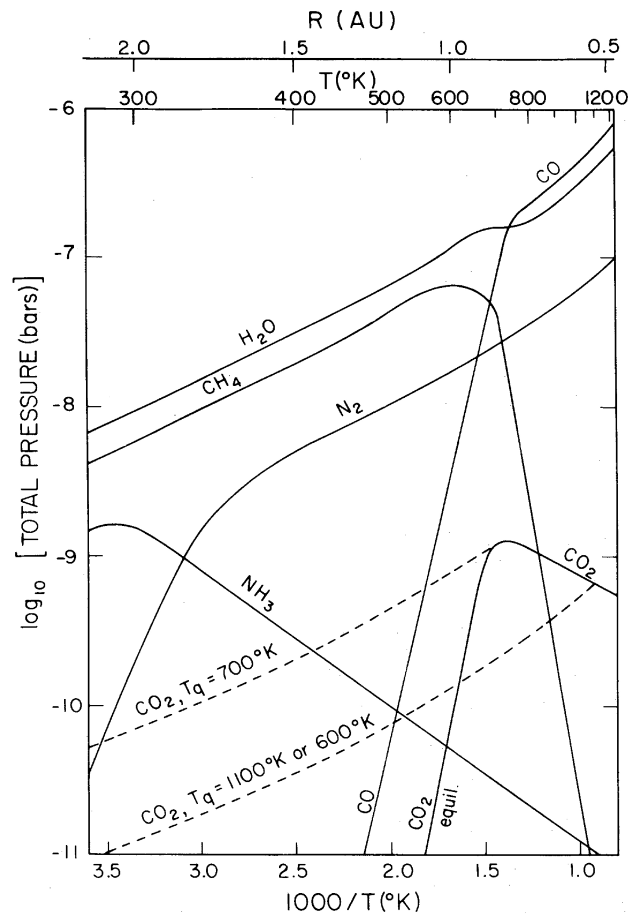


Figure 1.5: A typical solar nebula volatiles chemical composition at equilibrium for a range of pressure and temperature, from Lewis & Prinn (1980). The dashed lines are CO_2 non-equilibrium abundances at a quenching temperature T_q .

Both reaction however proceeds via multisteps. Lets consider the carbon reaction as an example. This reaction limiting step was originally proposed to be:



although cf. the work of (Yung et al., 1988) where another possible reaction limiting step is discussed.

In our case, the chemical conversion timescale is given by:

$$\tau_{chem} \sim \frac{[\text{CO}]}{d[\text{CO}]/dt} = \frac{[\text{CO}]}{k_f[\text{H}_2][\text{CH}_2\text{O}]} \quad (1.29)$$

where $[X]$ is X 's equilibrium concentration, and k_f is chemical reaction rate constant. Lewis & Prinn (1980) originally calculated for CO conversion:

$$\tau_{chem}^{CO} \sim 3 \times 10^9 \text{ s}$$

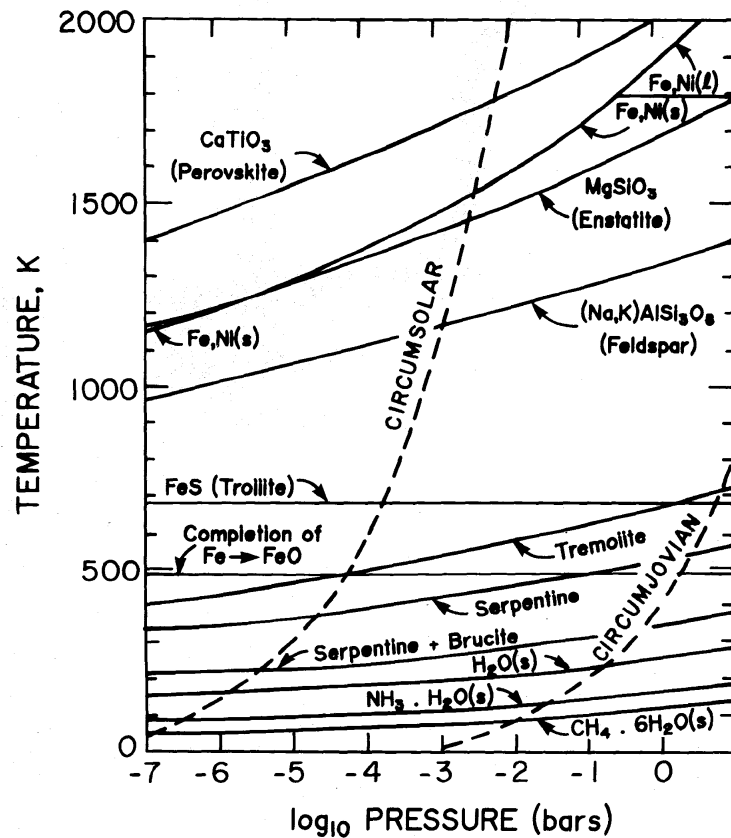


Figure 1.6: A typical solar nebula refractories chemical composition at equilibrium for a range of pressure and temperature, from Prinn (1993).

for this gas phase reaction. One should also ideally take into account the surface catalyzed and other gas-grain reactions, but their effects were found by Lewis & Prinn (1980) to be negligible. These results show that $\tau_{chem}^{CO} \gg \tau_{mix}^{CO}$, leading to the chemical quenching and CO as the main C bearing volatiles at all temperatures. Similar arguments can be made to explain why N_2 is also the main Nitrogen bearing volatile throughout the disk.

Disk chemistry observations

Observations wise, directly measuring the abundances of these volatiles in the disks midplanes is very challenging. Different parts of the disks can be observed at different wavelengths. IR observations for example will probe the optically thin regions of the disk, with the far IR sensitive to the surface and near-mid IR more sensitive to the inner sub-surface warm regions. On the other hand, mm and sub-mm observations probe the optically thick (mostly midplane) regions of the disk. However, since H_2 (and N_2) is a diatomic homo-nuclear molecule, it is almost unobservable. For this reason, relative abundances need to be normalized with respect to another element. Carr & Najita (2008)

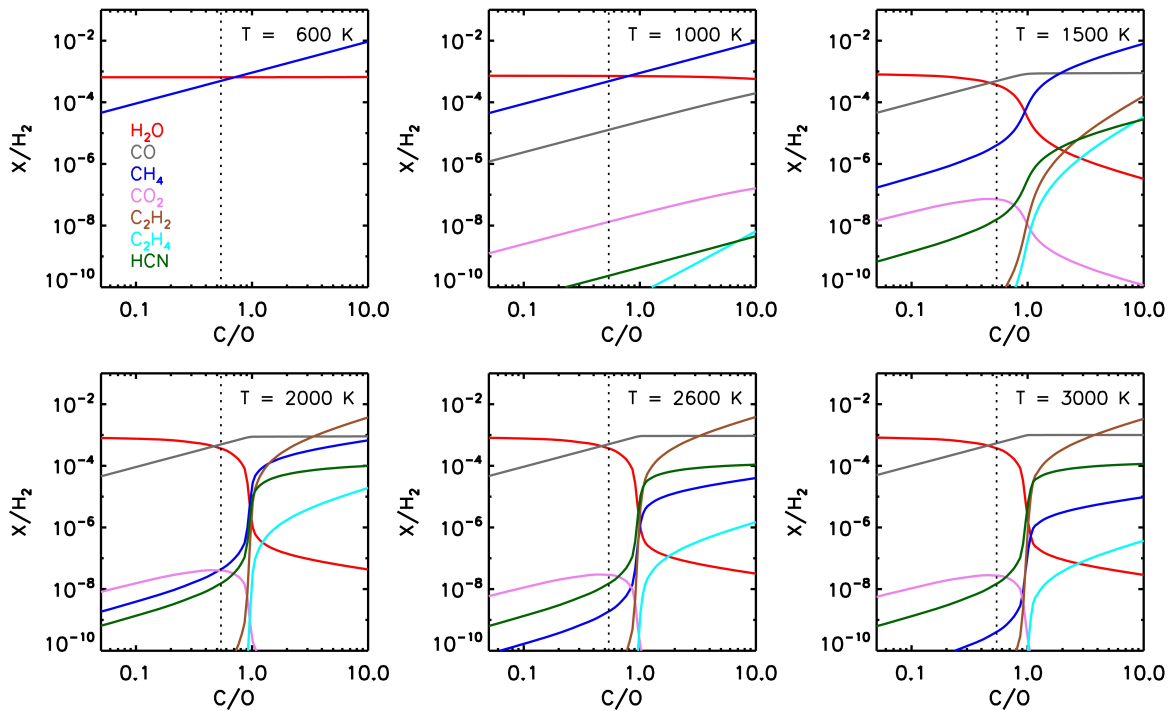


Figure 1.7: The C,H,O,N bearing volatiles equilibrium abundances for different temperatures and a range of C/O ratios, from Madhusudhan (2012).

reported the detection of organic molecules and water in the inner 3 AU of AA Tau in the IR wavelengths using IRS/Spitzer. Their main results are shown in Table 2.2. They inferred a H₂O/CO abundances ratio of 1.3, and CO₂/CO ratio between 0.004 and 0.26 (the species were measured at different temperatures (table 2.2)). These values are compatible with the abundances derived from equilibrium calculations. Their derived mean gas temperature of 900 K for CO indicates a higher than quenching limit temperature. The only nitrogen bearing species reported in this work is HCN. Moreover, to date, there is also no definitive detection of NH₃ in disks, only upper limits (Salyk et al., 2011; Mandell et al., 2012). In the mm wavelengths, radio-interferometers in the pre-ALMA era were only capable of probing the disk regions around 15-30 K, mostly beyond the CO iceline. Observations by Dartois et al. (2003); Piétu et al. (2007) and others however showed that even in these regions, important amounts of CO vapor is still present. This was attributed however to vertical and radial turbulent mixing (Semenov et al., 2006), in addition to photodesorption (Hersant et al., 2009). Measurements in the inner warm regions where planets formation takes place have only recently become accessible. Qi et al. (2013) for example used ALMA to image for the first time the CO iceline in a solar analogue (TW Hya), using N₂H⁺ as tracer. They inferred a CO iceline location around 30 AU. Favre et al. (2013) on the other hand, also using ALMA, made the first (indirect) measurement for the CO/H₂ ratio inside of the CO iceline, also for TW Hya. They found

however an unexplained CO depletion by an order of magnitude. This observation and others will be discussed in more details throughout this manuscript.

Molecule	T (K)	N (10^{16} cm $^{-2}$)	R^* (AU)	Abundance to CO
H ₂ O	575 ± 50	65 ± 24	2.1 ± 0.1	1.3
OH	525 ± 50	8.1 ± 5.2	2.2 ± 0.1	0.18
HCN	650 ± 100	6.5 ± 3.3	0.60 ± 0.05	0.13
C ₂ H ₂	650 ± 150	0.81 ± 0.32	0.60†	0.016
CO ₂	350 ± 100	0.2 – 13	1.2 ± 0.2	0.004 – 0.26
CO	900 ± 100	49 ± 16	0.7 ± 0.1	1.0

*The equivalent radius for the emitting area A ($R = [A/\pi]^{1/2}$).

†Area was set to that derived for HCN.

Table 2.2: The observed molecular abundances and column densities in AA Tau, from Carr & Najita (2008).

The D/H ratio in protoplanetary disks

Another important chemical probe of our own solar system is the Deuterium/Hydrogen (D/H) ratio measured in a large number of bodies. The D/H ratio is usually interpreted as an indicator of the formation temperature of ices. Ices forming at relatively high temperatures will have a lower D/H ratio than ices forming at relatively lower temperatures. The chemical reason behind this can be summarized by the following reaction:



where, at temperatures higher than few hundred kelvins, the HDO in water will react with the nebular H_2 resulting ordinary water and HD . This will decrease the D/H ratio in water from the initial high interstellar value to the lower values found in today's solar system.

Several models have been put forward to quantify this phenomenon. Drouart et al. (1999) and Mousis et al. (2000) are some of the earliest examples who tried to couple the mechanisms affecting the D/H ratio in disks (chemistry and the turbulent diffusion of HDO and water following their concentration gradients) to a simple evolutionary protoplanetary disk model. These models agreed on a monotonic D/H enrichment profile increasing with distance from the sun, as seen in Fig. 1.8. Fig. 1.9 on the other hand shows an up-to-date summary of D/H measurements in solar system bodies. The protosolar D/H value is defined to be the Jovian/Saturnian atmospheric value since these are gas dominated planets that accreted large amounts of nebular H_2 . Comets have on average higher D/H ratio than planets, which is expected since they are dominated by ices. The icy moon Enceladus have a cometary D/H ratio, which also conforms to theory since the Saturnian system formed in the same general area as comets. The D/H ratio was also measured in Uranus and Neptune and found to lower than in comets but higher than the protosolar value, for reasons not yet well understood. This measurement is discussed in Chapter 3.

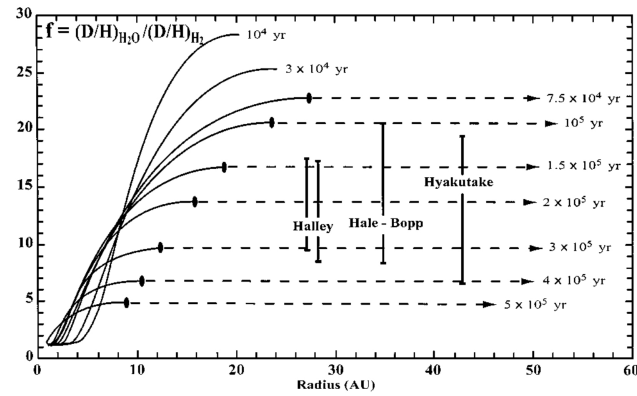


Figure 1.8: The D/H enrichment in the disk as a function of location and time, compared to several cometary values. From Mousis et al. (2000).

Earth’s D/H ratio is not well understood either, but it seems that chondritic meteorites were more presented than comets in Earth’s water budget. A variety of values is also observed among the comets themselves, to be discussed in Chapter 4.

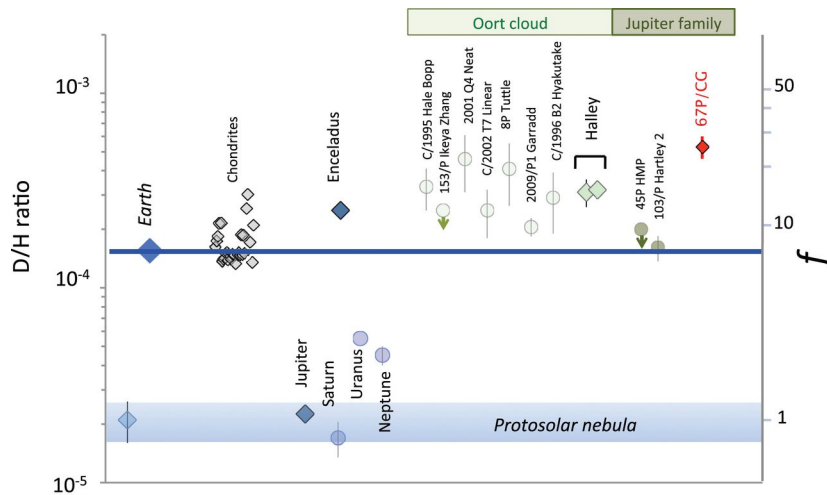


Figure 1.9: The D/H measurements in different solar system bodies including most comets to date. From Altwegg et al. (2015).

1.2 Basics of planets formation

Now that we have discussed the physics and chemistry of protoplanetary disks, we can proceed to introduce the basics of planets formation theory, focusing on giant planets. There are two planetary formation models currently discussed in the literature: the gravitational instability model where planets form quickly in one step from unstable disk

regions, and core accretion, where planets form over longer time periods from solids gradual growth then gas accretion onto the core.

1.2.1 Gravitational instability model

One widely discussed model of giant planets formation is the direct gravitational collapse of an unstable disk fragment (Boss, 1997). It has been shown that a rotating Keplerian disk is unstable to axisymmetric perturbations if:

$$Q = \frac{c_s \Omega}{\pi G \Sigma} < 1 \quad (1.31)$$

where Q is known as the Toomre parameter. If we increase the temperature or the rotational speed of the disk, it will become more stable. If on the other hand we increase its mass, then it will close toward gravitational instability. We develop equation 1.31 into:

$$\frac{H}{R} \lesssim \frac{M_d}{M_*}$$

where $\frac{M_d}{M_*}$ is the disk/star mass ratio and $\frac{H}{R}$ the disk's height/radius ratio. For a typical disk with $\frac{H}{R} \sim 0.1$, we need $\frac{M_d}{M_*} \sim 0.1$ for a gravitational collapse to occur, which is close to the observed disks upper mass limit. Assuming a characteristic size of the instability $\sim H$, we can estimate the mass of the resulting planet as: $M_p = \Sigma H^2 \sim 1 M_{Jup}$. The most straightforward predictions of this model is a coreless giant planet with solar-like chemical composition. Both of these constraints have been ruled out for our solar system giant planets, were solid cores have been detected in all of them, and are all thought to be enriched in heavy elements with respect to the solar value. Although this does not exclude this mechanism as a possibility for some exoplanets (Boss, 2011), it does severely constraint it for our solar system (although cf. recent works such as Nayakshin et al. (2014) on the core assisted gas capture instability).

1.2.2 Core accretion model

The most prominent and widely accepted theory for planets formation is through core accretion (Pollack et al., 1996), where the “bottom up” formation starts from small dust particles that coagulate together growing in size through chemical sticking and then gravitational attraction till reaching a mass sufficient for gas accretion to takes place, leading to a gaseous planet. In this section we take a chronological approach in explaining this mechanism.

Gas-solids interaction

Before diving into the details of solids growth, it is crucial to understand how these solids interact with the much more abundant gas in the nebula. A gas particle in a typical disk has a mean free path in the order of 1 cm. This implies that any dust

particle smaller than this size will feel the gas as individual particles, interacting with it mainly via collisions while following the gas mean flow. On the other hand, particle approaching and greater than this size will feel the gas as a fluid and get gradually decoupled (Weidenschilling, 1977). Lets consider a spherical solid dust particle with radius R_s and density ρ_s in a our slightly sub-Keplerian disk with mean free path λ , density ρ_g and a thermal velocity v_{th} .

For $R_s < \lambda$ (Epstein regime), the dust particle will collide with the gas particles, losing energy by each collision. The dust will feel the drag force:

$$F_D = -\frac{4\pi}{3}\rho R_s^2 v_{th} v_{rel} \quad (1.32)$$

where v_{rel} is the gas-dust relative velocity.

For $R_s > \lambda$ (Stokes regime), the particle (on a truly Keplerian orbit) will feel the slightly sub-Keplerian gas as a fluid, and thus will be affected by a residual gravity due to gas pressure gradient. In this case we have:

$$F_D = -\frac{C_D}{2}\pi R_s^2 \rho_g v_{rel}^2 \quad (1.33)$$

where C_D is the drag coefficient dependent on the fluid Reynold number R_e and v_g is the gas radial velocity. Lets now define the particle's stopping time (the drag time scale) as:

$$t_f = \frac{m v_{rel}}{F_D} \quad (1.34)$$

Lets consider now the particle's equations of motion:

$$\frac{dv_r}{dt} = \frac{v_\phi^2}{r} - \Omega_K^2 r - \frac{1}{t_f}(v_r - v_r^{gas}) \quad (1.35)$$

$$\frac{d}{dt}(r v_\phi) = -\frac{r}{t_f}(v_\phi - v_\phi^{gas}) \quad (1.36)$$

where v_r is the particle's radial velocity with respect to the star and v_ϕ its angular velocity. As long as the particle is relatively coupled to the gas ($t_f \Omega_k \ll 1$) we get the gas drag regime where:

$$v_{rel} = t_f \frac{1}{\rho_g} \frac{\partial P}{\partial r} \quad (1.37)$$

In this case, particles will lose energy due to friction or collisions and spiral inward toward the central star. On the hand, for particles decoupled from the gas ($t_f \Omega_k \gg 1$) we have the perturbed Keplerian and high R_e regimes:

$$v_{rel} = \frac{r}{t_f} \frac{1}{g \rho_g} \frac{\partial P}{\partial r} \quad (1.38)$$

where g is the central gravity. In this case, particles will feel the headwind, and according to their size either drift slowly or not at all. In Fig. 1.10 we can find typical drift velocities

for different particles sizes and gas densities. This classical result shows that particles in the metric size will feel strong gas drag, drifting inward to the star very rapidly (in 100 yr at 1 AU). How do planets form if particles around this size cannot survive for more than a 100 yr is a classical problem referred to as “the meter barrier”. Smaller (sub-centimetric) and larger (kilometric) particles on the other hand, although do feel the drag, can survive much longer ($\sim 10^5 - 10^6$ yr).

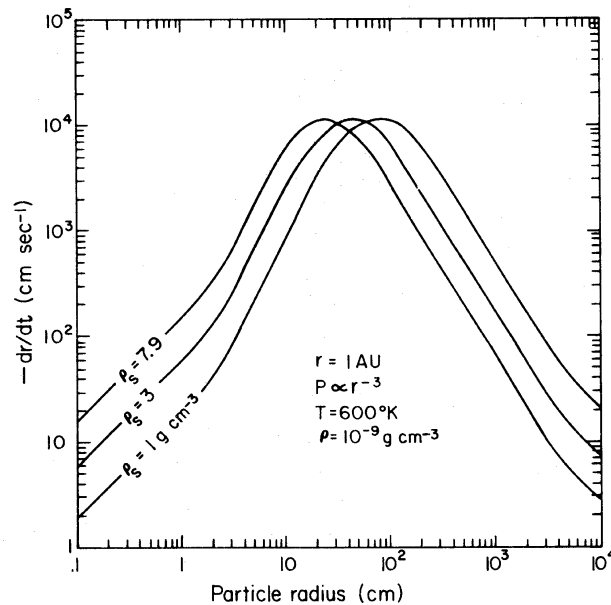


Figure 1.10: Solids drift velocities in disks due to gas drag, from Weidenschilling (1977). Metric boulders spiral towards the sun very fast, resulting in the metric barrier problem.

From dust to pebbles

Let’s consider a very simple typical young disk where all solids are micrometric dust particles, with a gas-to-dust ratio of 100 inside the water’s snowline (3.5 AU) and 70 beyond it. The first step towards planets formation is the μm dust growth into larger centimetric to decimetric (pebbles) solids. This proceeds mainly via dust coagulation (Blum & Wurm, 2008), although vapor condensation on pre-existing dust can play a significant role. Dust coagulation happens via two modes: cluster-cluster and particle-cluster agglomeration. In Both modes a cluster of particles will coagulate with either an individual particle of another cluster via Van der Waals forces. The efficiency of this type of growth depends on many factors, such as the collision velocity, sticking probability and collisions outcomes. A collision’s outcome can be sticking, bouncing or fragmentation, depending on the particles velocities and masses (Fig. 1.11). Particles need a relative velocity to collide. This can originate from Brownian motion, gas drag or turbulence. The sticking probability depends also on the velocity but more importantly on the chemical

composition of particle. Ice particles have higher sticking probability than refractories. Typical μm to $\text{cm} - \text{dm}$ growth timescales are around 10^3 to 10^4 yr, orders of magnitude lower than the disk lifetime. Another possible dust growth mechanism is volatiles condensation (Ros & Johansen, 2013) where vapors (mainly water and CO) will condense on the surface of a dust particle just beyond an iceline. The particle will then grow larger in size and condense more vapors. Moreover, the newly condensed ice on the particle's surface can increase substantially its sticking efficiency, thus assisting growth via coagulation. This was shown to be an efficient growth mechanism, with timescales around $10^3 \Omega_K^{-1}$. This channel will be discussed in more details later.

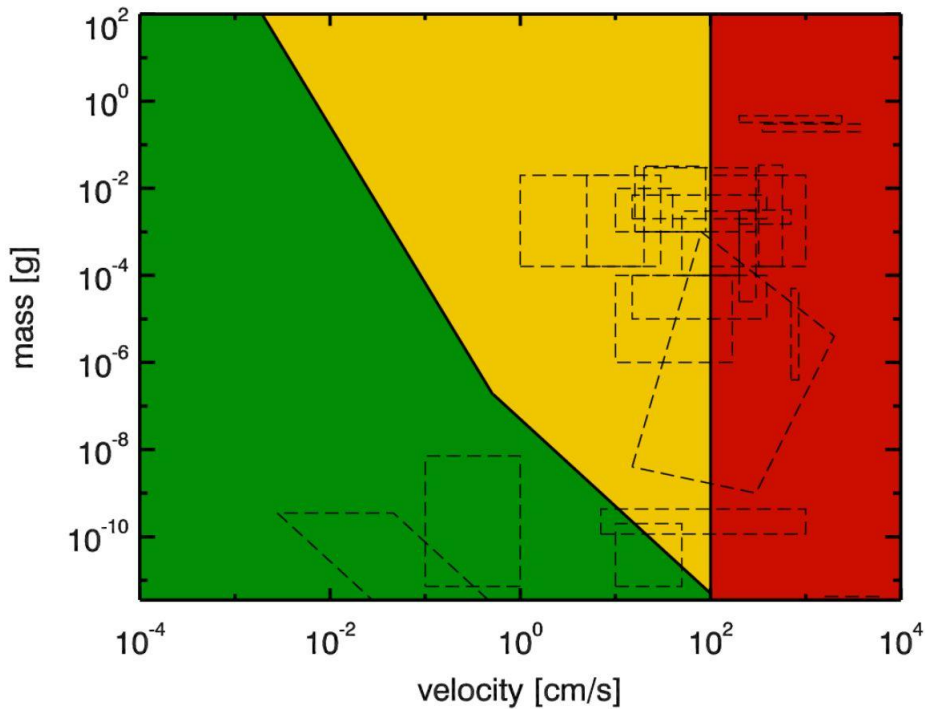


Figure 1.11: Dust collisions outcome as a function of their relative speed and mass, from Blum (2010). Green region represent sticking, yellow is for bouncing and red for fragmentation. Dashed shapes are the experimental results.

From pebbles to planetesimals

While coagulation and condensation were always suspected as the main ingredients of dust growth to pebbles, how do pebbles grow to kilometeric planetesimals through the meter barrier is a question that provoked a lot of research over the years. The currently accepted picture is that kilometeric planetesimals form directly from pebbles through gravitational collapse on timescales shorter than radial drift (Youdin & Goodman, 2005; Johansen et al., 2007). The first step in this mechanism is pebbles settling in the disk midplane, increasing the solids density in this layer. Roughly, settling will take place

if:

$$S_t \equiv \frac{\rho_s R \pi}{\Sigma_g} > \alpha \quad (1.39)$$

where S_t is the dimensionless Stokes number and α the turbulence parameter. The next step is the pebbles pile up in transient but long lived high pressure regions excited in the turbulent gas flow. Equations 1.37 and 1.38 show that since gas drag follows the pressure gradient, a pressure maximum will stop the particle's drift. This pile up will be increased further by streaming instability, where local particles clumps reduce the headwind for the upcoming particles resulting in runaway pile up of pebbles into clumps and filaments. These two effects, together, will decrease the local gas-to-solids ratio in the pebbles clumps to the order of unity, resulting in their rapid gravitational collapse into planetesimals typically with radii in the order of ~ 100 km.

From planetesimals to giant planets

In the core accretion model, giant planets formation proceeds essentially in two main steps: the growth of the planet's core to the critical mass (M_c) of about 10 Earths masses (M_\oplus), followed by the hydrostatic growth and then collapse (runaway accretion) of the envelope (Pollack et al., 1996). The first step is time critical, since the core's formation should be done before the disk's dissipation in few Myr. It was thought classically that planetesimals grow to M_c by oligarchic growth through runaway planetesimals accretion, but this channel always suffered from very long timescales allowing to barely form Jupiter, and usually fails for Uranus and Neptune. We define the distance from the planet over which its gravity dominates over the stellar gravity as the Hill radius R_H :

$$R_H = \left(\frac{M_p}{3M_*} \right)^{1/3} \quad (1.40)$$

Roughly speaking, a planet can only accrete solids inside its feeding zone with a half width of few times its R_H . The growth rate of a protoplanet is given by:

$$\dot{M}_p = \frac{\sqrt{3}}{2} \Sigma_s \Omega \pi r^2 F_g \quad (1.41)$$

where Σ_s is the solids density, r the distance to the protoplanet and F_g the gravitational focusing factor dependent on the protoplanet-solids relative velocity and the escape velocity $v_{esc} = \sqrt{\frac{2GM}{R}}$. Classical simulations show that 5 Myr is needed to grow a protoplanet to M_c through planetesimals accretion at 5 AU, and it goes up to 50 Myr at 10 AU (much longer than the disk lifetime). This is due to most planetesimals being simply scattered by the protoplanet, leading to the accretion of only a small fraction of the planetesimals entering R_H .

A much faster mechanism has started to get acceptance recently, where cores grow through pebbles accretion instead of planetesimals (Lambrechts & Johansen, 2012). The secret behind this efficiency is gas drag. While planetesimals interaction with the protoplanet is purely gravitational, pebbles continue to interact also with the gas via gas drag,

causing them to lose energy and spiral inward toward the protoplanet. This channel was found to be several orders of magnitude faster than classical oligarchic growth, and could grow cores far from the star 100 to 10000 times quicker. Once the protoplanet has reached M_c , it will begin accreting the gas disk, although slowly at the beginning. This hydrostatic accretion phase will proceed till the gaseous envelope starts dominating the planet's mass. At this point, no hydrostatic solution exists for the envelope, and the local disk's gas will collapse quickly onto the protoplanet forming its massive envelope. This collapse will be limited by either gap opening within the disk or the disk's evaporation.

Planetary migration

A paradigm change for planets formation theory followed the detection of the first closed-in hot Jupiter 51 Pegasi b (Mayor & Queloz, 1995). Since a Jupiter mass planet core can't form quickly enough inside of the snowline, such planets should have come from elsewhere in the disk ("migrated"). Planets migration is a natural and inevitable outcome of a planet's gravitational interaction with a gaseous disk (Kley and Nelson, 2012). Let's consider a low (Earth to Neptune) mass planet on a circular orbit in a disk. The superposition of sound waves, excited at the Lindblad resonances in the differentially rotating disk, will create 2 wakes (spiral arms) at the inner and outer resonances. The external wave will follow the planet, and thus exert a negative torque on it. The inner wave on the other hand will exert a positive torque on the planet. Since one-sided Lindblad torques scale as H^{-3} . Assuming further that $H/r \sim 0.1 - 0.01$, we conclude that the inner torque on the planet is much larger than the outer torque, and thus the planet will be driven inward. This is the "type I" migration with a characteristic velocity $\propto M_p^2$ and a time scale $\tau_I \sim 10^5$ yr, much shorter than the disk lifetime. A migration halting processes in thus needed for planets to survive, such as a truncated inner disk, turbulence, or a planetary trap. Another process that can affect type I migration is the corotation torques exerted from the Horseshoe region on the planet. By taking into account this process in a more realistic (non isothermal) disk, the migration direction can be reverted under certain conditions.

Lets now consider more massive (Jovian) planets, with $R_H \geq H$. Such planet, through the same forces acting in type I migration, will open a gap in the disk if (Crida et al., 2006):

$$P = \frac{3}{4} \frac{H}{R_H} + \frac{50}{q R_e} \leq 1 \quad (1.42)$$

Once a gap has been opened, the planet's migration will halt. The gap, and the planet trapped in its middle, will then follow the viscous evolution of the disk. Since the disk's gas global evolution will push the gap inward toward the star, the planet will also move inward: this is the "type II" migration. The characteristic timescale in this case is $\tau_{II} = \tau_{visc} = 1/(\alpha H^2 \Omega_p)$. This type of migration is fundamentally comparable to the disk's life time and is thus slow.

The planet's final composition

The final planet's chemical composition is dictated by the compositions of both its core and envelope, in addition to its interior convective state (Guillot et al., 1994; Leconte & Chabrier, 2012). In the case of a completely decoupled envelope (no core erosion), then the planet is expected to have the same chemical composition of the local disk's gas that collapsed onto the core and formed the envelope. If on the other hand, the planet's core was partially or completely eroded, then the planet's atmospheric composition should reflect this dual origin. Even if the planet's core was eroded, a strong internal convection is needed for a well mixed and fully equilibrated envelope. If the envelope is not chemically fully equilibrated with the core, then even deep measurements does not necessarily reflect the planet's bulk composition.

Moreover, a planet's bulk composition can be affected by its migration history. Jovian and Neptune-like planets can acquire important fraction of their mass during migration (Alibert et al., 2005; Terquem & Papaloizou, 2007). In this case, the planet's atmospheric composition can reflect a different accretion location than its core.

1.3 Chemical composition of planets and small bodies

A primary source of data on how do planets form is their chemical composition. The chemical composition of the solar system's small bodies can also shed a light on the properties of the disk regions where they formed. The main goal of this work is to establish a framework connecting the chemical composition of the solar system bodies to processes in the protosolar nebula. In this section I summarize the current knowledge on the composition of bodies. I will discuss only the measurements, leaving interpretations for next chapters.

1.3.1 Giant planets

Jupiter

The best studied giant planet is by far Jupiter. It is the gas giant where we have the most detailed informations about its chemical composition. This is due mainly to the Galileo spacecraft that entered its atmosphere in 1995 up to depths of 23 bar, and did the only in situ measurements of a giant planet's atmosphere to date (Young et al., 1996). At these depths, the probe was below Jupiter's weather layer (the stratosphere). For this reason, the abundances found by Galileo are usually interpreted to be the deep bulk chemical composition of Jupiter. For such interpretations of the tropospheric measurements to be valid, we are implicitly assuming the planet's interior to be well mixed, and thus convective. Jupiter's chemical composition as seen mostly by Galileo's neutral mass spectrometer and helium-abundance interferometer can be found in table 2.3 (elementary abundances with respect to hydrogen) and table 2.4 (elementary abundances with respect to hydrogen, normalized to solar value). Interpreting these values is not trivial. First,

we notice how most elements (including noble gases) are enriched by a factor 2-3 with respect to the solar value. This is a very strong indicator that Jupiter formed via core accretion, since formation via gravitational instability would lead the planet to having a solar chemical abundance. Second, Helium and Neon are apparently depleted. This is usually interpreted by He - Ne droplets raining in to the planet's core. Finally, Oxygen also seems to be depleted. This contradicts predictions from core accretion models, since Jupiter's formation beyond the water snowline through core accretion should have led to water enrichment, and in any case, would have excluded such depletion. However, this value is usually attributed to Galileo's entering a locally depleted thermal hot spot, arguing that the bulk water abundance should be higher. How did Jupiter acquire its current exact chemical composition is still a major unresolved problem, but several models have been proposed in order to explain quantitatively the observed enrichments, each with its advantages and weaknesses:

1. Volatiles enrichment by their trapping in either crystalline clathrates-hydrates or amorphous ices, accreted later by Jupiter (Gautier et al., 2001; Hersant et al., 2004; Alibert et al., 2005; Mousis et al., 2012; Owen et al., 1999). In these scenarios the volatiles are acquired in solid phase. This model requires a very cold formation region for Jupiter ($\leq 40K$), and thus are probably incompatible with the dynamical models (Walsh et al., 2011), specially if the presence of a dead zone in the midplane kept the low temperature regions far out in this disk (Qi et al., 2013; Martin and Livio, 2014), where solids density is very low. Other problems in these models is the assumption that $\sim 50\%$ of sulfur existed as the volatile H_2S throughout the disk, which might not be the case where it probably existed mostly as the much more refractory FeS (Lodders, 2004), although cf. the models of Pasek et al. (2005); Ciesla (2015). Moreover, both models imply a cometary D/H ratio for Uranus and Neptune building blocks (assuming well mixed planetary interiors), what was recently excluded in both planets (Feuchtgruber et al., 2013). Finally, and maybe most importantly, Phosphine (PH_3 , the main volatile phase of phosphorus), is not yet detected in comets, with only upper limits available (Agúndez et al. (2014a) and references herein). It was though detected in a circumstellar region, and found to contain only 2% of the solar phosphorus abundance (Agúndez et al., 2014b). This hints that maybe phosphine was absent from the nebula, and not available for trapping by either models, specially knowing that the refractory phases of phosphorus have an almost solar abundance in CI chondrites (Lodders, 2003).
2. Jupiter's late formation from a chemically evolved disk (Guillot and Hueso, 2006; Monga and Desch, 2015). In these scenarios, the disk evaporation along with dust settling and drifting particles sublimation enrich the midplane in volatiles, where Jupiter will form later and accrete these volatiles in gaseous phase. Again, the major problem of this model is its non-compatibility with Jupiter's migration, as stated by the Guillot and Hueso (2006). A massive disk is needed for Jupiter's (and Saturn's) migration that shaped the inner disk (Walsh et al., 2011; Kley and Nelson, 2012).

3. Jupiter’s formation on a refractory carbons “tar” line (Lodders, 2004). In this model, the enrichments observed are merely an artifact of normalization with respect to hydrogen. When normalized to sulfur instead, the author found solar abundances for most elements (Table 5.1). She therefore proposed that the hydrogen in Jupiter is locked in its metallic interior, depleting the outer envelope in hydrogen and giving the apparent enrichments. Only carbon remain enriched after the normalization with respect to sulfur. The author hence proposed that Jupiter formed on a tar line, leading to this moderate enrichment. No realistic origin for this line has been proposed.

More detailed discussions on these models and others can be found in Mousis et al. (2014).

Element	Jupiter	Solar System	CI Chondrites	Jupiter/Solar System	Jupiter/CI Chondrites
H.....	2.60×10^6	5.46×10^6	1236	0.476	2104
He.....	$(2.05 \pm 0.05) \times 10^5$	5.27×10^5	1.36×10^{-4}	0.389 ± 0.010	$(1.51 \pm 0.04) \times 10^9$
Ne.....	32 ± 4	483	5.29×10^{-7}	0.066 ± 0.008	$(6.1 \pm 0.8) \times 10^7$
Ar.....	23.6 ± 4.7	23.0	2.16×10^{-6}	1.03 ± 0.20	$(1.1 \pm 0.2) \times 10^7$
Kr.....	0.0121 ± 0.0022	0.0124	3.69×10^{-8}	0.98 ± 0.18	$(3.3 \pm 0.6) \times 10^5$
Xe.....	0.00116 ± 0.00022	0.00121	7.86×10^{-8}	0.96 ± 0.18	$(1.5 \pm 0.3) \times 10^4$
C.....	2727 ± 520	1591	174	1.71 ± 0.33	16 ± 3
N.....	922 ± 416	438	12.4	2.10 ± 0.95	74 ± 34
P.....	1.69 ± 0.65	1.88	1.88	0.90 ± 0.35	0.90 ± 0.35
O _{gas}	779^{+506}_{-364} ^a	2454^b	984^b	$0.33^{+0.21}_{-0.15}$	$0.81^{+0.51}_{-0.37}$
O _{rock}	$\equiv 722^c$	722^c	722^c	$\equiv 1.0$	$\equiv 1.0$
O _{total}	1501^{+506}_{-364}	3176	1706	$0.47^{+0.16}_{-0.12}$	$0.82^{+0.30}_{-0.21}$
S.....	$\equiv 100$	$\equiv 100$	$\equiv 100$	$\equiv 1.0$	$\equiv 1.0$

Table 5.1: The measured chemical composition of Jupiter normalized with respect to sulfur (from Lodders (2004)).

Saturn

Although no in situ measurements have been made to date in Saturn’s atmosphere, a wealth of informations is still available (a recent review can be found in Mousis et al. (2014)). This is due mostly to the Cassini space probe orbiting Saturn for more than decade. A summary of our current knowledge on Saturn chemical composition can also be found in tables 2.3 and 2.4. Carbon (methane) and phosphorus (phosphine) abundances were measured using the Cassini Composite Infrared Spectrometer (CIRS). Sulfur (H₂S) and Nitrogen (ammonia) abundances on the other hand were measured from older (and inherently less reliable) centrimetric wavelengths observations. These values are also interpreted as the deep tropospheric well mixed bulk composition of Saturn. As for Jupiter, Saturn is enriched in most measured heavy elements. This is also in favor of core accretion theory. Moreover, Saturn appear to be more metals rich than Jupiter, where carbon for example is about 10 times solar, comparing to 4 times solar for Jupiter. The reason why Saturn is more enriched than Jupiter in volatiles is also an open fundamental question.

Table 2.3: Abundances in Jupiter and Saturn, from Mousis et al. (2014).

Species	Jupiter			Saturn		
	X/H ₂	$\Delta(X/H_2)$	Reference	X/H ₂	$\Delta(X/H_2)$	Reference
CH ₄	2.37×10^{-03}	5.70×10^{-04}	Wong et al. (2004)	5.33×10^{-3}	0.23×10^{-3}	Fletcher et al. (2009)
NH ₃	6.64×10^{-04}	2.54×10^{-04}	Wong et al. (2004)	$4-6 \times 10^{-4}$	–	Briggs & Sackett (1989)
H ₂ O ^(a)	4.90×10^{-04}	1.60×10^{-04}	Wong et al. (2004)	??	??	
PH ₃	2.11×10^{-06}	1.00×10^{-07}	Fletcher et al. (2009)	7.30×10^{-06}	0.48×10^{-06}	Fletcher et al. (2009)
H ₂ S	8.90×10^{-05}	2.10×10^{-05}	Wong et al. (2004)	3.90×10^{-04}	0.45×10^{-04}	Briggs & Sackett (1989)
He	1.36×10^{-01}	2.70×10^{-03}	von Zahn et al. (1998)	1.35×10^{-1}	0.25×10^{-1}	Conrath & Gautier (2000)
Ne ^(b)	2.95×10^{-05}	–	Niemann et al. (1998)	??	??	
Ar	1.82×10^{-05}	3.60×10^{-06}	Mahaffy et al. (2000)	??	??	
Kr	9.30×10^{-09}	1.70×10^{-09}	Mahaffy et al. (2000)	??	??	
Xe	8.90×10^{-10}	1.70×10^{-10}	Mahaffy et al. (2000)	??	??	

^(a)This is a lower limit; ^(b)this is an upper limit.

Uranus and Neptune

Since no space probe was dedicated to date to Uranus and Neptune (apart from Voyager’s fly by), we know little about their compositions (a review can be found in Gautier & Owen (1989)). The first effort to measure the carbon abundance in Uranus and Neptune was through the Voyager IRIS experiment, but no emission spectrum was detected due to their low atmospheric temperatures. Later ground based observations however were able to constraint the methane abundances in these planets to around $40-80 \times$ solar value. This carbon enrichment is an order of magnitude higher than for Jupiter and Saturn. Attempts were also made in order to constrain the nitrogen abundance on these planets from models of radio spectra. This method showed an apparent depletion in nitrogen by one to two orders of magnitudes in both planets. Interpreting the results is challenging though, since this apparent depletion might be due simply to opaque clouds or the nitrogen condensing below the observed atmospheric levels. Another possible interpretation is that these values do reflect the real bulk nitrogen abundances in Uranus and Neptune, and thus both are surprisingly poor in nitrogen. These observations will be discussed throughly in chapter 3.

Table 2.4: Enrichments in Jupiter and Saturn relatives to Protosun, from Mousis et al. (2014).

Species	Jupiter		Saturn	
	E	$\Delta E^{(a)}$	E	$\Delta E^{(a)}$
C	4.40	1.14	9.90	1.05
N	4.18	2.08	2.5–3.8	–
O ^(b)	0.42	0.15	??	??
P	3.34	0.36	11.54	1.35
S	2.94	0.70	12.88	1.52
He	0.72	0.04	0.71	0.14
Ne ^(c)	0.12	–	??	??
Ar	2.62	0.86	??	??
Kr	2.23	0.61	??	??
Xe	2.18	0.61	??	??

^(a)Error is defined as $(\Delta E/E)^2 = (\Delta X/X_{\text{planet}})^2 + (\Delta X/X_{\text{Protosun}})^2$; ^(b)this is a lower limit;
^(c)this is an upper limit.

1.3.2 The solar system's small bodies

Lots of informations can also be derived from the compositions of the solar system's small primitive bodies: comets and asteroids. C-type asteroids are the most primitive asteroids in the solar system. They are thought to have never been heated to more than 150 K. The spectra of these asteroids is very similar to CI chondrites, and are thus believed to be their parent bodies. CI chondrites and the solar system (solar photosphere) compositions are summarized in table 2.5. We notice how these chondrites have a very solar like composition, with the exception of the depleted volatile elements that were present in gas phase and thus not accreted (Anders & Grevesse, 1989; Wood, 2005). Comets are a mix of dust and ices with relative dust/gas ratios ranging possibly from 0.5 to 4 (Singh et al., 1992; Fulle et al., 2015), although with a factor 2 uncertainty. While the volatile abundances can be mostly measured from the ground when the ices start sublimating, the dust's composition must be measured in situ. A plethora of cometary ices observations has been acquired over the years across the spectrum. A recent review can be found in Fig. 1.12 from Mumma & Charnley (2011). The most abundant volatile in comets is water, which is the main oxygen bearing species. Next come CO and CO₂ with comparable abundances up to 30% with respect to water, although most comets seem to be on average more rich in CO than in CO₂ (Mumma & Charnley, 2011). Methane abundance is very low with 1.6% tops. Ammonia (NH₃) is the main nitrogen bearing species detected in comets, with an upper abundance of only 1.4%. This value is an order of magnitude lower than the solar nitrogen abundance. Molecular nitrogen (N₂) evaded detection for a very long time, but was finally resolved with ROSINA/Rosetta Rubin et al. (2015). It was found also to be an order of magnitude below solar value, confirming

Element	Halley		Solar System	CI-Chondrites
	Dust	Dust and Ice		
H ₂	2,025	4,062	2,600,000	492
C	814	1,010	940	70.5
N	42	95	291	5.6
O	890	2,040	2,216	712
Na	10	10	5.34	5.34
Mg	= 100	= 100	= 100	= 100
Al	6.8	6.8	7.91	7.91
Si	185	185	93.1	93.1
S	72	72	46.9	47.9
K	0.2	0.2	0.35	0.35
Ca	6.3	6.3	5.69	5.69
Ti	0.4	0.4	0.223	0.223
Cr	0.9	0.9	1.26	1.26
Mn	0.5	0.5	0.89	0.89
Fe	52	52	83.8	83.8
Co	0.3	0.3	0.21	0.21
Ni	4.1	4.1	4.59	4.59

Table 2.5: The observed dust and ice chemical compositions of 1P/Halley, from Jessberger & Kissel (1991). The solar system (photosphere) and chondrites compositions are also included for comparison.

the long speculated problem of nitrogen depletion in comets.

The dust composition in comets was first measured in-situ in 1P/Halley by Giotto. The results are given in table 2.5 from Jessberger & Kissel (1991), along with the ices compositions, and the solar and CI chondrites compositions for comparison. Interestingly, almost half of Halley's carbon and oxygen are found in dust. Additionally, refractories in Halley can't account for the nitrogen missing from the volatile phases.

Another comet we have visited is 81P/Wild, where samples were returned to Earth for analysis by the Stardust mission. The summary of this mission can be found in Fig. 1.13 from Flynn et al. (2006). The abundances of C,H,O and N were not determined for the sample. A striking result from this mission is the apparent one order of magnitude depletion in sulfur with respect to chondrites, which is not expected. The origin of this depletion is debated, and can be resulting from the analysis method itself. Another interesting result is the presence of very high temperature minerals among the collected samples, necessitating a delivery mechanism for these minerals from their formation region to the comets area.

All these informations show how do comets and their compositions relate directly to the physical processes taking place in the protoplanetary disk. It is the same basic physical and chemical properties of the disk that will affect everything from small bodies to giant

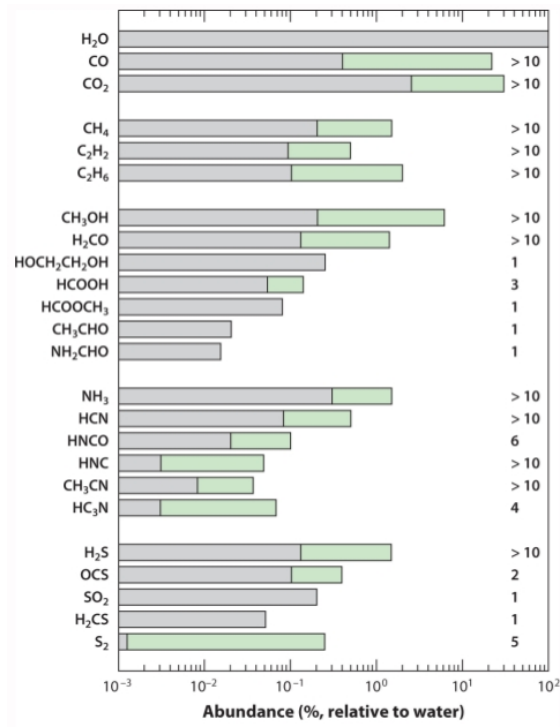


Figure 1.12: The observed abundances of cometary volatiles with respect to water, from Mumma & Charnley (2011).

planets.

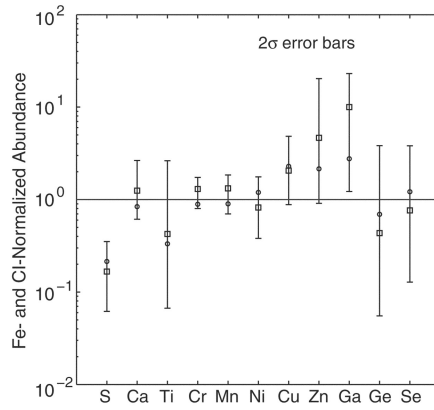


Figure 1.13: The measured refractory chemical composition of 81P/wild, from Flynn et al. (2006).

Bibliography

- Alibert, Y., Mordasini, C., Benz, W., & Winisdoerffer, C. 2005, *A&A*, 434, 343
- Altwegg, K., Balsiger, H., Bar-Nun, A., et al. 2015, *Science*, 347, 1261952
- Anders, E., & Grevesse, N. 1989, *Geochim. Cosmochim. Acta*, 53, 197
- Asplund, M., Grevesse, N., Sauval, A. J., & Scott, P. 2009, *ARA&A*, 47, 481
- Baines, K. H., Mickelson, M. E., Larson, L. E., & Ferguson, D. W. 1995, *Icarus*, 114, 328
- Benneke, B. 2015, arXiv:1504.07655
- Blum, J., & Wurm, G. 2008, *ARA&A*, 46, 21
- Blum, J. 2010, *Research in Astronomy and Astrophysics*, 10, 1199
- Boss, A. P. 1997, *Science*, 276, 1836
- Boss, A. P. 2011, *ApJ*, 731, 74
- Briggs, F. H., & Sackett, P. D. 1989, *Icar*, 80, 77
- Carr, J. S., & Najita, J. R. 2008, *Science*, 319, 1504
- Conrath, B. J., & Gautier, D. 2000, *Icar*, 144, 124
- Crida, A., Morbidelli, A., & Masset, F. 2006, *Icar*, 181, 587
- Dartois, E., Dutrey, A., & Guilloteau, S. 2003, *A&A*, 399, 773
- Drouart, A., Dubrulle, B., Gautier, D., & Robert, F. 1999, *Icar*, 140, 129
- Favre, C., Cleeves, L. I., Bergin, E. A., Qi, C., & Blake, G. A. 2013, *ApJL*, 776, L38
- Fletcher, L. N., Orton, G. S., Teanby, N. A., & Irwin, P. G. J. 2009, *Icar*, 202, 543
- Flynn, G. J., Bleuet, P., Borg, J., et al. 2006, *Science*, 314, 1731
- Fulle, M., Della Corte, V., Rotundi, A., et al. 2015, *Lunar and Planetary Science Conference*, 46, 2420

- Gautier, D., & Owen, T. 1989, *Origin and Evolution of Planetary and Satellite Atmospheres*, 487
- Guillot, T., Gautier, D., Chabrier, G., & Mosser, B. 1994, *Icar*, 112, 337
- Hernández, J., Hartmann, L., Megeath, T., et al. 2007, *ApJ*, 662, 1067
- Hersant, F., Wakelam, V., Dutrey, A., Guilloteau, S., & Herbst, E. 2009, *A&A*, 493, L49
- Hueso, R., & Guillot, T. 2005, *A&A*, 442, 703
- Jessberger, E. K., & Kissel, J. 1991, *IAU Colloq. 116: Comets in the post-Halley era*, 167, 1075
- Johansen, A., Oishi, J. S., Mac Low, M.-M., et al. 2007, *Natur*, 448, 1022
- Kley, W., & Nelson, R. P. 2012, *ARA&A*, 50, 211
- Lambrechts, M., & Johansen, A. 2012, *A&A*, 544, A32
- Lecante, J., & Chabrier, G. 2012, *A&A*, 540, A20
- Lewis, J. S., & Prinn, R. G. 1980, *ApJ*, 238, 357
- Lynden-Bell, D., & Pringle, J. E. 1974, *MNRAS*, 168, 603
- Madhusudhan, N., Harrington, J., Stevenson, K. B., et al. 2011a, *Natur*, 469, 64
- Madhusudhan, N. 2012, *ApJ*, 758, 36
- Madhusudhan, N., Crouzet, N., McCullough, P. R., Deming, D., & Hedges, C. 2014, *ApJL*, 791, L9
- Mahaffy, P. R., Niemann, H. B., Alpert, A., et al. 2000, *JGR*, 105, 15061
- Mandell, A. M., Bast, J., van Dishoeck, E. F., et al. 2012, *ApJ*, 747, 92
- Mayor, M., & Queloz, D. 1995, *Natur*, 378, 355
- Mousis, O., Gautier, D., Bockelée-Morvan, D., et al. 2000, *Icar*, 148, 513
- Mousis, O., Fletcher, L. N., Lebreton, J.-P., et al. 2014, *Planet. Space Sci.*, 104, 29
- Mumma, M. J., & Charnley, S. B. 2011, *ARA&A*, 49, 471
- Nayakshin, S., Helled, R., & Boley, A. C. 2014, *MNRAS*, 440, 3797
- Niemann, H. B., Atreya, S. K., Carignan, G. R., et al. 1998, *JGR*, 103, 22831
- Piétu, V., Dutrey, A., & Guilloteau, S. 2007, *A&A*, 467, 163

- Pollack, J. B., Hubickyj, O., Bodenheimer, P., et al. 1996, *Icar*, 124, 62
- Prinn, R. G., & Fegley, B., Jr. 1981, *ApJ*, 249, 308
- Prinn, R. G. 1993, *Protostars and Planets III*, 1005
- Qi, C., Öberg, K. I., Wilner, D. J., et al. 2013, *Science*, 341, 630
- Ros, K., & Johansen, A. 2013, *A&A*, 552, A137
- Rossi, L. Cardozo-Filho, & R. Guirardello 2009, *Fluid Phase Equilibria*, Volume 278, Issues 1–2, Pages 117-128
- Rubin, M., Altwegg, K., Balsiger, H., et al. 2015, *Science*, 348, 232
- Salyk, C., Pontoppidan, K. M., Blake, G. A., Najita, J. R., & Carr, J. S. 2011, *ApJ*, 731, 130
- Semenov, D., Wiebe, D., & Henning, T. 2006, *ApJL*, 647, L57
- Shakura, N. I., & Sunyaev, R. A. 1973, *A&A*, 24, 337
- Sharp, C. M., & Huebner, W. F. 1990, *ApJS*, 72, 417
- Singh, P. D., de Almeida, A. A., & Huebner, W. F. 1992, *AJ*, 104, 848
- Terquem, C., & Papaloizou, J. C. B. 2007, *ApJ*, 654, 1110
- von Zahn, U., Hunten, D. M., & Lehmacher, G. 1998, *JGR*, 103, 22815
- Weidenschilling, S. J. 1977, *MNRAS*, 180, 57
- White, W. B., Johnson, S. M., & Dantzig, G. B. 1958, *J. Chem. Phys.*, 28, 751
- Wong, M. H., Mahaffy, P. R., Atreya, S. K., Niemann, H. B., & Owen, T. C. 2004, *Icar*, 171, 153
- Wood, J. A. 2005, *Chondrites and the Protoplanetary Disk*, 341, 953
- Youdin, A. N., & Goodman, J. 2005, *ApJ*, 620, 459
- Young, R. E., Smith, M. A., & Sobek, C. K. 1996, *Science*, 272, 837
- Yung, Y. L., Drew, W. A., Pinto, J. P., & Friedl, R. R. 1988, *Icar*, 73, 516

Further reading & General references

Armitage, P. J. 2010, *Astrophysics of Planet Formation*, by Philip J. Armitage, pp. 294. ISBN 978-0-521-88745-8 (hardback). Cambridge, UK: Cambridge University Press, 2010.

Armitage, P. J. 2011, *ARA&A*, 49, 195

Benz, W., Ida, S., Alibert, Y., Lin, D., & Mordasini, C. 2014, *Protostars and Planets VI*, 691

Encrenaz, T., Bibring, J.-P., & Blanc, M. 1987, Paris : InterEditions : Editions du CNRS, c1987.

Helled, R., Bodenheimer, P., Podolak, M., et al. 2014, *Protostars and Planets VI*, 643

de Pater, I., & Lissauer, J. J. 2001, *Planetary Sciences*, by Imke de Pater and Jack J. Lissauer, pp. 544. ISBN 0521482194. Cambridge, UK: Cambridge University Press, December 2001.

Dutrey, A., Semenov, D., Chapillon, E., et al. 2014, *Protostars and Planets VI*, 317

Johansen, A., Blum, J., Tanaka, H., et al. 2014, *Protostars and Planets VI*, 547

Mordasini, C., Klahr, H., Alibert, Y., Benz, W., & Dittkrist, K.-M. 2010, arXiv:1012.5281

Pontoppidan, K. M., Salyk, C., Bergin, E. A., et al. 2014, *Protostars and Planets VI*, 363

Testi, L., Birnstiel, T., Ricci, L., et al. 2014, *Protostars and Planets VI*, 339

Youdin, A. N. 2010, *EAS Publications Series*, 41, 187

Chapter 2

A new volatile distribution model and application to WASP 12b

2.1 An introduction to exoplanets

2.1.1 Overview

The last decade of planetary sciences was characterized by the exoplanets revolution with the discovery of (to date) thousands of exoplanets orbiting host stars other than our own (see Winn & Fabrycky (2015) for a recent review). These exoplanets were discovered using three techniques:

1. Radial velocity, where planets are detected due to their gravitational influence on the host star's radial velocity with respect to Earth, as measured through the Doppler effect. This method allows to infer the mass of the perturbing planet, but is limited only to Jovian mass bodies orbiting very close to their host stars.
2. Transit photometry, where planets transiting their host star aligned with the line of sight of the observer will cause a slight dip in the star's photometric light curve. This method allow the determination of the planet's radius, and is the origin of my exoplanetary detections to date with the *Kepler* space observatory (Rowe et al., 2015).
3. Direct imaging through the use of coronagraphs to block the stellar light. This method was used to find giant planets orbiting unexpectedly far from their host stars.

Fig. 2.1 shows an up-to-date plot showing the masses of confirmed exoplanets as a function of their semi-major axis, in addition to their radii. Two main populations are interesting to consider. The first (mostly in orange) are the “Hot Jupiters” (hereafter HJs), namely the Jovian mass planets orbiting very close (semi-major axis less than 0.1 AU) to their host stars. This type of planets is surprisingly absent from our own solar system. They have very high atmospheric temperatures allowing to possibly constraint

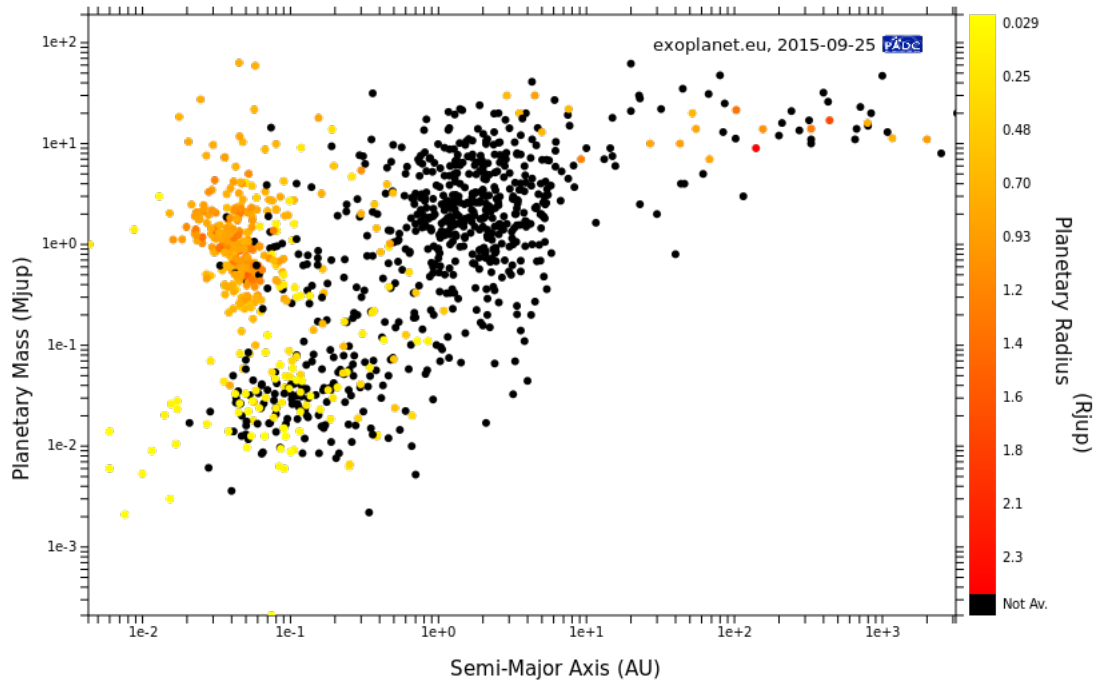


Figure 2.1: A graph showing the mass, radius, and semi-major axis of confirmed exoplanets to date.

their atmospheric compositions. The second interesting population (mostly in yellow) are the also hot Super-Earths and Mini-Neptunes. These planets planets with masses ranging from 2 to 10 Earths masses also on very closed in orbits. They seem to be very abundant in surveys, although also absent from our solar system.

2.1.2 WASP-12b’s atmospheric composition

The one major unmeasured elemental abundance in our solar system’s giant planets is Oxygen. This is due to water condensing at the relatively high temperature of 150 K, thus forbidding any tropospheric vapor phase measurements. In hot exo-Jupiters however, the tropospheric temperatures are much higher, permitting the detection of water and other C and O bearing volatiles (CO, CH₄, CO₂ and others). One of the first attempts of constraining the C/O ratio in a hot-Jupiter was by Madhusudhan et al. (2011) for WASP-12b. WASP-12b is a 1.4 M_J (Jovian mass) planet orbiting its host star at a distance of 0.023 AU. It is thus receives strong stellar radiation flux, in addition to the strong tidal heating also due to its proximity to the host star. These effects increase its dayside atmosphere’s temperature to more than 2500 K, forbidding the formation of a cold trap for water and allowing the possibility of measuring its bulk abundance, in addition to the

other volatiles. A statistical retrieval technique that combines a 1-D atmospheric model with a Markov-chain Monte Carlo sampler was used to compute thousands of models in order to explore the parameters (thermal-pressure profiles and chemical compositions) space and fit the 7 narrowband photometric thermal emissions observations (4 Spitzer space telescope and 3 ground based observations). The main results of Madhusudhan et al. (2011) (shown in Fig. 2.2) concluded a best fitting model for WASP 12b's atmosphere with $C/O \geq 1$ and $C/H = 2 \times 10^{-5} - 1 \times 10^{-3}$, to compare with the stellar host values of $C/O \sim 0.56$ and $C/H \sim 6 \times 10^{-4}$. This indicate that WASP 12b is poor in both oxygen and carbon with respect to the solar abundances.

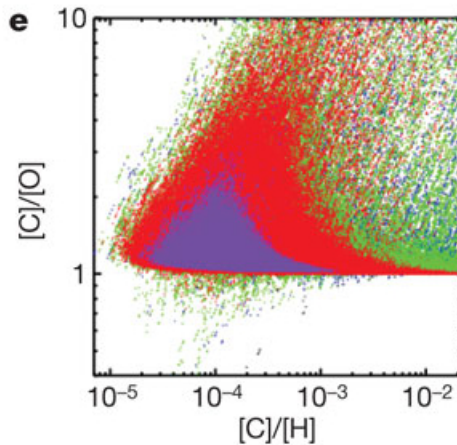


Figure 2.2: The C/O and C/H ratios in WASP 12b as constrained by Madhusudhan et al. (2011) using multi-band photometric observations and their statistical retrieval code. The purple, red, green, and blue, colored dots correspond to individual models with χ^2 less than 7, 14, 21, and 28, respectively. The most probable models (violet) hence favor a sub-solar C/H ratio and supersolar C/O ratio in WASP 12b's atmosphere.

2.2 The problematic of WASP 12b's formation

The observation of a super-solar C/O ratio along with a sub-solar C/H ratio in WASP 12b discussed in section 2.1.2 was unexpected for several reasons :

1- As discussed in section 1.3.1, all of the four giant planets in our own solar system are enriched in volatiles with respect to the solar value in what seems a systematics effect. These enrichments are considered a triumph for the core accretion model of planetary formation, since the alternative gravitational instability model predicted solar abundances for all elements. WASP 12b however seems to be poor in carbon, what necessitate an explanation since the formation models discussed in Chapter 1 are generic and should take place in any system, leading to solar or super-solar carbon abundance in the giant planets atmospheres. New formation channels are hence necessary to explain the carbon

depleted WASP 12b.

2- WASP 12b's higher than or equal to unity C/O ratio along with its low carbon abundance imply that it accreted less oxygen than carbon, which is not expected from the formation models discussed in section 1.3.1. The first two formation scenarios will both lead to oxygen enrichments, and the third can't avoid enriching the carbon abundance. A formation model is needed that allows for both elements (C and O) to be depleted, although carbon to a lesser degree in order to explain the measured C/O ratio.

These observations led me to the first question I will try to answer in this manuscript:

How do the C/H and O/H ratios vary with time/location in a protoplanet disk and what can they tell us about the formation of WASP 12b ?

In this chapter, I will start by discussing previous works on WASP 12b's formation, followed by an introduction to earlier relevant works I based my own approach on, to finally discuss the new model I elaborated to tackle the problem along with the results and perspectives.

2.3 The formation of WASP 12b in the literature

2.3.1 Clathrates formation models

One of the first attempts to explain the chemical composition of WASP 12b was by Madhusudhan et al. (2011). In this paper, the authors considered a statistical-thermodynamical model that calculates the compositions of WASP 12b's building blocks (shown in Fig. 2.3) through a formation sequence where these ices trap important amounts of volatile gases via clathration. This work concluded that WASP 12b's atmospheric C/O ratio is inconsistent with the host star's composition, even if enriched in heavy elements by icy planetesimals dissolved in the planet's envelope, and suggested that it may have been formed in an O-depleted part of the protoplanetary disk. This model moreover cannot account for the carbon depletion in WASP 12b's atmosphere.

2.3.2 Static formation models

Another model trying to explain the chemical composition of WASP 12b was by Öberg et al. (2011). These authors considered the very simple case of a completely static nebula with three C and O bearing volatiles: CO, H₂O, and CO₂ with the relative abundances of 1.5/0.9/0.3 (giving a solar C/O ratio). They assumed no volatiles transport or nebular evolution in their model, but only the total solid and gas phase compositions changes due to the presence of the different snowlines. Since these volatiles condense at different temperatures: 135 K, 45 K and 20 K respectively for water, CO₂ and CO as assumed by

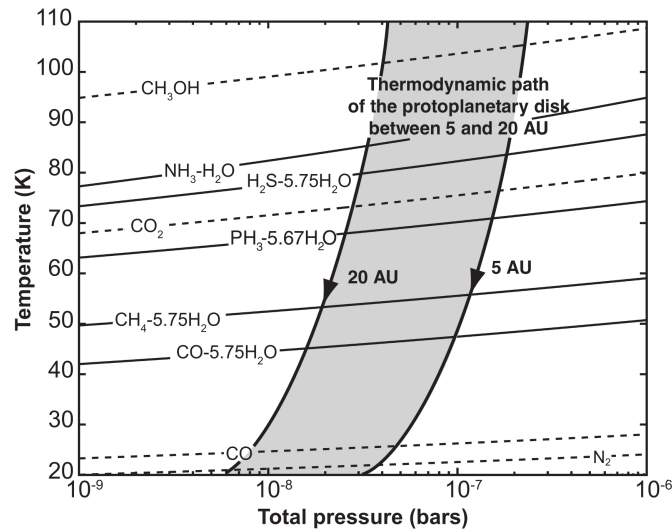


Figure 2.3: The chemical composition of the protoplanetary disk in the clathration model used by (Madhusudhan et al., 2011) as a function on temperature and pressure.

the authors, the chemical composition of the separate gas and solids phases will depend on the location in the disk. Their results are presented in Fig. 2.4 showing the dependence of the gas and solid phases C/O ratio on the location. This model allow the formation of a giant planet with a C/O ratio in the order of unity through the accretion of gas between the CO and CO_2 icelines, where the C/O ratio in the gas phase is 1. The problem with this model is twofold. First, it does not explain the sub-solar carbon abundance in WASP 12b, since this model lead to a near solar C/H ratio. Second, it neglected the dynamical and thermodynamic processes like gas drag, vapor diffusion and ices sublimation that may affect the abundances of volatiles in protoplanetary disks. However, this model showed the importance of considering different chemical elements along with their respective ice-lines, an aspect that was incorporated in the model I developed.

2.4 Water distribution models

Motivated by the shortcomings of the previous scenarios, I decided to elaborate a new model that takes into account the multi-volatiles approach of Öberg et al. (2011), but also incorporates dynamical elements affecting the distribution of volatiles in the disk. This dynamical aspect of the model is based on previous works presented in this section.

2.4.1 The cold finger effect

The water distribution in the solar nebula have always been the subject of intense research due to its significant role in planets formation.

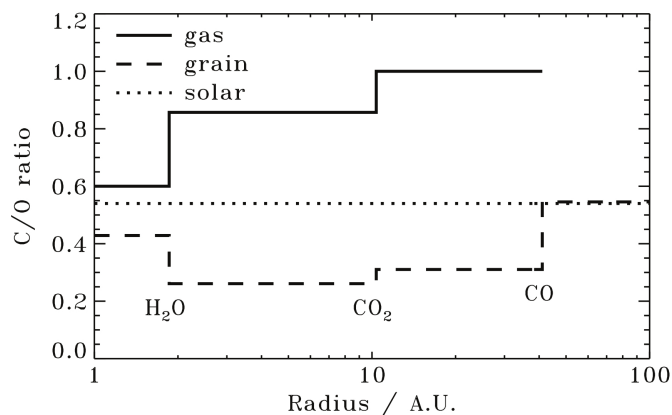


Figure 2.4: The static C and O bearing elements distribution model of (Öberg et al., 2011), along with the inferred gas and solid phase C/O ratio.

A significant early study is Stevenson & Lunine (1988), introducing the so called “cold finger effect”. These authors considered the simple but robust situation of a turbulent disk with a water snowline. Inside of the snowline, by definition, water is only in vapor form, while outside of it, water is present only as ice. A sharp vapor concentration gradient is thus present at the snowline’s position. Due to turbulence, this vapor will diffuse following its concentration gradient till it crosses the snowline and condenses into ices. Gradually over time (timescales around 10^5 yr), this effect will deplete the water vapor inside of the snowline and will increase the ices density in the 0.5 AU just beyond it as shown in Fig. 2.5. The authors hence proposed that Jupiter could have formed on this ices density peak.

2.4.2 vapor replenishment

A major aspect of the picture ignored by Stevenson & Lunine (1988) was the ices feedback. These authors assumed the ices to remain immobile in place beyond the water snowline, and did not study their subsequent evolution. This was later done by Cyr et al. (1998) (C98) who considered the entire water-ice cycle. In this model, in addition to the vapor outward diffusion, the authors considered the ices inward movement due to gas drag, in addition to their sublimation. Ices can hence drift inward and sublimate, resupplying the outward diffusing vapor. This cyclic model is illustrated in Fig. 2.6. This work concluded that according to the considered nebular model, and assuming that most of the ices are in the fastest moving sizes (10-100 cm), different patterns of vapor depletion and enrichment as a function of time and distance can exist. The general trend they found though is that the outward diffusion is faster than the inward replenishment, leading to a depleted inner nebula and an enhanced C/O ratio assuming a constant carbon abundance inside of the snowline.

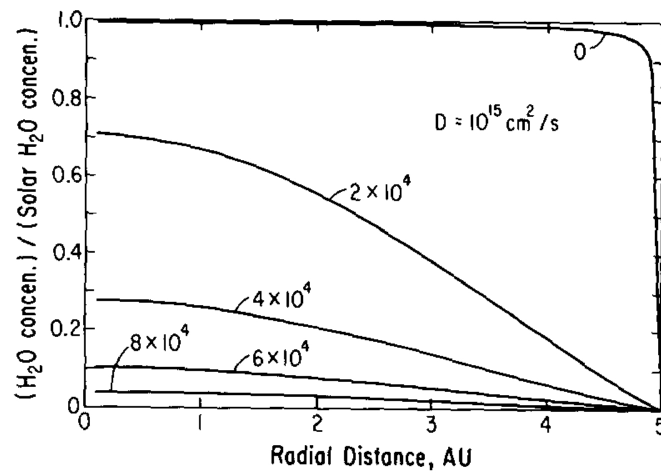


Figure 2.5: The water vapor concentration evolution inside the snowline as a function of time (in years) in the model of Stevenson & Lunine (1988). The gradual depletion is caused by the outward diffusion of the vapor.

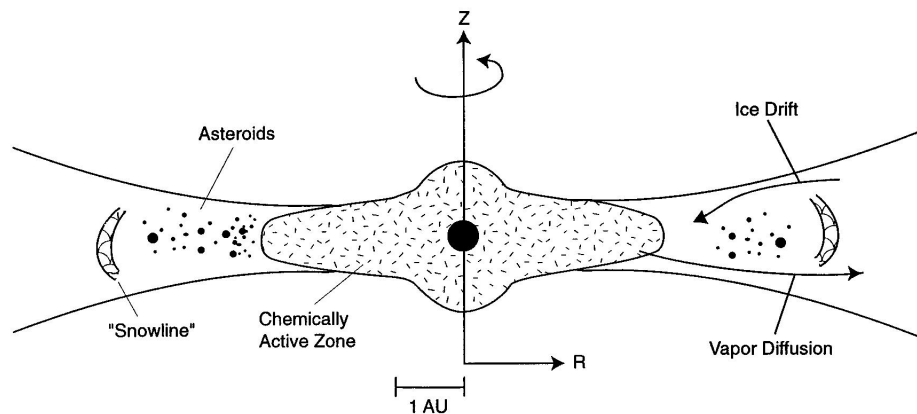


Figure 2.6: The water distribution cycle from Cyr et al. (1998).

2.4.3 Modern models

A more modern and sophisticated water distribution model was presented by Ciesla & Cuzzi (2006) who considered water vapor and solids in a 3 size distribution (dust, migrators and planetesimals). The model then tracked the concentration evolution of each bin through a fully dynamical model incorporating a large number of processes that C89 ignored such as accretion, coagulation, collisional destruction etc. The goal of the model was to obtain a detailed description of the distribution of water, and the authors

concluded that a large variety of possible depletions and enhancements patterns can exist for the vapor and all of the solids sizes, also according to the disk properties. Due to the complexity of the model and the large number of elements incorporated in it however, a single simulation took between 1000 and 3000 computer hours in parallel on the 2 SGI Origins clusters at NASA Ames and Goddard.

2.5 Published article summary

The first goal of this thesis (tackled in the following article) is to explain the C/O and C/H ratios in WASP 12b. For this reason, I chose to construct a simple model inspired by C98, but while considering both water and CO. The objective was not to have a complete picture of volatiles evolution, but a more basic understanding of how do carbon and oxygen bearing species behavior differ and how does it affect the C/O ratio. This model, at heart, should hence be interpreted more as a chemical model, not a complete volatiles distribution model such as Ciesla & Cuzzi (2006).

All of the three models discussed above show that water vapor depletion inside of its snowline is possible under certain conditions. If we naively suppose the carbon vapor phase to be constant through time and location, this will naturally enhance the C/O ratio inside the water snowline. However, the same physical processing affecting water should also affect carbon. For this reason, my approach was to build a modernized model analogues to C98 but taking into account both water and CO. Instead of the Cassen (1994) disk model used by C98, I used the newer model of Hueso & Guillot (2005). I also used a more sophisticated gas drag formalism taking into account the nebular turbulence, while C98 considered the classical drag in a laminar disk. Another important difference is the use of a bimodal dust-pebbles particles size distribution, instead of the size spectrum with metric particles used by C98. This is motivated by the recent results highlighting the importance of pebbles in planets formation and showing how do large kilometric bodies form directly through the gravitational collapse of pebbles. I used the same vapor diffusion law as C98, and assumed the vapor condensation into dust once it crossed the snowline to be instantaneous, and that this dust is coupled to an outward advective nebula stopping it from diffusing inward in dust form. I finally implemented typical sublimation and dust coagulation (assuming a constant dust surface density) routines into the model. The used numerical methods are discussed in Appendix A.

The model will calculate first the total vapor replenishment timescale by evaluating the total time needed for a dust particle to grow into a pebble, drift inward and sublimate. The replenishment timescale and pebbles sublimation locations are then inputed as a source function into the vapor diffusion module that is evolved with time. For a typical protosolar like disk with standard parameters ($\alpha = 10^{-2}$, $\Sigma_{dust} = 1 \text{ g cm}^{-2}$, $t_{coag}^{1AU} = 10^3 \text{ yr}$, water iceline at 3.8 AU and CO snowline at 30 AU), my model shows that the outward vapor diffusion is faster than the inward replenishment for both water and CO, leading to vapor depletion inside of both icelines. However, the gradual CO depletion takes place

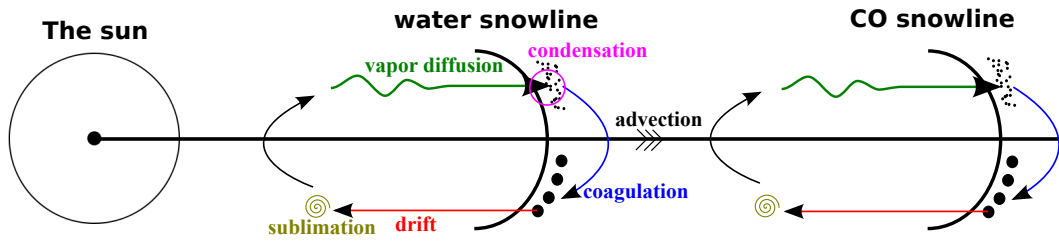


Figure 2.7: A sketch for our water and CO transport model showing the main ingredients.

on a longer timescale (by an order of magnitude) than water. This is due to the diffusive timescale dependency on the diffusion length scale: $t_{diff} \propto r_{diff}^2$ where r_{diff} is the sun-iceline distance. The main conclusion of this work is that vapor CO will dominate the nebula inside of the water's snowline as the sole carbon and oxygen bearing elements for most of the disk's lifetime, enhancing the C/O ratio to about unity in this region. Any planet (WASP 12b) accreting its envelope inside of the water's iceline will have a near unity C/O ratio, regardless of the disk's initial C/O ratio. Moreover, since even CO is depleted with respect to its nominal value, the bulk carbon budget in the planet will be subsolar, explaining the low carbon abundance in WASP 12b. The nominal scenario I propose is the planet's core formation outside of the water's snowline, then its envelope accretion during its migrating inside of the snowline (assuming a decoupled core-envelope).

2.6 Published article

CARBON-RICH PLANET FORMATION IN A SOLAR COMPOSITION DISK

MOHAMAD ALI-DIB¹, OLIVIER MOUSIS¹, JEAN-MARC PETIT¹, AND JONATHAN I. LUNINE²

¹ Université de Franche-Comté, Institut UTINAM, CNRS/INSU, UMR 6213, Observatoire de Besançon, BP 1615,
F-25010 Besançon Cedex, France; mdib@obs-besancon.fr

² Center for Radiophysics and Space Research, Space Sciences Building, Cornell University, Ithaca, NY 14853, USA

Received 2013 November 26; accepted 2014 February 20; published 2014 April 3

ABSTRACT

The C to O ratio is a crucial determinant of the chemical properties of planets. The recent observation of WASP 12b, a giant planet with a C/O value larger than that estimated for its host star, poses a conundrum for understanding the origin of this elemental ratio in any given planetary system. In this paper, we propose a mechanism for enhancing the value of C/O in the disk through the transport and distribution of volatiles. We construct a model that computes the abundances of major C- and O-bearing volatiles under the influence of gas drag, sublimation, vapor diffusion, condensation, and coagulation in a multi-iceline 1+1D protoplanetary disk. We find a gradual depletion in water and carbon monoxide vapors inside the water's iceline, with carbon monoxide depleting slower than water. This effect increases the gaseous C/O and decreases the C/H ratio in this region to values similar to those found in WASP 12b's day side atmosphere. Giant planets whose envelopes were accreted inside the water's iceline should then display C/O values larger than those of their parent stars, making them members of the class of so-called carbon-rich planets.

Key words: planets and satellites: atmospheres – planets and satellites: composition – planets and satellites: formation – protoplanetary disks

1. INTRODUCTION

The C/O ratio is a key parameter for the chemical composition and evolution of the atmospheres of giant planets since it controls the relative abundances of C- and O-bearing species. Studies suggest that at equilibrium, as the C/O ratio increases (≥ 0.8) in the gas phase, all the available O goes into organics, CO, CO₂ and CH₃OH, so that the gas phase becomes H₂O-free and the remaining C is in the form of CH₄ (Fortney et al. 2010; Madhusudhan et al. 2011b). The CO/CH₄/CO₂ ratios in planetary atmospheres are also affected by the possible existence of non-equilibrium chemistry effects due to dynamical mixing and photochemistry (Venot et al. 2012). The C/O ratio is also crucial for understanding the chemical evolution of protoplanetary disks (Cyr et al. 1999; Prinn 1993).

Based on comparisons between a grid of model predictions and six narrowband photometry points for the dayside atmosphere of the hot Jupiter (HJ) WASP 12b, Madhusudhan et al. (2011a) found a best fitting model of $C/O \geq 1$ and $C/H = 2 \times 10^{-5} - 1 \times 10^{-3}$, to compare with the stellar host values of $C/O \sim 0.56$ and $C/H \sim 6 \times 10^{-4}$. These authors concluded that WASP 12b probably has a superstellar C/O but with a substellar C/H ratio. Because giant planets are expected to have stellar or superstellar metallicities (Kuchner & Seager 2005), new formation models consistent with the properties of WASP 12b have been proposed. For instance, Öberg et al. (2011) considered the H₂O, CO, and CO₂ snowlines in a protoplanetary disk model, and found an increase of the gaseous C/O ratio (compared to the C/O ratio of the stellar host) in the disk regions boxed by these snowlines, even reaching ~ 1 between the CO and CO₂ snowlines. They proposed that WASP 12b might have accreted its gaseous envelope in this area but they neglected the dynamical and thermodynamic processes like gas drag, diffusion, and sublimation that may affect the abundances of volatiles in protoplanetary disks. On the other hand, Madhusudhan et al. (2011b) have shown that WASP 12b's atmospheric C/O is inconsistent with an atmosphere of the host star's composition, even if en-

riched in heavy elements by icy planetesimals dissolved in the planet's envelope, and suggest that it may have been formed in an O-depleted part of the protoplanetary disk.

Here, we present a fully dynamical and multi-snowline model describing the transport and distribution of C and O bearing volatiles in protoplanetary disks, which is inspired by the original idea of Cyr et al. (1998). The model is used to compute the C/O ratio as a function of the radial distance in order to constrain the possible formation locations of carbon-rich HJs.³ In Section 2 we present the different components of our model. Our results are presented in Section 3. In Section 4 we discuss the implications and predictions of our model for the formation of carbon-rich HJs, and in particular for WASP 12b.

2. MODEL PRESCRIPTION

Here we describe the processes that affect the distribution of volatile abundances in protoplanetary disks. In our approach, we assume that H₂O and CO are the main C- and O-bearing species. We track their respective evolutions near their snowlines, due to multiple effects described below.

2.1. The Protoplanetary Disk

The backbone of our model is the protoplanetary disk model of Hueso & Guillot (2005) and Guillot & Hueso (2006). This is a standard one-dimensional α -viscosity disk model, where the viscosity is assumed to be generated by turbulence characterized by the free parameter α according to the formalism of Shakura & Sunyaev (1973):

$$\nu = \alpha C_s H. \quad (1)$$

This model follows Beckwith et al. (1990) in the (gas+dust) opacity expression and Ruden & Pollack (1991) in the expressions of the isothermal sound speed C_s , and the mid-plane density ρ_c . The authors also take into account the disk's self-gravity

³ In this manuscript, "carbon-rich" refers to high C/O ratio, regardless of the C/H value.

in calculating the scale height H . The temperature is calculated by assuming a geometrically thin disk heated by both star illumination and the dissipation of viscous energy. The disk is supposed to be optically thick in the radial direction, but the heat can be transported efficiently vertically.

Finally, we chose to use the mean gas radial velocity obtained by Hughes & Armitage (2010) from their 1+1D α -disk model. In 1+1D and two-dimensional models, in contrast with one-dimensional models, the mean advective gas flow experienced by solid particles in the midplane is outward, but the vertically integrated movement is inward as a result of accretion. In all simulations, we used the disk properties obtained from Hueso & Guillot (2005) using their inward gas velocity, but imposed the outward velocity from Hughes & Armitage (2010) in the solid tracking modules only.

2.2. The Evolution of Solids

Three important processes affecting solids are incorporated into our model: advection due to solid–gas interaction, sublimation, and coagulation. The behavior of solids in protoplanetary disks depend strongly on their size (Weidenschilling 1977). Small submillimetric particles will remain almost completely coupled to this gas and *advent* outward along with it, although at a slightly lower velocity due to residual gravity. Large particles on the other hand will feel the gas “headwind” and get decoupled, drifting inward. This motion is called the gas drag. The exact decoupling size is derived from our model. We model this transport using the approach of Stepinski & Valageas (1996) which incorporates analytically the effects of the disk’s turbulence into the gas drag originally predicted by Weidenschilling (1977). Stepinski & Valageas (1996) modeled turbulence by dividing the density and velocity of the particles into mean and fluctuating parts. The gas turbulent velocity is introduced through the Schmidt number⁴ used explicitly to express the correlation terms between the mean radial and transverse solids velocities. In the presence of turbulence, the solids will diffuse due to the collective action of turbulent eddies advecting particles in all directions, resulting in additional “pressure” and “viscosity” terms in the expression determining the mean radial velocity of the solids. In our model the gas turbulent velocity is calculated self-consistently in the Hueso & Guillot (2005) framework of the overall disk model. The relative radial and transverse solids velocities are finally expressed following Equations (15) and (16) of Stepinski & Valageas (1996):

$$2\overline{v_\phi} - \frac{\overline{v_r}}{\Omega_k t_{s*}} = -\frac{1}{\overline{\rho}} \frac{\partial \overline{P}}{\partial r} \frac{1}{\Omega_k} \quad (2)$$

$$2\overline{v_r} + \frac{\overline{v_\phi}}{\Omega_k t_{s*}} = -\overline{V_r} - 3r^{-1/2} \frac{\partial}{\partial r} \left(r^{1/2} \frac{v}{\text{Sc}} \right) + \frac{(D - 3v)}{\text{Sc}} \frac{1}{\overline{\rho_d}} \frac{\partial \overline{\rho_d}}{\partial r}, \quad (3)$$

where \overline{P} and $\overline{\rho}$ are the gas mean pressure and density, Ω_k is the Keplerian frequency, $\overline{v_\phi}$ is the mean relative transverse velocity between particles and gas, $\overline{v_r}$ the mean relative radial velocity, $\overline{V_r}$ the mean gas radial velocity (from Hughes & Armitage 2010), t_{s*} the stopping time of the particle, Sc the Schmidt number, D the diffusion coefficient, r the heliocentric distance, and $\overline{\rho_d}$ the global solid particles density. For numerical

⁴ The ratio of the viscous to mass diffusion rates.

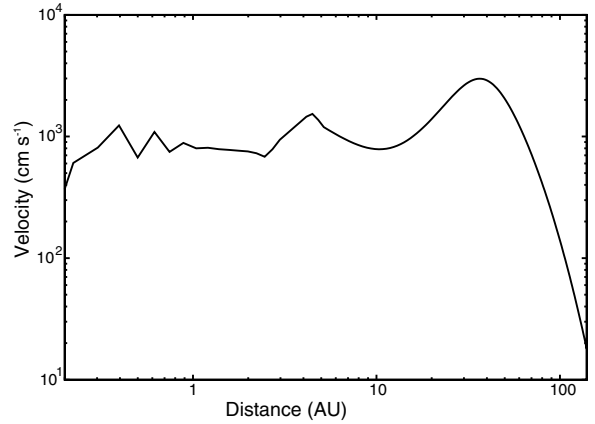


Figure 1. Mean absolute radial velocity of decimetric pebbles as a function of distance. Although this velocity explicitly depends on the particle’s density, no significant difference has been found between H₂O and CO ices. Particles placed at 28 AU (CO pebbles) are faster than those at 3.8 AU (H₂O) due to the non-linear propagation of gas density in the equations. The movement direction is always inward. This is equivalent to and reproduces the major aspects of Figure 2 (third panel) of Stepinski & Valageas (1996).

simplicity, we follow Stepinski & Valageas (1996) in choosing $D = 3v$, a value consistent with more detailed numerical values of D (Canuto & Battaglia 1988), and which cancels the third term in the second equation. The presence of a strong vertical magnetic field though might affect the value of D (Johansen et al. 2006). These equations are coupled to the disk model and are solved using a globally convergent Newton method (Press et al. 1992). This module replicated successfully the results of Stepinski & Valageas (1996) within a small factor probably due to the different disk models used. The results of this module are presented in Figure 1. Our model assumes that the particles have settled in the midplane, where they feel the outwardly moving gas. A solid particle will settle if its dimensionless Stokes number⁵ is larger than α . We follow Birnstiel et al. (2010) in expressing this parameter as:

$$St = \frac{\rho_s R \pi}{\Sigma_g 2} \quad (4)$$

with ρ_s the single solid particle’s density, R its radius, and Σ_g the gas surface density. In the case of our decimetric pebbles, we obtain $St \sim 0.1$ and 0.7 , respectively, for H₂O and CO particles at the locations of their snowlines. These values are one order of magnitude higher than the viscosity parameter used in our calculations ($\alpha = 10^{-2}$), implying that our assumption of settled particles is valid.

Sublimation modeling is based on the simplified approach of Supulver & Lin (2000). We ignore the condensation of gas on the particle since it is assumed to be minimal in the inner hot regions. We finally write the theoretical maximum sublimation rate of a particle ($\text{g cm}^{-2} \text{s}^{-1}$) as

$$\chi_{s,\text{max}} = -\sqrt{m/(2\pi kT)} P_p \quad (5)$$

and derive the particle’s radius decrease rate (cm s^{-1}) in the form

$$\frac{dR}{dt} = -\frac{0.63 \times v_s P_p}{\sqrt{2} \times \pi m k T}, \quad (6)$$

⁵ Defined as the ratio between the stopping and eddy turnover times.

where P_p is the equilibrium vapor pressure on a flat surface for H₂O (Haynes et al. 1992)⁶ or CO (Goodwin 1985),⁷ v_s is the volume of single molecules, k the Boltzmann constant, m is the particle's mass, and T is its surface temperature. We multiply the sublimation rate by 0.63 following the experimental results of Haynes et al. (1992).

We model the dust coagulation into larger particles following Ciesla & Cuzzi (2006; Equation (26)):

$$\Delta\Sigma^{\text{coag}} = \Sigma_d(1 - \exp^{-\Delta t/t_{\text{coag}}^r}) \quad (7)$$

with

$$t_{\text{coag}}^r = t_{\text{coag}}^{1\text{AU}} \times \frac{\Omega(1\text{ AU})}{\Omega(r)} \quad (8)$$

where Σ_d is the dust surface density, $\Omega(r)$ is the Keplerian angular rotation velocity at distance r and t_{coag}^r is the average timescale for larger bodies (in this case decimetric pebbles) to grow from the local dust supply at distance r . We choose $t_{\text{coag}}^{1\text{AU}} = 10^3$ yr, which is the lowest value considered by Ciesla & Cuzzi (2006) and others since we do not grow our particles all the way to meter scale in this work. The solids in fact are not allowed to grow larger than 10 cm, since most of the solid mass density in disks is supposed to be in pebbles of this size scale (Lambrechts & Johansen 2012). We also choose $\Sigma_d = 1$ g cm⁻², an average value obtained at $t = 10^5$ yr in seven runs made by Ciesla & Cuzzi (2006), as the average dust surface density at both snowlines since we were not able to find any detailed modeling of this quantity in cases relevant to our model. It is assumed to be constant with respect to time; modeling the expected individual evolutionary trajectories of the surface densities of dust and pebbles is a substantial numerical undertaking beyond the scope of this work.

2.3. The Evolution of Vapors

Two processes affecting volatile vapors are included: vapor diffusion and condensation into solid dust. Any existing volatile vapor is coupled to the H₂ gas, advecting along with it but diffusing according to its own gradient. The diffusion is modeled following the approach depicted in Stevenson & Lunine (1988), Cyr et al. (1998) and others:

$$\frac{\delta c}{\delta t} - \frac{2D}{r} \frac{\delta c}{\delta r} - D \frac{\delta^2 c}{\delta r^2} + S(r, t) = 0, \quad (9)$$

where c is the vapor concentration ($c = 1$ for stellar abundance) and $S(r, t)$ is the source function due to replenishment. This equation is solved and evolved using the explicit Forward Time-Centered Space method (Press et al. 1992). Once the vapor attains a low enough temperature (160 K for H₂O, 25 K for CO), it condenses into solid ice. We assume that the vapor, following the cold finger effect, condenses instantaneously and completely either on existing submillimetric dust or directly as pure ice, leading in both cases to the formation of typical 10⁻² cm sized dust particles. This sets a boundary condition for Equation (9) of $c = 0$ for the vapor concentration at the iceline's positions. The particles are then advected outward along with the gas while coagulating into the pebbles that will later replenish the vapor. This concentration of dust at the snowline position might induce an additional diffusive motion. This could result

in an extra source term just interior to the snowline. This effect is neglected in the following and will be discussed in Section 4.

The diffusion of the vapors described by Equation (9) is key to our results. It describes the evolution of both H₂O and CO vapors in addition to H₂ gas. Any difference in the behavior of the different gases in the nebula is due to the boundary conditions used to solve this equation. Physically this translates into the presence of snowlines at different locations. In the presence of turbulent diffusion, the behavior of the various gases is different due to the presence (or absence), and location, of their snowlines. The flux of the vapor is dominated by the turbulent diffusion. The presence of a snowline will induce a concentration gradient resulting in an outwardly directed vapor flux. In the absence of replenishment, the region inside the snowline will become depleted on a timescale $t_{\text{diff}} = r^2/D$, where r is the diffusion distance (up to the snowline, if present). This implies different diffusion timescales for H₂O and CO and thus relative depletion between the two species. In the case of the nebular H₂ gas for which no snowline is present, r in the above equation is the centrifugal radius R_c .⁸ Using Equation (8) from Hueso & Guillot (2005), we find $R_c \sim 178$ AU in the case of our disk model.⁹

For a CO snowline located at 28 AU, we find $t_{\text{diff}}^{\text{H}_2} \sim 40 \times t_{\text{diff}}^{\text{CO}}$, implying that the H₂ diffusive timescale is much longer than that of any condensing species considered in our model. This allows us to use a stationary disk model for the rest of our calculations and decouples the evolution of volatile vapors from that of the nebular gas. This permits our model to track directly the concentrations (defined as the ratio of the vapor to H₂ gas surface density) instead of the vapor surface density.

For a more realistic modeling, one has to add replenishment to the model discussed above, as initially proposed by Stevenson & Lunine (1988). The replenishment is mainly caused by the inward drift and sublimation of the particles created from the condensation of gas into dust at the snowline, and the dust's subsequent coagulation into larger particles. A simple model including this effect was elaborated by Cyr et al. (1998). In our model, these replenishing particles are assumed to be entirely in the form of decimetric pebbles. In the presence of a permanent sink term like a static kilometric planetesimal (Cuzzi & Zahnle 2004; Ciesla & Cuzzi 2006), the vapor is always depleted no matter what may be the replenishment speed. In the absence of a permanent sink, the replenishment rate is crucial to the results. Fast replenishment will cause an enrichment of the vapor abundance inside the snowline, while slow replenishment will still result in vapor depletion. In our model the replenishment rate is defined as $S(r, t) = c_{\text{rep}}/t_{\text{rep}}$ where c_{rep} is the total concentration of the replenishing material present at the snowline position as a function of time, and t_{rep} is the longest time duration between the coagulation and sublimation timescales, which is the factor that controls the replenishment speed. We neglect the time an inward pebble needs after its formation is complete in order to reach the snowline since it is too short compared to the other considered timescales. Vapor depletion will only result if t_{rep} is sufficiently long. The main goal of our model is to calculate accurate replenishment rates to track the concentrations of volatiles inside and at their snowlines.

⁶ $P_p = 1.013 \times 10^6 \exp(-5940/T_p + 15.6)$ dyn cm⁻².

⁷ <http://www.nist.gov/data/PDFfiles/jpcrd281.pdf>

⁸ The radial limit in the disk where the gas stops getting accreted inward and start dispersing outward.

⁹ Using the parameters detailed in Section 3.

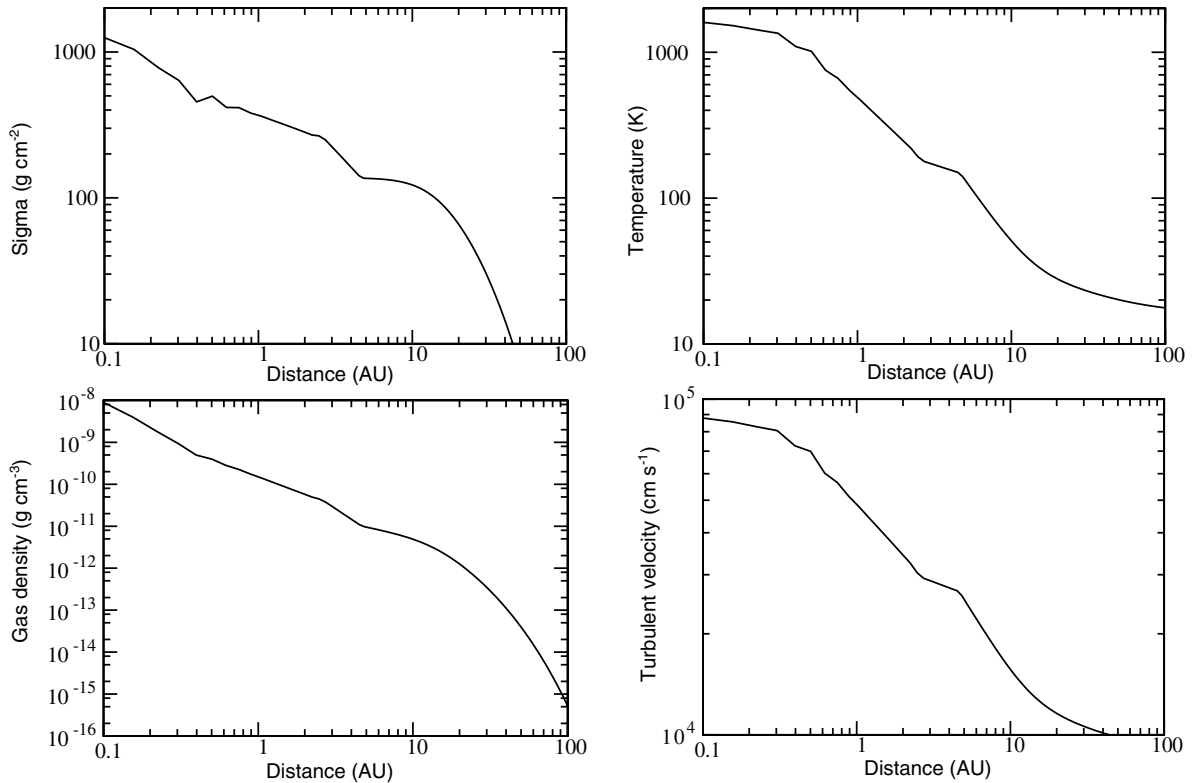


Figure 2. Surface density (top left), temperature (top right), density (bottom left), and turbulent velocity (bottom right) profiles in the midplane of the employed disk model.

3. RESULTS

A typical simulation starts with a decimetric pebble (H_2O or CO) near its corresponding snowline. This particle is large enough to be decoupled from the gas. It will drift inward at the velocity determined by the transport module and will start sublimating. The time needed for sublimation and the distance traveled before it happens are calculated by the sublimation module. These values are communicated to the vapor diffusion module through the source function. The diffusion module then evolves the vapor concentration inside the snowline. The removed vapor will condense instantaneously at the snowline into 0.1 mm sized dust. This dust, coupled to the gas, will start diffusing outward while coagulating into 10 cm sized pebbles, where it will get decoupled and start drifting inward, repeating the cycle.

For the rest of this work, we will use the disk properties at 10^5 yr. The disk is supposed to be stationary since modeling the temporal migration of snowlines requires detailed modeling of the accumulated ices present beyond them, which is beyond the scope of this work. The implication of this assumption on the results should be minimal since the planetary formation timescale is thought to be shorter than the disk evolution timescale (Lissauer et al. 2009).

The initial conditions of the disk model are $\alpha = 0.01$ (same value used by Hughes & Armitage 2010), $M_{\text{cloud}} = 1 M_{\odot}$, $\Omega_{\text{cloud}} = 3.0 \times 10^{-14} \text{ s}^{-1}$, $T_{\text{cloud}} = 10 \text{ K}$, $M_{0,\text{star}} = 0.1 M_{\odot}$, and $T_{\text{star}} = 4000 \text{ K}$. At 10^5 yr, this leads to a star and disk system with respective masses of 0.7 and $0.015 M_{\odot}$, although

our system continues to evolve and converges rapidly toward 1 and $0.02 M_{\odot}$. The disk properties obtained are typical for protoplanetary disks (Hueso & Guillot 2005) and give gas surface densities compatible with results reported by Hughes & Armitage (2010). The disk surface density, temperature, turbulent velocity, and density profiles we use are given in Figure 2. Water vapor condenses into crystalline ice at $\sim 160 \text{ K}$, and the CO condensation temperature is $\sim 25 \text{ K}$ (Lide 2002). This places the H_2O and CO snowlines in our disk model at 3.8 AU and 28 AU, respectively. The location of the CO snowline in our model is comparable to that recently inferred at $\sim 30 \text{ AU}$ in TW Hya (Qi et al. 2013). We assume an initial homogeneous disk C/O ratio of solar value ~ 0.55 (Asplund et al. 2009).

Table 1 shows the results from the transport, sublimation, and coagulation modules. For H_2O solids near the snowline, millimeter-sized particles and smaller move outward while particles equal to and larger than 1 cm move inward. The decoupling size for H_2O particles (where they change direction) is between those two values. Ten centimeter-sized pebbles will drift inward for $\sim 1.0 \times 10^3$ yr before sublimation, crossing a distance of $\sim 2.8 \text{ AU}$. This contradicts the results of Ciesla & Cuzzi (2006) who reported inward traveling distances for particles of no more than a few tenths AU. This difference might be attributed to the different velocity profiles, disk models, and parameters used (Ciesla & Cuzzi 2006 used larger α values). Due to the use of an exponential law for depicting its rate, the sublimation occurs almost at the very end of the particle's inward travel. The vapor concentration is thus enhanced in a narrow region both for H_2O and CO . On the other hand, 10^{-2} cm sized

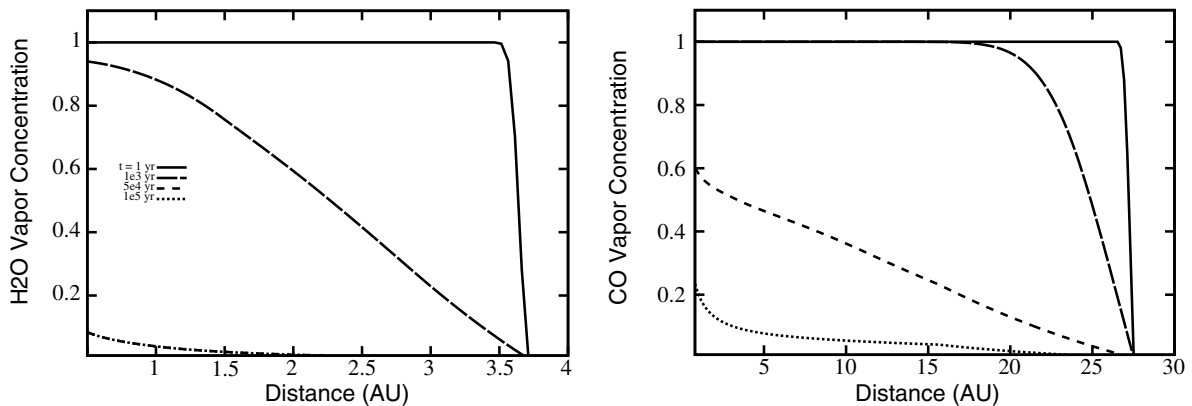


Figure 3. Vapor concentrations of H₂O (left panel) and CO (right panel) inside their respective icelines as a function of time and distance to the star. In both cases there is a gradual depletion in the concentration due to diffusion being faster than replenishment. CO depletion is much slower than H₂O, leading to a CO-dominated inner nebula. H₂O is depleted in 10^4 yr (not shown), and CO in 10^5 yr.

Table 1
Velocity, Evolution Time, and Distance for Chosen Solid Sizes as Found by Our Model

Size (cm)	H ₂ O			CO		
	Velocity (cm s ⁻¹)	Δt (years)	ΔR (AU)	Velocity (cm s ⁻¹)	Δt (years)	ΔR (AU)
10^{-2}	+38.5	2.2×10^4	+1.78	+34.8	2.2×10^4	+1.61
10^{-1}	+25.3	2.2×10^4	+1.17	-11.0	5.9×10^5	-14.1
1	-106.0	1.1×10^4	-2.4	-469.6	1.8×10^4	-18.0
10	-1370.3	1.0×10^3	-2.8	-2647.5	3.5×10^3	-19.7

Notes. Positive and negative velocities mean outward and inward drifts, respectively. Δt is the time taken by 1–10 cm particles to drift from their starting positions until sublimation and for 10^{-2} – 10^{-1} cm gas-coupled dust to coagulate into pebbles (in this case $\Delta t \equiv t_{\text{coag}}^+$). ΔR is the distance traveled by inwardly drifting particles from their iceline to their sublimation location. The particles are placed initially on their iceline.

dust will advect outward and coagulate with other particles for 2.2×10^4 yr before reaching pebble size. Although this seems to correspond to a traveled distance of ~ 1.6 AU, the real traveled distance should be shorter, since the particle will stop advecting outward once it reached the decoupling size.

In the case of CO, the decoupling size of particles is between 10^{-2} and 10^{-1} cm. Decimetric pebbles will move inward for 3.5×10^3 yr before sublimating, corresponding to a travel distance of 19.7 AU from their starting position. Coupled 10^{-2} cm CO particles also need 2.2×10^4 yr in order to coagulate into pebbles, the same timescale as for H₂O particles, since our approach is species independent and that dust surface densities are assumed equal near both icelines.

In the case of H₂O, the sublimation timescale of decimetric pebbles is close to the coagulation timescale of 10^{-2} cm dust (into pebbles), with the latter slightly longer than the former. In the case of CO, the timescale for the sublimation of pebbles timescale is much shorter than the dust coagulation timescale. For these reasons, in both cases the replenishment rate is limited by the dust coagulation time ($\sim 2.2 \times 10^4$ yr), with CO being more sensitive to this parameter than H₂O due to its smaller sublimation timescale.

The evolution of the vapor concentrations is presented in Figure 3. In both cases, the vapor diffusion is much faster than replenishment. The replenishment rate is not enough to counter the effect of diffusion, due to the long coagulation timescales limiting this rate. These long timescales act as a temporary sink term that significantly slows down the replenishment. This leads to a gradual depletion in vapor concentration inside the

iceline, analogous to the depletion reported by Cyr et al. (1998), although faster and with lower vapor concentrations due to the different models used. This depletion is compensated by an increase in the solids surface density near the iceline itself. The comparison of the two panels of Figure 3 shows that the vapor depletion is much faster for H₂O than for CO. This is caused by the CO iceline that is much farther out than H₂O’s iceline, giving CO vapor a longer distance to travel before condensation. The H₂O vapor concentration profile reaches a quasi-depleted stationary state in 2×10^4 yr. This is faster than the “no radial drift” case in Cyr et al. (1998), which is mainly due to our closer snowline and higher D . This relatively short diffusive timescale for H₂O supports our assumption of a stationary nebula, since the disk’s gas evolves over a 10^5 – 10^6 yr timescale (Hueso & Guillot 2005). Finally, our model was able to reproduce some of the results of Cuzzi & Zahnle (2004) using the correct parameters, and considering meter-sized bodies instead of pebbles.

4. IMPLICATIONS FOR CARBON-RICH PLANET FORMATION

The difference in the timescales needed to deplete water and CO vapors from the region inside the H₂O snowline leads to a gas phase composition compatible with the observed abundances in WASP 12b’s dayside atmosphere. For a long period of time, CO vapor is the major C- and O-bearing species in that region, increasing the gas C/O ratio of the area up to ~ 1 (Figure 4). The C/O in this case is never exactly equal to or higher than unity because the residual water vapor

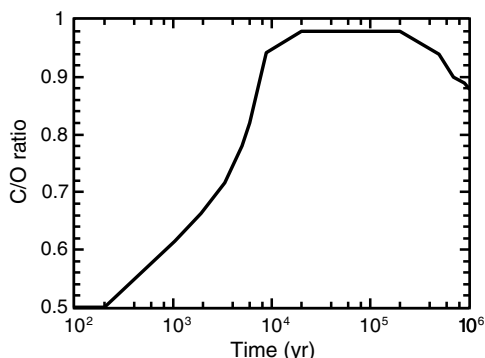


Figure 4. C/O ratio at 2 AU as a function of time. Early in the disk, H₂O vapor depletes much faster than CO vapor does, leading to a progressive increase of the C/O ratio with time. When the H₂O concentration reaches its minimum value, the CO concentration starts to decrease slowly, thus decreasing the C/O ratio in the gas phase.

slightly decreases the ratio. Even if the CO vapor exists in much higher concentrations than H₂O in this region, it is still depleted with respect to the initial stellar abundance, leading to a substellar C/H value. For example, Figure 3 shows that at $t = 5.0 \times 10^4$ yr and for $r = 2$ AU, $c_{\text{H}_2\text{O}} \sim 0.01$, but $c_{\text{CO}} \sim 0.55$, giving $\text{C/O} \sim 0.98$ and $\text{C/H} \sim 0.55$ times the solar value. Any giant planet accreting its envelope from this region in the disk, assuming no core–envelope coupling, should have an atmospheric superstellar C/O ~ 1 and a substellar C/H, corresponding to the properties of the so-called carbon-rich planets.

A plausible scenario is that WASP 12b’s core was formed through a streaming instability (Youdin & Goodman 2005) at or beyond the location of the water snowline where the solids surface density is high (since water vapor is depleted and concentrated as solids at its snowline location in 10^4 yr), then accreted its atmosphere in the inner region where the C/O ratio is superstellar (D’Angelo & Lubow 2008). This scenario assumes that the core does not mix with the accreted atmosphere. The opposite case of a well-mixed envelope would explain a planet with a higher oxygen but lower carbon abundance than its host star. Absent detailed information on the formation location of the planet’s core and its subsequent evolution, we can also assume that the entire planet formed in the region inside the water snowline. Our nominal (first) scenario differs from the one postulated by Öberg et al. (2011). It has the advantage of ending the formation of WASP 12b in the inner region of the disk, which is much closer to its observed location than in the scenario of Öberg et al. (2011). It is then not necessary to invoke long distance migration to explain the observed abundances. It also contradicts their conclusion that superstellar C/O with substellar C/H are compatible only with a planet accreting its atmosphere beyond the water snowline. Further, solid grains do not need a C/O ratio ~ 0.4 inside the snowline, since according to our dynamical model, H₂O ice is quickly depleted. The same can be said for the CO ice grains inside the corresponding CO snowline.

Since the first report of the C/O ratio in WASP 12b dayside atmosphere, it has been the subject of many follow-up studies and observations. Some of those confirmed the initial inferred abundances (Föhning et al. 2013), and others disagreed (Swain et al. 2013). In the generic volatiles transport model we presented, we made no assumptions regarding WASP 12b. The

results are independent from its atmospheric observations. We used a typical protoplanetary disk code and added generic, well-studied physical effects. Therefore, even if future studies definitely ruled out the superstellar C/O ratio in WASP 12b, our results will still be valid and informative since it would help constrain the possible formation location and migration history of planets. Our model is also independent of the absolute positions of the icelines. What is relevant is the relative positions between the two.

Another important parameter in our model is the coagulation timescale. It controls the CO replenishment rate since it is higher than the sublimation timescale, which is not the case for H₂O. For an improbable $\tau_{\text{coag}}^{\text{iceline}} \leq 3.5 \times 10^3$ yr, the CO replenishment will become faster than diffusion, allowing for simultaneously superstellar C/H and C/O ratios inside the water’s iceline since H₂O would still be depleted but CO might be enhanced above solar value if there is enough replenishing matter beyond the snowline. This would result in solids depleting at the snowline and thus excluding this location as a planet-forming region. The growth timescale can also be affected if we take into account the continuous condensation of vapor on dust in addition to the considered coagulation. Ros & Johansen (2013) found that for $\alpha \sim 0.01$, the condensation of millimeter-sized dust into 10 cm sized pebbles is possible in $10^3 \Omega_k^{-1}$, corresponding in our model to 10^3 and 10^4 yr respectively near the water and CO snowlines. These timescales would lead to similar results as inferred from our model. It is worth mentioning also that in our model we made the implicit assumption that CO is not trapped in water ice clathrates. This should not affect our main results though since the clathration temperature (~ 45 K; Lunine & Stevenson 1985) would act as a CO snowline, although a more complete model that includes clathrate transport can give important information in this regard. In all cases, the water vapor will be depleted much quicker than CO, and the inferred C/O ratio will hold. The C/H ratio on the other hand might be affected by such processes. Finally the observation of a CO snowline by Qi et al. (2013) hints in favor of CO behaving similar to water.

An important approximation made in our model is to neglect the effect of ices drifting in from beyond the snowlines on the replenishment rates. We do account for the inward drift of pebbles, with some delay due to coagulation time and time to return to the snowline. Furthermore, the sublimation of pebbles is a rather slow process as shown in Table 1 and act as a source a few AUs inside the snowline. What we are not considering is the return of microscopic dust grains inside the snowline.

Since we assume that the condensation or adsorption of vapor is an instantaneous phenomenon at this scale, then sublimation of any returning grain would also be instantaneous. As shown in Section 2, the main gas motion in the midplane is a strong outward advection which carries the microscopic grains. The condensation of vapor at the snowline creates a dust concentration gradient peaking at this position. This gradient will cause an isotropic diffusion of the dust, inducing inward movement for a some fraction of the microscopic grains. These grains will immediately sublimate as soon as they reach interior of the snowline, effectively counteracting the vapor gradient imposed by the cold finger effect. This effect slows down the depletion of the vapors. In our calculations we assumed the dominance of outward advection which will substantially mute the inward diffusion due to the much lower advection timescale and the non-null condensation time in realistic situations.

Even considering only the diffusive motion, pebbles will eventually grow from the grains (Ros & Johansen 2013) and

finally allow the formation of a planetary core at the water snowline. This core will act as a permanent sink rapidly accreting the newly condensed dust (Cuzzi & Zahnle 2004; Ciesla & Cuzzi 2006), allowing water to be depleted in 10^4 yr and our scenario to hold. This core will then migrate inward and accrete its envelope from the C/O enhanced gas.

With current technology, only alkali metals, H_2O , CO , CO_2 , and CH_4 are observable in exoplanet atmospheres (Tessenyi et al. 2013). In the near future, with the arrival of *James Webb Space Telescope* (*JWST*), E-ELT, and other new astronomical facilities, additional species should be detectable, so it might be useful to use our model to predict the abundances of other elements. N should be among the most abundant observable metals in giant planets atmospheres after O and C. In protoplanetary disks, N_2 (a volatile) is assumed to be the major N-bearing species (Prinn 1993). If we assume that WASP 12b accreted its atmosphere inside the water snowline, N should be accreted in gaseous form leading to a stellar or slightly substellar (due to vapor depletion) NH_3 abundance in the deep atmosphere at equilibrium. Since all volatiles are accreted in gaseous form in the envelope, we exclude a possible N enrichment induced by its trapping in clathrate hydrates in the nebula.

We thank an anonymous referee and S. J. Weidenschilling for their useful comments that helped us improve our manuscript. We thank T. Guillot and R. Hueso for having provided us with their accretion disk model. Special thanks go to K. Ros for discussions on condensation timescales. M.A.D. is supported by a grant from the city of Besançon. O.M. acknowledges support from CNES. J.I.L. acknowledges support from the *JWST* program through a grant from NASA Goddard.

REFERENCES

- Asplund, M., Grevesse, N., Sauval, A. J., & Scott, P. 2009, *ARA&A*, 47, 481
 Beckwith, S. V. W., Sargent, A. I., Chini, R. S., & Guesten, R. 1990, *AJ*, 99, 924
 Birnstiel, T., Dullemond, C. P., & Brauer, F. 2010, *A&A*, 513, A79
 Canuto, V. M., & Battaglia, A. 1988, *A&A*, 193, 313
 Ciesla, F. J., & Cuzzi, J. N. 2006, *Icar*, 181, 178
 Cuzzi, J. N., & Zahnle, K. J. 2004, *ApJ*, 614, 490
 Cyr, K. E., Sears, W. D., & Lunine, J. I. 1998, *Icar*, 135, 537
 Cyr, K. E., Sharp, C. M., & Lunine, J. I. 1999, *JGR*, 104, 19003
 D'Angelo, G., & Lubow, S. H. 2008, *ApJ*, 685, 560
 Fortney, J. J., Shabram, M., Showman, A. P., et al. 2010, *ApJ*, 709, 1396
 Föhring, D., Dhillon, V. S., Madhusudhan, N., et al. 2013, *MNRAS*, 435, 2268
 Goodwin, R. D. 1985, *JPCRD*, 14, 849
 Guillot, T., & Hueso, R. 2006, *MNRAS*, 367, L47
 Haynes, D. R., Tro, N. J., & George, S. M. 1992, *JPhCh*, 96, 8502
 Hueso, R., & Guillot, T. 2005, *A&A*, 442, 703
 Hughes, A. L. H., & Armitage, P. J. 2010, *ApJ*, 719, 1633
 Johansen, A., Klahr, H., & Mee, A. J. 2006, *MNRAS*, 370, L71
 Kuchner, M. J., & Seager, S. 2005, arXiv:astro-ph/0504214
 Lambrechts, M., & Johansen, A. 2012, *A&A*, 544, A32
 Lide, D. R. 2002, *CRC Handbook of Chemistry and Physics: A Ready-reference Book of Chemical and Physical Data*, ed. D. R. Lide (83rd ed.; Boca Raton: CRC Press)
 Lissauer, J. J., Hubickyj, O., D'Angelo, G., & Bodenheimer, P. 2009, *Icar*, 199, 338
 Lunine, J. I., & Stevenson, D. J. 1985, *ApJS*, 58, 493
 Madhusudhan, N., Harrington, J., Stevenson, K. B., et al. 2011a, *Natur*, 469, 64
 Madhusudhan, N., Mousis, O., Johnson, T. V., & Lunine, J. I. 2011b, *ApJ*, 743, 191
 Öberg, K. I., Murray-Clay, R., & Bergin, E. A. 2011, *ApJL*, 743, L16
 Press, W. H., Teukolsky, S. A., Vetterling, W. T., & Flannery, B. P. 1992, *Numerical Recipes in Fortran 77* (2nd ed.; Cambridge: Cambridge Univ. Press)
 Prinn, R. G. 1993, *Protostars and Planets III* (Tucson, AZ: Univ. Arizona Press), 1005
 Qi, C., Öberg, K. I., Wilner, D. J., et al. 2013, *Sci*, 341, 630
 Ros, K., & Johansen, A. 2013, *A&A*, 552, A137
 Ruden, S. P., & Pollack, J. B. 1991, *ApJ*, 375, 740
 Shakura, N. I., & Sunyaev, R. A. 1973, *A&A*, 24, 337
 Stepinski, T. F., & Valageas, P. 1996, *A&A*, 309, 301
 Stevenson, D. J., & Lunine, J. I. 1988, *Icar*, 75, 146
 Supulver, K. D., & Lin, D. N. C. 2000, *Icar*, 146, 525
 Swain, M., Deroo, P., Tinetti, G., et al. 2013, *Icar*, 225, 432
 Tessenyi, M., Tinetti, G., Savini, G., & Pascale, E. 2013, *Icar*, 226, 1654
 Venot, O., Hébrard, E., Agúndez, M., et al. 2012, *A&A*, 546, A43
 Weidenschilling, S. J. 1977, *MNRAS*, 180, 57
 Youdin, A. N., & Goodman, J. 2005, *ApJ*, 620, 459

2.7 Methods & Caveats

2.7.1 The protoplanetary disk

The Hueso & Guillot (2005) model

The advantage of this relatively simple disk model is that it combines accuracy with simplicity. The model contains most of the major physics involved in disks and is able to explain the properties and evolutionary histories of DM Tau and GM Aur as shown by Hueso & Guillot (2005). Its simplicity translates by the small number of free parameters that needs to be inputted in advance for the model to function. Practically, on the input side, we need to choose the properties of the collapsing cloud (mass, rotational frequency and temperature), in addition to the properties of the central star (initial mass, radius, temperature, and UV flux), the fundamental disk parameters (turbulent α value and some numerical grid related parameters), and finally a surface density profile. The code will then evolve the cloud + star + disk system according to the laws discussed in chapter 1. On the output side, the code will give most of the physical quantities then needed for the volatiles transport model such as the profiles of the surface density, angular velocity, viscosity, midplane temperature, scale height, pressure, radial and turbulent velocities of the gas. The limitations of this model reside also in its relative simplicity. First it does not incorporate processes affecting the innermost regions of the disk and thus the accretion rates such as the presence of a Jupiter-mass planet. This However should have a minimal impact on the properties of the disk of interest to this work, since I am considering the young disk prior to the formation of first planetesimals. Additionally, this model does not take into account non viscous interactions affecting the disk such as wind and tidal stripping in addition to photoevaporation. These processes affect the long term evolution of the disk, and should not play a significant role on the shorter timescales when the first planets are still forming. Finally, and most importantly, this model artificially increases the viscosity in the case of a disk gravitational instability. These instabilities can arise mostly in very massive disks, in contrast with DM Tau and GM Aur who seems to be currently fully stable. However, as we will see in chapter 3, local gravitational instabilities can play a major role in affecting the disk's chemical composition. For this part of the thesis however, I will assume the disk to be fully stable.

Although this is a dynamical disk model, in this work I chose to use a static disk profile for my calculations for simplicity. Incorporating the fully time-dependent disk model to the volatiles transport model is an important future step. A important aspect of such work would be the snowlines position change as a function of time along with the accumulated ices evolution. Other protoplanetary disk models, such as passive disks heated only by the star, can also be considered.

The Hughes & Armitage (2010) model

Although I used the overall disk profiles issued from the model of Hueso & Guillot (2005), I assumed that the dust particles in the midplane feel an outward advective gas

such in Hughes & Armitage (2010) from their 1+1D α -disk model. In this model based on the earlier work of Takeuchi & Lin (2002), the mean gas flow in the midplane is outward, but the vertically integrated movement is inward resulting in accretion. The authors thus define two types of flows in the disk: an inward accretion flow on the disk's surface, and an outward midplane flow where the velocity is calculated using the azimuthally symmetric Navier-Stokes equation as shown in Fig 2.8. These two types of flows result in a meridional circulation in the disk. The outward midplane flow and associated circulation was invoked by these authors to explain the presence of minerals such as crystalline silicates and CAIs (that can only form at very high temperatures) in comets that formed in the outer cold nebula. This is due to the small dust being strongly coupled to the gas and following its mean advective flow in the presence of minimal gas drag. This is of capital importance since I assumed in this work that once icy dust have been formed beyond the snowline, they will get advected outward with the midplane gas flow instead of diffusing inward. Although the presence of an outward midplane flow is convenient and does allow elegant solutions for major problems, whatever it does really occur in disks or if it is just a numerical model artifact is an open question. Fromang et al. (2011) for example demonstrated using high resolution Magneto-Hydro-Dynamical (MHD) simulations of turbulent protoplanetary disks that this meridional circulation can be no more than an artifact of the α parametrization of viscosity, and is not present when the turbulence is caused directly by Magneto-Hydro-Instability (MHD). The simulations by Fromang et al. (2011) are not fully conclusive though. These are very size and time limited calculations that ended with the system still evolving. Moreover, they did not consider the possibility of an MRI inactive dead zone (see Chapter 4) in the midplane. Therefore this subject is still very much in flux. Future results from MRI simulations or classical models should also be taken into account.

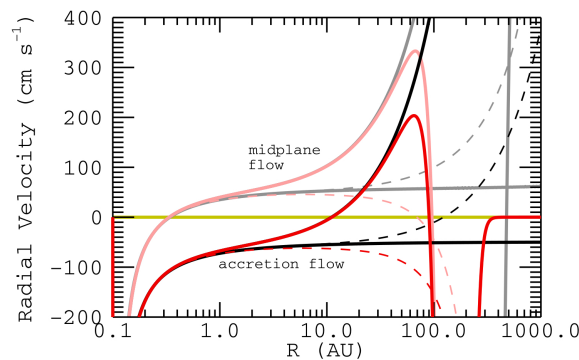


Figure 2.8: Radial advection velocities of the disk gas (black/gray) and dust (red/pink) from ?. Solid colors represent accretion flow and paler colors represent midplane flow case. Solid lines are for $t=0$ and dashed lines for $t=1$ Myr.

2.7.2 Gas drag & dust diffusion

As discussed in the published work and Annex A.3, in the gas drag formulation, I chose a special case for the viscosity that nullified the last term in equation A.16. Although this term has minimal effect on the drift velocities of large pebbles, it is more important for smaller gas-coupled dust such as these forming from the condensation of vapor just beyond an iceline. This term is proportional to the dust density gradient, and is thus responsible for the dust diffusion following their concentration gradient. If no other process quench this effect, we would hence expect the newly forming dusty ices to diffuse inward and re-sublimate, thus forbidding the vapor depletion inside of the snowline from taking place. As stated earlier, this aspect was neglected in my model since I assumed an outward advective midplane that will move the newly forming dusty ices outward away from the snowline faster than their inward diffusion. Ideally though, both effects should be taken into account, specially since the direction and magnitude of advection in disks is still unclear as discussed above. This however would necessitate a more profound understand of the dust evolution in order to calculate its gradient at each time step.

2.7.3 On the validity of WASP 12b’s measurements

The same technique of Madhusudhan et al. (2011) has been more recently reapplied to two more exoplanets: HD209458 and HD189733. As shown in Fig. 2.9, both were found to be depleted in water with respect to the solar value by up to several orders of magnitude. These results were challenged however by new analysis techniques doubting the technique

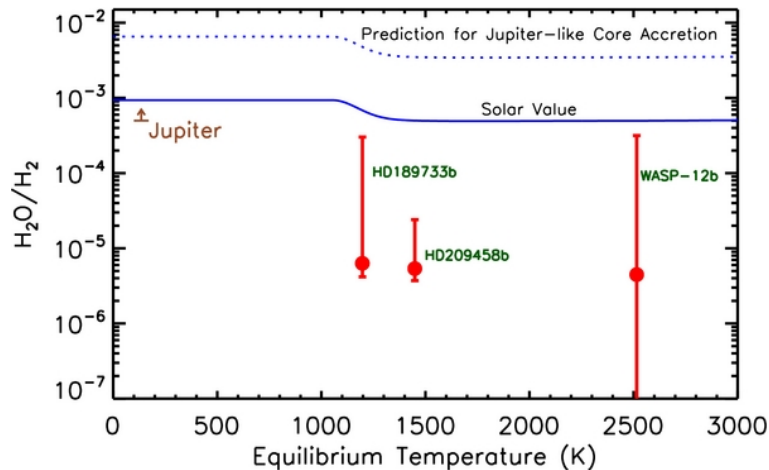


Figure 2.9: The water abundance in three exoplanets as constrained by Madhusudhan et al. (2014).

used to retrieve these abundances. By using a new approach incorporating the advantages of both the atmospheric retrieval methods and direct forward measurements, Benneke (2015) concluded that a sub-unity C/O ratio is much more probable for these planets. Although our model was motivated by the supersolar C/O ratio in WASP 12b, it is

independent from this constraints and the calculations remain valid even if the observation was proven to be wrong.

2.7.4 The cold finger effect vs observations

The cold finger effect and the resulting vapor depletion inside of the snowline with solids enhancement beyond it is the major mechanism at play in my model. One can ask though how realistic is this result ? Aren't there any hidden effects muting this mechanism ? Here I put the cold fingers effects face to face with recent observations, and show how it can give a neat explanation to a multiple of seemingly unrelated disks measurements.

CO depletion in TW Hya

TW Hya is an isolated T Tauri star in a face on position about 150 parsec away in the Hydra constellation (Kastner et al., 1997; Qi et al., 2008). It is our closest and thus most studied pre-main sequence system. The central star is a spectral type K7 with a mass of around $0.8 M_{\odot}$ (Qi et al., 2013). The gas rich disk has an estimated mass of $\sim 0.04 M_{\odot}$, a size of ~ 100 AU, and is 3-10 Myr old (Andrews et al., 2012). All of this indicates that TW Hya is a solar analogue, with its disk potentially resembling our own original protosolar nebula.

Recently, Qi et al. (2013) used ALMA to indirectly measure for the first time the CO iceline position in TW Hya (first inference in a solar analogue) from N_2H^+ emission. The presence of vapor CO will at the same time slow down the formation of N_2H^+ (by acting as H_3^+ sink) and accelerate its destruction by capturing one of its protons. N_2H^+ can thus only be present in the absence of CO vapor. Since ALMA function at submillimetric wavelengths, it is more sensitive to the disk's midplane, allowing this method to detect the CO iceline in the planets forming region of the disk. Qi et al. (2013) hence inferred a CO iceline location around 30 AU. This strengthen the case for TW Hya being a benchmark for planets forming disks, since the snowline's position is compatible with standard models (Hueso & Guillot, 2005; Martin and Livio, 2014).

A natural parallel step to the detection of the CO iceline in TW Hya is the characterization of its CO vapor. This was done by Favre et al. (2013), who tried to measure (for the first time) the CO/ H_2 ratio in the warm ($T \geq 20$ K, hence inside the CO iceline) region of this same system, again using ALMA. Due to the intrinsic difficulties in directly detecting CO and H_2 in disks midplanes, the authors took the indirect approach of measuring the species isotopes ratio ($C^{18}O/HD$), then calculating the implied $^{12}CO/H_2$ ratio through assumptions on the oxygen and hydrogen isotopic ratios. This can be summarized in their derived equation:

$$\chi(CO) = 1.76 \times 10^{-5} \left(\frac{^{16}O/^{18}O}{557} \right) \left(\frac{R_{obs}}{1.05 \times 10^{-3}} \right) \left(\frac{\chi(HD)}{3 \times 10^{-5}} \right) \frac{f_u(HD, J_u = 1)}{f_u(C^{18}O, J_u = 2)} \quad (2.1)$$

where R_{obs} is the ratio between the observed number of $C^{18}O$ and HD molecules in their respective upper states, $\chi(HD)$ the HD/ H_2 ratio and $f_u(X)$ the fractional population in

the upper state. The authors found, as a function of a fixed warm molecular layer's temperature, $\chi(\text{CO}) = 0.1 - 3 \times 10^{-5}$, which is at least an order of magnitude lower than the canonical value of 10^{-4} . Taken at face value, this implies a strong CO vapor depletion inside of its snowline in the disk's midplane.

The CO/H₂ ratio was also measured in the UV wavelengths by France et al. (2014) in the T Tauri RW Aur using COS/HST, who inferred on the other hand an almost canonical value of 1.6×10^{-4} . Although RW Aur is a younger disk than TW Hya allowing chemical evolution as possible explanation for the CO abundance difference, it is more probable that UV observations are probing the inner hot regions of the disk and is more contaminated by surface emissions than sub-mm wavelengths. In this vision, the disk is depleted in vapor only in the midplane beyond a certain radius.

The CO vapor depletion in TW Hya is unexpected and necessitates an explanation. Favre et al. (2013) initially suggested that CO transformation into CO₂ or hydrocarbons with higher condensation temperatures than CO. The newly formed molecule will thus freeze out and permanently remove the CO from the disk. Chemistry was then explored further in the detailed model of Cleaves et al. (2015) incorporating the chemical code of Fogel et al. (2011) that includes photo and ionic chemistries. This study concluded though that this type of chemistry alone is not capable of explaining all of the observed depletion, and that an additional sink (such as a physical disk specific process) of CO must be present.

Another model was presented more recently by Reboussin et al. (2015) including a detailed gas-grain chemical model that follows the evolution of the disk composition, starting from a dense prestellar core composition. These authors concluded that at high densities, and due mainly to grain surface reactions, CO will transform into CO₂. The canonical CO abundance can hence only be reached for temperatures above 30-35 K.

In this thesis I advance a new interpretation for this measurement, mainly that the observed CO depletion is caused by the cold finger effect. The volatile vapors diffusion following their concentration gradients as initially proposed by Stevenson and Lunine (1988) will remove the vapors from inside of their snowlines leading to the measured depletion. In Ali-Dib et al. (2014) (Fig. 2), I showed how the non null inward replenishment of vapor will lead to a residual amount on vapor in the inner disk, while keeping the rest of the disk depleted. This explains neatly both observations: the CO depleted warm molecular layer, and the almost unaltered inner disk region. The depletion by more than an order of magnitude found by my model is compatible with the values derived by Favre et al. (2013).

If my explanation is correct, then a particles growth rate enhancement and even an overabundance of CO ices should be present beyond its iceline. Observations relevant to this theory are presented next.

Dust excess on icelines

Another interesting T Tauri system observed recently by ALMA is HL Tau (Partnership et al., 2015). This was the first observation of a protoplanetary disk with very high angular resolution from 10 to 3.5 AU, allowing to resolve the disk at this scale. The resulting imaging revealed a pattern of bright and dark rings visible at all wavelengths (2.9, 1.3, and 0.87 mm continuum emission), as shown in Fig. 2.10. The presence of these rings and

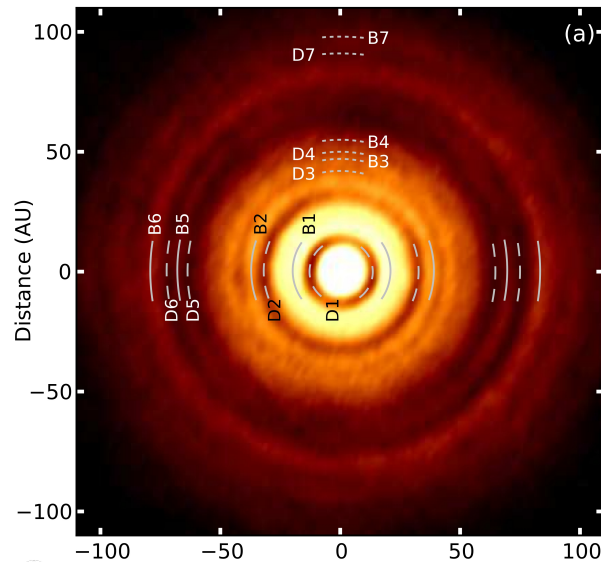


Figure 2.10: The HL Tau disk as seen by ALMA. Seven dark and 7 bright rings are resolved from the high angular resolution used, (from Partnership et al. (2015)).

gaps is a smoking gun evidence for planets formation related processes. The exact nature of what is happening though is still very much in flux. An interesting interpretation was put forward by Zhang et al. (2015), who proposed that the three most prominent dips might be evidence for pebbles growth near major icelines. Their conclusion is based on these two points (Fig. 2.11):

- The coincidence of the expected major volatiles snowlines positions with the gaps seen in the 0.87 mm observations. The thermal profile used was obtained from the HL Tau modeling of Men'shchikov et al. (1999).
- The spectral index variation inside the gaps indicates a possible bimodal growth distribution.

The spectral index α is expected to approach 2 (the black body limit) in optically thick regions, and is approximated by $2 + \beta$ in the optically thin regions, where β depends on the particles maximum size. Zhang et al. (2015) suggested a simple model where centimetric particles dominate the opacity if present (leading to $\alpha \sim 2$), while mm-sized grains dominate the mass-specific dust opacity where pebbles have grown to decimetric

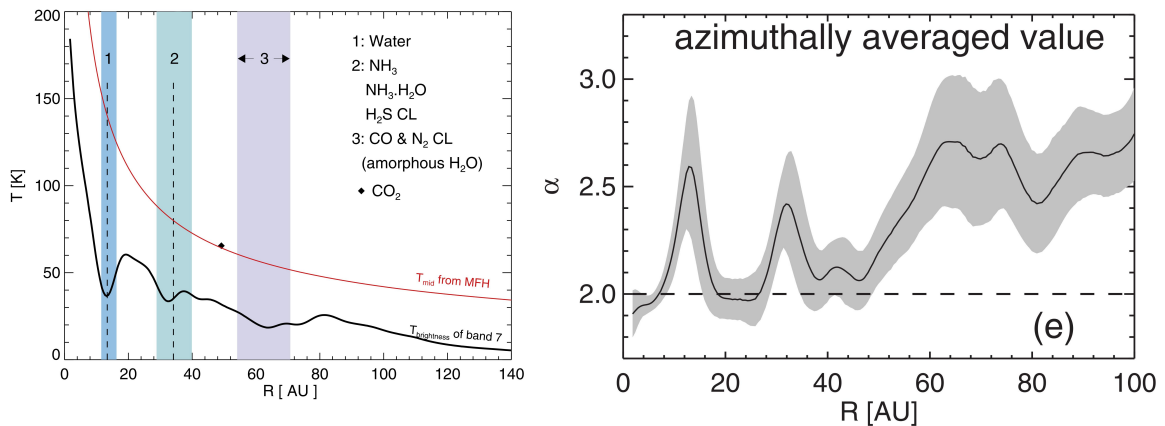


Figure 2.11: From Zhang et al. (2015). Left: The thermal profile of HL Tau along with the expected major condensation icelines and clathrates (CL) formation positions. The red curve is the midplane temperature and black curve the brightness temperature from 0.87 mm. Right: The azimuthally averaged continuum spectral index in HL Tau.

pebbles leading to $\alpha > 2$. This indicates a particles growth enhancement in the regions with $\alpha > 2$ just near the icelines transforming the first population (centimetric particles) into decimetric pebbles.

This possible pebbles growth enhancement beyond icelines is expected from both Ros & Johansen (2013) and my model. If confirmed, it does point out to the cold finger effect as being a major pebbles forming mechanism.

Formation of Enstatite chondrites

Enstatite chondrite meteorites are the most reduced solids of the solar system (Wood, 2005). They have a unique mineralogy with species such as MgS and CaS found in no other chondritic family, and are usually rich in MgSiO_3 while containing almost no FeO (Weiss and Elkins-Tanton, 2013).

Although Enstatites are among the rarest meteoritic type we find on Earth, there is some evidence that Enstatite like bodies dominated the terrestrial planets region in the protosolar nebula. Mercury (Nittler et al., 2011), Earth (Javoy et al., 2010), and Mars (Sanloup et al., 1999) are all thought to have originated from Enstatite like materials, due to resemblances in the isotopic compositions. This does not exclude other chondritic types contributions to the building blocks of these planets though, specially for Mars.

Several models have been put forward to explain the formation of Enstatites, such as condensation with slow nucleation kinetics or at high pressures, but they all failed to reproduce some aspects of their mineralogy. More recent models suggest their formation in a extremely reduced disk environment. (Hutson & Ruzicka, 2000) for example showed how an $\sim 85\%$ removal of water vapor in addition to a refractory elements fractionation can reproduce the major aspects of Enstatites composition (Fig. 2.12). They went forward

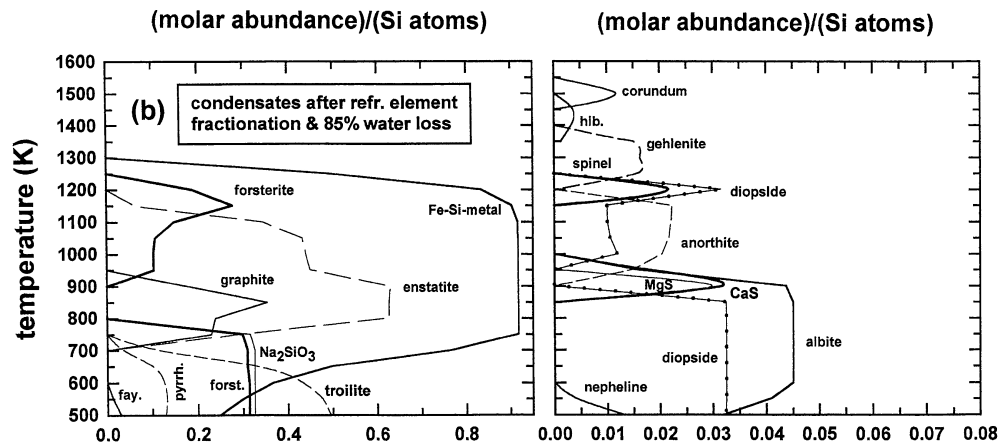


Figure 2.12: From Hutson & Ruzicka (2000). Left: A chemical equilibrium model starting from solar abundances but with 85% water removal and refractory elements fractionation. Right: The measured Enstatite chondrites mineralogical composition.

to propose that the water depletion due to the cold finger effect could have been the mechanism depleting the inner nebula from water and allowing Enstatites to form.

Bibliography

- Ali-Dib, M., Mousis, O., Petit, J.-M., & Lunine, J. I. 2014, *ApJ*, 785, 125
- Andrews, S. M., Wilner, D. J., Hughes, A. M., et al. 2012, *ApJ*, 744, 162
- Benneke, B. 2015, arXiv:1504.07655
- Cassen, P. 1994, *Icar*, 112, 405
- Ciesla, F. J., & Cuzzi, J. N. 2006, *Icarus*, 181, 178
- Cleeves, L. I., Bergin, E. A., Qi, C., Adams, F. C., & Oumlberg, K. I. 2015, *ApJ*, 799, 204
- Cyr, K. E., Sears, W. D., & Lunine, J. I. 1998, *Icarus* 135, 537
- Favre, C., Cleeves, L. I., Bergin, E. A., Qi, C., & Blake, G. A. 2013, *ApJL*, 776, L38
- Fogel, J. K. J., Bethell, T. J., Bergin, E. A., Calvet, N., & Semenov, D. 2011, *ApJ*, 726, 29
- France, K., Herczeg, G. J., McJunkin, M., & Penton, S. V. 2014, *ApJ*, 794, 160
- Fromang, S., Lyra, W., & Masset, F. 2011, *A&A*, 534, A107
- Hueso, R., & Guillot, T. 2005, *A&A*, 442, 703
- Hughes, A. L. H., & Armitage, P. J. 2010, *ApJ*, 719, 1633
- Hutson, M., & Ruzicka, A. 2000, *Meteoritics and Planetary Science*, 35, 601
- Javoy, M., Kaminski, E., Guyot, F., et al. 2010, *Earth and Planetary Science Letters*, 293, 259
- Kastner, J. H., Zuckerman, B., Weintraub, D. A., & Forveille, T. 1997, *Science*, 277, 67
- Madhusudhan, N., Harrington, J., Stevenson, K. B., et al. 2011a, *Natur*, 469, 64
- Madhusudhan, N., Mousis, O., Johnson, T. V., & Lunine, J. I. 2011, *ApJ*, 743, 191
- Madhusudhan, N., Crouzet, N., McCullough, P. R., Deming, D., & Hedges, C. 2014, *ApJL*, 791, L9

- Martin, R. G., & Livio, M. 2014, *ApJL*, 783, L28
- Men'shchikov, A. B., Henning, T., & Fischer, O. 1999, *ApJ*, 519, 257
- Nittler, L. R., Starr, R. D., Weider, S. Z., et al. 2011, *Science*, 333, 1847
- Öberg, K. I., Murray-Clay, R., & Bergin, E. A. 2011, *ApJL*, 743, L16
- Partnership, A., Brogan, C. L., Perez, L. M., et al. 2015, *arXiv:1503.02649*
- Qi, C., Wilner, D. J., Aikawa, Y., Blake, G. A., & Hogerheijde, M. R. 2008, *ApJ*, 681, 1396
- Qi, C., Öberg, K. I., Wilner, D. J., et al. 2013, *Science*, 341, 630
- Reboussin, L., Wakelam, V., Guilloteau, S., Hersant, F., & Dutrey, A. 2015, *arXiv:1505.01309*
- Ros, K., & Johansen, A. 2013, *A&A*, 552, A137
- Rowe, J. F., Coughlin, J. L., Antoci, V., et al. 2015, *ApJS*, 217, 16
- Sanloup, C., Jambon, A., & Gillet, P. 1999, *Physics of the Earth and Planetary Interiors*, 112, 43
- Stevenson, D. J., & Lunine, J. I. 1988, *Icarus* 75, 146
- Takeuchi, T., & Lin, D. N. C. 2002, *ApJ*, 581, 1344
- Weiss, B. P., & Elkins-Tanton, L. T. 2013, *Annual Review of Earth and Planetary Sciences*, 41, 529
- Winn, J. N., & Fabrycky, D. C. 2015, *ARA&A*, 53, 409
- Wood, J. A. 2005, *Chondrites and the Protoplanetary Disk*, 341, 953
- Zhang, K., Blake, G. A., & Bergin, E. A. 2015, *ApJL*, 806, L7

Chapter 3

The formation of Uranus and Neptune on the CO iceline

In addition to increasing the C/O in the inner nebula, my model have another consequence: the permanent accumulation of solids beyond the iceline due to vapor diffusion and condensation being faster than replenishment. For water, this hints to a natural formation spot for Jupiter at the water snowline as originally proposed by Stevenson & Lunine (1988). For CO on the other hand, this implies a relatively narrow spot very rich in carbon situated around 30 AU, compatible with the composition and formation location of Uranus and Neptune, two planets that puzzled formation models for a long time. This shifted my attention to these planets, where I tried to use my model to explain their chemical composition from their formation at the CO iceline.

3.1 On pebbles growth via vapor condensation

In this particular work, instead of calculating the time needed for pebbles to grow using a coagulation module, I chose to use the growth timescales from Ros & Johansen (2013) (RJ13). In RJ13, pebbles grow in the disk just beyond the iceline due to the diffusing vapor condensation (Fig. 3.1). I made this choice due to RJ13's detailed model fundamental compatibility with the snowlines picture, instead of my more general (and simpler) dust coagulation module.

In this model, vapor just inside of the snowline will diffuse outward due to turbulence then condensate (following a standard condensation law analogues to my sublimation equation) onto existing solids, growing in size. They assumed moreover that vapor will preferably condense on already grown particles instead of the small dust. Solids on the other hand can drift or diffuse inward and sublimate instantaneously. A large number of particles was used in a Monte-Carlo scheme in order to track the overall evolution of the system. Their main conclusion is that, for $\alpha = 0.01$, decimetric pebbles can grow efficiently beyond the snowline on a timescale of $1000 \Omega_K^{-1}$, or about 10^3 and 10^4 yr near the water and CO condensation fronts, respectively.

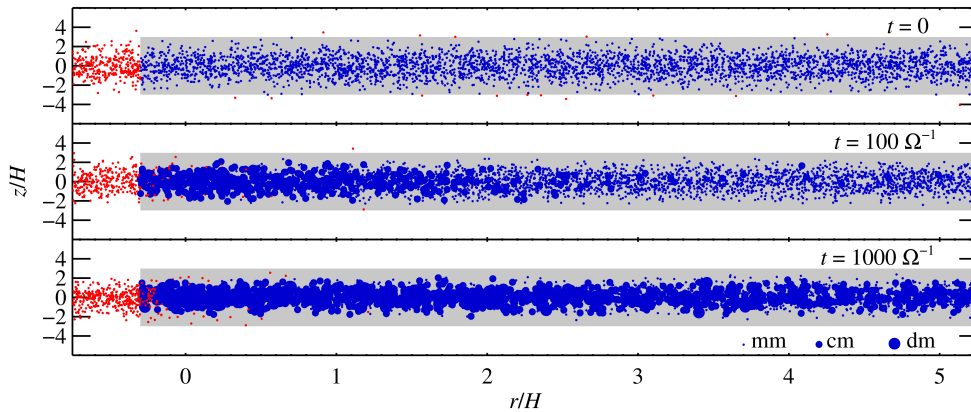


Figure 3.1: A sketch of the particles growths model of RJ13 (from their paper). Vapor particles (red) will diffuse across the snowline, condensate onto existing dust (blue) and grow in size. Decimetric pebbles are shown to grow on a $1000 \Omega_K^{-1}$ timescale.

3.2 Published article summary

The constraints we have on the formation of Uranus and Neptune can be summarized as follows:

1. Classically it is hard to form the cores of these planets quickly enough in the outer tenuous nebula to allow for gas accretion before the disk's dispersal.
2. The chemical composition of these planets is also hard to reconcile with formation scenarios since both planets are equally very enriched in carbon (10 times more than Jupiter), but possibly very depleted in nitrogen. Jupiter (and possibly Saturn) on the other hand is uniformly enriched in all volatile elements.
3. A recent determination of the D/H ratios in these planets using PACS/Herschel inferred a value much lower than in comets, which is unexpected for planets dominated in mass by water ices thought to be accreted in the comets region. Moreover, the D/H ratios of the original proto-ices that formed these planets were also constrained using an interior structure model, and found to be also sub-cometary.

I hence proposed a formation scenario based on the volatiles transport model than can address all these issues at once:

1. The solids peak predicted by my model beyond the CO iceline decreases the gas/dust ratio by an order of magnitude, possibly allowing the formation of planetesimals in this location via gravitational instability, and helping the later core growth via pebbles accretion.
2. Since an important fraction of the accreted solids is CO ices, the planets forming in this region will naturally be very rich in carbon. Additionally, since the N_2 iceline

is located slightly (few AUs) further out than the CO iceline, and since N_2 is same depleted in vapor form inside of its snowline for the same reasons as CO, the CO iceline area (and any planet that form around it) will be very poor in nitrogen. The planets forming at the CO iceline will be rich in carbon but poor in nitrogen.

3. In this case, the water inside of Uranus and Neptune should have two origins: a major fraction as CO that reacted with the accreted nebular H_2 leading the water with proto-solar D/H ratio and methane, and a minor cometary water fraction. My calculations show that this model explains neatly the currently measured bulk D/H values in Uranus and Neptune.

3.3 Published article

3.4 Methods & Caveats

3.4.1 On the main C and N bearing species in disks

This work assumes that CO and N₂ are the main carbon and nitrogen bearing elements throughout the disk. Here I discuss the validity of this assumption.

Carbon

As discussed in section 1.1.2, non equilibrium chemical models hint to CO being the main carbon bearing volatile in disks. Other models however have shown the importance and effects of the gas-grain processes on the chemistry of dense clouds (Hasegawa et al., 1992) and disks (Semenov & Wiebe, 2011). Wherever these effects do play an important effect on the nebula's chemistry or not is debated. What is certain though is that CO is the major carbon bearing specie in both comets (thus the cold region of the disk), and the inner hot nebula (as discussed in section 1.1.2), and hence I assumed that it was the major carbon bearing volatile in the disk. Another major carbon bearing volatile is CO₂ that can be produced from CO via two possible reactions (Lodders, 2003):



that can be dominant if CH₄ formation is kinetically inhibited as in the models of Prinn & Fegley (1981), and:



that takes place at temperatures below 650 K. However, again, although CO₂ is present in comets in amounts higher than what we expect at equilibrium (see section 1.3.2), it is still minor in comparison to CO. So although these processes might have converted some CO to CO₂, it did leave CO as the main C bearing volatile, since otherwise this would have been seen in comets. Finally, even if significant amounts of carbon were present as CO₂, it won't affect the main results as long as it leaves CO abundance order of magnitude.

Nitrogen

The other assumption I made in this work is that N₂ is the main nitrogen bearing volatile in the disk. As discussed in section 1.3.2, molecular nitrogen is very deficient in comets, but so is NH₃. The case for considering that N₂ was dominant in the protosolar nebula originates, in addition to the non-equilibrium chemical models discussed before, from the ¹⁴N/¹⁵N ratio in the solar system. This isotopic ratio was measured in a large number of our solar system's bodies. Of interest to this discussion are the values found in the solar wind, Jupiter, Saturn, and comets, summarized in table 3.1.

Table 3.1 indicate the presence of two distinct nitrogen reservoirs in the nebula. On one side of the equation we have the high solar value. Since N₂ is the main N bearing specie in interstellar clouds (Owen et al., 2001; van Dishoeck et al., 1993), the solar value ¹⁴N/¹⁵N should also be found in the primordial nebular N₂. On the other hand we have

Table 3.1: Selected $^{14}\text{N}/^{15}\text{N}$ ratio measurements in solar system bodies.

Target	$^{14}\text{N}/^{15}\text{N}$	Form of Nitrogen	Primordial form	Reference
Solar wind	442 ± 100	N_2	N_2	Marty et al. (2010)
Jupiter	435 ± 65	NH_3	N_2	Owen et al. (2001)
Saturn	≥ 500	NH_3	N_2	Fletcher et al. (2014)
Comets	127 ± 32	NH_3	NH_3	Rousselot et al. (2014)

the low cometary value in NH_3 , thought to represent the primordial interstellar nature of these icy grains Roueff et al. (2015). N_2 reduction into NH_3 at low temperatures as in the model of Prinn & Fegley (1981) however does not fractionate the nitrogen isotopic composition, since this can only happen in very low density cosmic rays dominated regions. We can deduce then that Jupiter and Saturn accreted most of their nitrogen in N_2 form, since otherwise we would expect a lower $^{14}\text{N}/^{15}\text{N}$ values in their atmospheres. This indicates that N_2 was the major nitrogen bearing species all the way to the orbit of Saturn. Although no $^{14}\text{N}/^{15}\text{N}$ measurements are available for Uranus and Neptune, it is more probable based on the previous discussion that N_2 was the main nitrogen bearing species in that region, since otherwise we should have found more NH_3 in comets.

3.4.2 The width of the ices over-density beyond the icelines

The results of this work depend crucially on the distance over-which newly formed ices concentrate beyond the CO iceline. Both the gas/solids ratio and the final carbon abundance in Uranus and Neptune depend directly on this parameter. I followed the prescription of Stevenson & Lunine (1988) in expressing this length scale over which most of the diffused CO vapor will condense as:

$$X_c = \delta \times \ln(\sqrt{D \times t}/2\delta) \quad (3.3)$$

see equation 1 from the published article. The free parameter in this equation is δ . It indicates the distance over which the saturation vapor pressure of the species changes significantly. Due to the lack of data, I used for both CO and N_2 the same δ value used by Stevenson & Lunine (1988) for water. The presented results can benefit greatly from more realistic values for this parameter based on ab initio calculations or experiments. Qualitatively, since the temperature gradient is less steep in the outer nebula than near the water snowline, I would expect this parameter's value to be higher. This is compatible with the results of Ros & Johansen (2013), who found from their model including a more detailed condensation process ices accumulation over a larger area with characteristic length $X_c \sim r/H$.

3.4.3 On the tropospheric CO in Uranus and Neptune

A major observational constraint unaddressed by this work is the difference in the tropospheric CO abundances between Uranus and Neptune. It was discussed in the pub-

lished work that only tropospheric (in contrast with stratospheric) CO measurements are relevant for formation models. Tropospheric CO was detected only in Neptune, and seems to be absent from Uranus where only stratospheric CO (with external origin) was detected. Assuming this difference is due to the formation processes of these planets and not to their interior evolution or observational biases, formation models should try and explain the difference between the two icy giants. Assuming the standard interpretation that Neptune's tropospheric CO originates from a very high internal water abundance, the absence of CO in Uranus should be interpreted hence as a lack of water with respect to Neptune. Future works taking into account the model presented above along with detailed formation and accretion tracks for these planets can give interesting insight on this subject.

Bibliography

- Ali-Dib, M., Mousis, O., Petit, J.-M., & Lunine, J. I. 2014, *ApJ*, 785, 125
- Fletcher, L. N., Greathouse, T. K., Orton, G. S., et al. 2014, *Icar*, 238, 170
- Hasegawa, T. I., Herbst, E., & Leung, C. M. 1992, *ApJS*, 82, 167
- Lodders, K. 2003, *ApJ*, 591, 1220
- Marty, B., Zimmermann, L., Burnard, P. G., et al. 2010, *Geochim. Cosmochim. Acta*, 74, 340
- Owen, T., Mahaffy, P. R., Niemann, H. B., Atreya, S., & Wong, M. 2001, *ApJL*, 553, L77
- Prinn, R. G., & Fegley, B., Jr. 1981, *ApJ*, 249, 308
- Ros, K., & Johansen, A. 2013, *A&A*, 552, A137
- Roueff, E., Loison, J. C., & Hickson, K. M. 2015, *A&A*, 576, A99
- Rousselot, P., Perali, O., Jehin, E., et al. 2014, *ApJL*, 780, L17
- Semenov, D., & Wiebe, D. 2011, *ApJS*, 196, 25
- Stevenson, D. J., & Lunine, J. I. 1988, *Icarus* 75, 146
- van Dishoeck, E. F., Blake, G. A., Draine, B. T., & Lunine, J. I. 1993, *Protostars and Planets III*, 163

Chapter 4

Nebular dead zone effects on the D/H ratio in chondrites and comets

When I first started working on my PhD in 2012, no measurement was as hotly debated as the Earth like water D/H ratio inferred in the Jupiter family comet (JFC) 103P/Hartley by HIFI/Herschel (Hartogh et al., 2011). To understand why, and how did this lead me to work on much smaller bodies (chondritic meteorites), first a quick introduction to cometary families and their D/H ratios.

4.1 A brief history of comets

The most fundamental property of comets is their dynamical orbits, dividing them into different dynamical families (cf. reviews by Morbidelli (2008); Morbidelli et al. (2008)). JFCs are comets with orbits dominated by Jupiter's gravity, and thus orbit roughly between it and the sun. They originate from the scattered disk beyond Neptune and migrate to their current orbits as the intrinsically short living centaurs. OCCs (Halley-type and long period comets) on the other hand, originate much further out in the Oort cloud, where gravitational perturbations disrupt their orbits and throw them into the inner solar system as shown in Fig. 4.1.

Dynamical models show that the Oort cloud originated as bodies distributed in the giant planets region and got later ejected via their gravitational interaction with mainly Jupiter and the galactic tides (Duncan et al., 1987). The formation location of the scattered disk objects on the other hand is less understood, but it has probably originated as bodies disrupted from the Kuiper belt via the gravitational interaction with Neptune. This implies that the OCCs formed closer to the sun (at higher temperatures) than JFCs, what should have resulted in lower D/H ratios for these comets. Of course this is not the case. As mentioned above the D/H measured in the JFC 103P/Hartley is in fact lower than the D/H ratio in OCCs as shown in Fig. 1.9. The D/H value found in Hartley (that was the first in a JFC) is still to date the lowest found in a comet. Although its Earth's

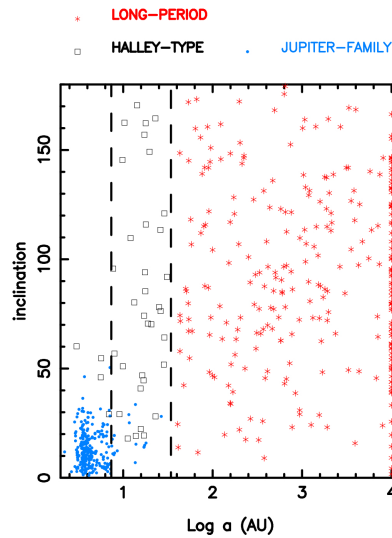


Figure 4.1: The three main cometary dynamical families as defined by their inclination and semi-major axis. From Morbidelli (2008).

VSMOW¹ like value was surprising and reignited the debate about the origin of water on Earth, the most shocking aspect is that it is lower than the Oort Cloud comets (OCC) D/H ratios range. If indeed JFCs formed further out from the sun than OCCs, then why do they seem to have a lower D/H ratio ?

For this reason, the D/H ratio found in Hartley needed an explanation. However, the mystery did not stop at this point. In 2015, another precise measurement of the D/H ratio in a JFC was made, this time in comet 67P/CG by the ROSINA mass spectrograph on board the European *Rosetta* space probe (Altwegg et al., 2015). This measurement was very anticipated for long time, since it was supposed to either confirm a systematic low D/H ratio in JFCs, or contradict the value found in Hartley. As shown in Fig. 4.1, the D/H ratio in 67P/CG turned out to be much higher than in Hartley, even higher than most OCCs. This of course added yet another layer of complexity to the equation.

Several explanations has been proposed to this problem. The first, advocated by Brown et al. (2012), is the possibility that the remote-sensing measurement does not reflect the bulk composition of 103P/Hartley. This interpretation is strengthened by the fact that the only 2 in-situ measurements we have (in Halley and CG) are compatible. Another possibility is that maybe the dynamical models of cometary origins need some revision. Indeed, in the model of (Brasser and Morbidelli, 2013), all of the cometary families originate from the same initial population (the primordial trans-Neptunian disk) around 10-40 AU.

My own initial intuition was the following: what if the thermal profile in the presolar nebula was not monotonic, and for some reason had a local peak JFCs region ? This would allow the OCCs to have their high D/H ratios, and JFCs to be distributed between

¹Vienna Standard Mean Ocean Water

those who formed on the thermal peak and have a low D/H ratio, and the rest that formed beyond the local thermal peak and have a much higher value. I then found a possible origin for this non-monotonic thermal profile in layered dead zone disks with midplane turbulence inhomogeneities, where the accumulation of matter at certain locations can result in such a local temperature peak. In practice though, I found that even for very young disks, the thermal peak is too close to the sun (maximum around 10 AU) to be relevant for comets. I hence shifted the discussion to another family of bodies where analogue problems are present: chondritic meteorites. In this chapter I discuss the D/H ratio variety found in the different chondritic families in the light of new dead zone physics.

4.2 An introduction to dead zones

We saw in chapter 1 that accretion in disks is unambiguous both observationally and theoretically. This accretion is maintained by disk turbulence generated by an unknown mechanism. A leading possible cause of turbulence in disks is magneto-rotational-instability (MRI) (Balbus and Hawley, 1991), arising from the magnetic coupling of gas parcels with different angular velocity. MRI, by definition, can function only if the gas is coupled to the magnetic field and is thus ionized with enough free electrons (cf. Turner et al. (2014) for a review). Two main sources of ionization are thought to dominate in disks: collisional (thermal) ionization and cosmic rays (Armitage, 2011). In the inner most one-tenths of AU, the temperature is hot enough due to solar irradiation for collisional (thermal) ionization to couple this part of the disk to the magnetic field. This mechanism is however inefficient beyond the inner most parts of the disks, where cosmic rays ionization dominate. Cosmic rays however can penetrate the disk only to a depth in the order of 100 g cm^{-2} . For a typical young disk (Fig 1.3), this means that only its surface layer will be ionized (thus MRI active), allowing accretion to take place. The disk's midplane in the planets forming region on the other hand, will be an MRI inactive "dead" zone with very weak turbulence (resulting in low macroscopic viscosity typically modeled by $\alpha \sim 10^{-4}$) and almost no accretion flow (Gammie, 1996). Finally, for the outer disk (beyond roughly 10-20 AU), the gas density is low enough for cosmic rays to penetrate the entire disk, and it is thus entirely MRI active.

The presence of a deadzone in a protoplanetary disk can have a range of important implications for its structure and evolution. In this chapter of the manuscript I am interested in the dead zone effect on the thermal profile of the disk. Since the outer part of the disk is MRI active, accretion should proceed in this part. Matter will thus be transported inward till reaching the deadzone where accretion will stop, leading to matter accumulation. Overtime, this will increase substantially the gas surface density in this part of the disk, leading to a local increase in temperature due to the viscous dissipation component as can be seen from equations 1.19 to 1.23. This will lead to a non monotonic thermal profile in the disk that can affect its chemistry (Martin and Lubow, 2013). In some cases, the temperature increase can reach a critical value necessary to reignite the MRI in the deadzone, leading to a disk wide instability and an accretion outburst similar

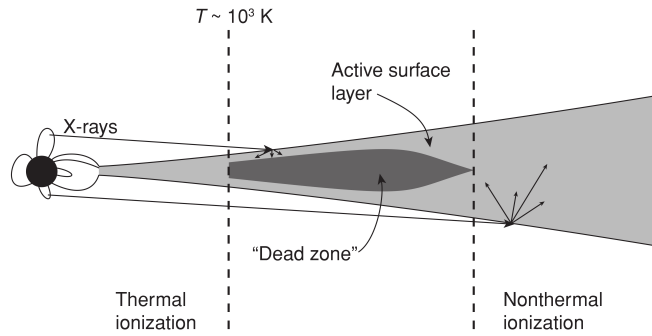


Figure 4.2: A sketch of a layered disk with an inner thermally ionized zone, a middle deadzone, an outer tenuous cosmic rays ionized MRI active zone, and the active surface layer (from Armitage (2011)).

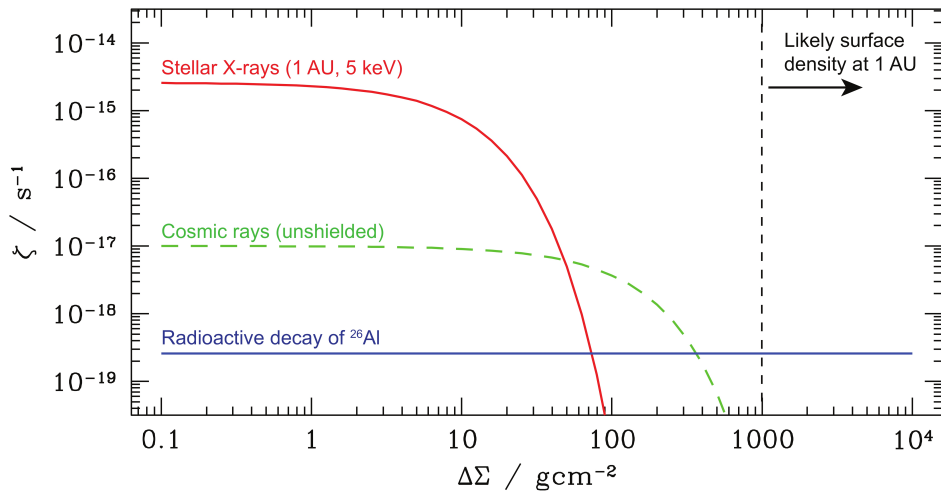


Figure 4.3: Ionization rate in a disk for different sources as a function of its column density (from Armitage (2011)).

to those seen in FU Orion stars (Martin and Lubow, 2013).

4.3 A few words on chondrites

The following is a brief introduction to chondritic meteorites gathered from Wasson and Kallemeyn (1988); Wood (2005); Wooden et al. (2005); Brearley (2006); Scott (2007); Krot et al. (2009); Weiss and Elkins-Tanton (2013). Chondrites are the most primitive and unaltered type of meteorites. They represent up to 86% of the total number of falls on Earth. Composition wise, three main components are characteristic of chondrites:

- Chondrules: Millimeter sized spherical solids formed through very rapid (minutes)

heating (to around 1000 K) of solids. They are primarily made of silicate minerals such as Olivine ($(\text{Mg,Fe})_2\text{SiO}_4$) and Pyroxene ($\text{Mg}_2\text{Si}_2\text{O}_6$ for example). In volume, they occupy between 20% and 80% of meteorites. Chondrules aging showed that they might be the oldest unaltered solids of the solar system. Understanding their formation is thus crucial to shed light on the solar system early evolution.

- **The matrix:** A fine grained sheet-like “matrix” with roughly similar bulk composition to chondrules. Matrices are thought to form at lower temperatures than chondrules and are chemically complimentary (the total composition of chondrules and the matrix are needed to reach solar like composition for a chondrite). Matrices usually occupy most of the remaining volume unoccupied by chondrules in the meteorite. Carbon rich “carbonaceous” chondrites are usually dominated by the matrix, while carbon poor (ordinary and enstatite) chondrites are more dominated by chondrules.
- **Calcium-Aluminum Inclusions:** CAIs are submillimetric to centimetric Calcium and Aluminum rich inclusions constituting in volume up to 5% of carbonaceous chondrites. These minerals can form only at very high temperatures (higher than chondrules), and their origin remain unclear. They are strong candidates (along with chondrules) for the oldest objects in the solar system.

Chondrites are usually divided into 3 broad classes: primitive volatile rich carbonaceous chondrites (CX, where X designates a prototype meteorite in a group), more altered volatile poor ordinary chondrites (H, L and LL), and the severely reduced enstatite chondrites (EH and EL). A summary of their main relevant characteristics is given in table 4.1.

Due to their more or less unaltered nature, chondrites are thought to originate from undifferentiated (thus small enough) parent bodies (asteroids or possibly even comets). Based on spectra similarities, CI chondrites are usually associated with C-type asteroids, and ordinary chondrites with S-type asteroids.

Chondritic group	Carbon abundance	Oxygen abundance	% of droplet chondrules
OC (type 3)	0.5%	1%	16%
CI	3.5%	20%	-
CM	2.5%	13%	5%
CR	1.5%	6%	<1%
CO	0.5%	1%	5%
CV	0.5%	1%	6%

Table 4.1: The main volatiles abundances in addition to the proportions of completely melted chondrules in major chondritic groups (compiled from Wood (2005)).

4.4 Published article summary

The water D/H ratio was measured in a large number of chondritic meteorites. Despite the different chondritic families probably forming in the same general area, large differ-

ences in the D/H ratios were found. Most surprisingly, the value measured in CR seems to be higher than that in CI chondrites (Fig. 4.4), although these last probably formed farther from the sun at lower temperatures as inferred from their water abundances (Fig. 4.5). The question I try to answer in this work is:

Why do we have such a diversity in chondritic D/H ratios and why do some chondrites who formed closer to the sun seem to have a higher D/H value ?

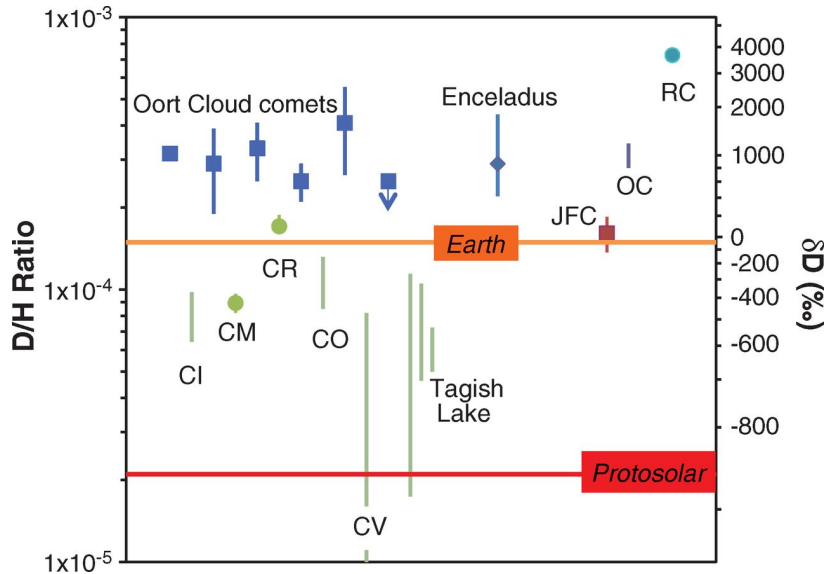


Figure 4.4: The D/H ratio in water for different chondritic families and other solar system bodies (from Alexander et al. (2012)).

In this work I use a snapshot of a layered disk model containing a dead zone with a non monotonic thermal profile to investigate if such models can offer a new solution to the problem. The new thermal profile contains a peak reaching around 700 K in the chondrites formation region around 3-5 AU. I couple this disk snapshot as an input for a D/H model taking into account chemistry, diffusion, and advection (ignored in earlier studies, numerical methods are discussed in Appendix B). I start from a uniform D/H enrichment value of $15 \times$ protosolar throughout the disk, and I leave it evolve for 4×10^5 yr, the time by which the snowline supposedly moved inward to 1 AU. As a result I find a new non monotonic D/H profile with a peak in the chondrites region possibly explaining the origin of their D/H variations (Fig. 5 in the submitted article). Most of chondritic families measured D/H ratios can be accounted for in the right relative formation order in the disk. I also tried to use a younger disk profile with a further out thermal peak to explain the low D/H ratio in 103P/Hartley, but the D/H reversal location found is still too close to be relevant for comets.

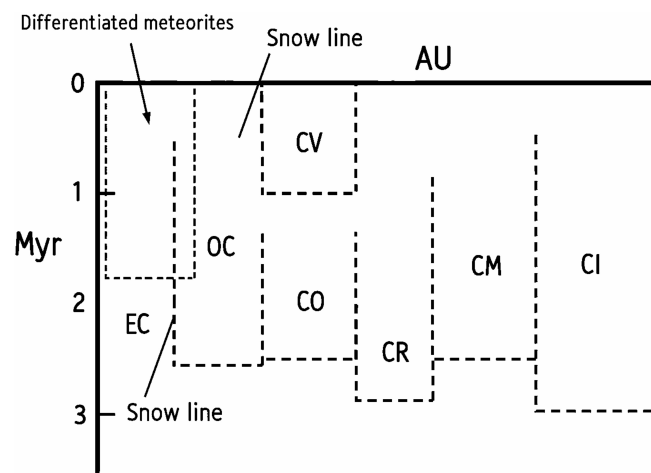


Figure 4.5: The relative formation locations of chondrites based on their volatiles abundances and the proportions of completely melted chondrules (from Wood (2005)).

4.5 Published article

The following paper was submitted to *Astronomy & Astrophysics* on 02/05/2015. It has been accepted on 11/08/2015 and is currently in press.

Nebular dead zone effects on the D/H ratio in chondrites and comets

M. Ali-Dib¹, R. G. Martin², J.-M. Petit¹, O. Mousis³, P. Vernazza³ and J. I. Lunine⁴

¹ Institut UTINAM, CNRS-UMR 6213, Observatoire de Besançon, Université de Franche-Comté, BP 1615, 25010 Besançon Cedex, France e-mail: mdib@obs-besancon.fr

² Department of Physics and Astronomy, University of Nevada, Las Vegas, 4505 South Maryland Parkway, Las Vegas, NV 89154, USA

³ Aix Marseille Université, CNRS, LAM (Laboratoire d'Astrophysique de Marseille) UMR 7326, 13388, Marseille, France

⁴ Center for Radiophysics and Space Research, Space Sciences Building, Cornell University, Ithaca, NY 14853, USA

Received ??; accepted ??

ABSTRACT

Context. Comets and chondrites show non-monotonic behavior of their deuterium-to-hydrogen (D/H) ratio as a function of their formation location from the Sun. This is difficult to explain with a classical protoplanetary disk model that has a decreasing temperature structure with radius from the Sun.

Aims. We want to understand if a protoplanetary disc with a dead zone, i.e., a region of zero or low turbulence, can explain the measured D/H values in comets and chondrites.

Methods. We use time snapshots of a vertically layered disk model with turbulent surface layers and a dead zone at the midplane. The disc has a non-monotonic temperature structure due to increased heating from self-gravity in the outer parts of the dead zone. We couple this to a D/H ratio evolution model in order to quantify the effect of such thermal profiles on D/H enrichment in the nebula.

Results. We find that the local temperature peak in the disk can explain the diversity in the D/H ratios of different chondritic families. This disk temperature profile leads to a non-monotonic D/H enrichment evolution, allowing these families to acquire their different D/H values while forming in close proximity. The formation order we infer for these families is compatible with that inferred from their water abundances. However, we find that even for very young disks, the thermal profile reversal is too close to the Sun to be relevant for comets.

Key words. protoplanetary disks – astrochemistry – Meteorites, meteors, meteoroids – Comets: general – Planets and satellites: composition

1. Introduction

The deuterium-to-hydrogen (D/H) ratio is one of the most discussed isotopic ratios in planetary sciences. This interest is due to the strong dependence the ratio has on the temperature of an icy body's formation location (Ceccarelli et al. 2014). In the interstellar medium (ISM), the water D/H ratio is measured at up to $\sim 9 \times 10^{-4}$ (Brown & Millar 1989), although the values are much higher in the organic matter of the interstellar hot cores ($\sim 1 \times 10^{-3}$) and cold clouds (up to $\sim 2 \times 10^{-2}$) (Dartois et al. 2003; Robert 2006; Parise et al. 2012). When a protoplanetary disk forms around a young star, these ices are heated to more than a few hundred K. At these high temperatures, gaseous HDO reacts with nebular H₂ to form water vapor and HD,



and this results in a decrease in the D/H ratio in water because $[\text{HD}]/[\text{H}_2]$ is lower than D/H in water, even accounting for chemical affinity (Lécluse & Robert 1994). The rate of this reaction depends strongly on the disk temperature. Therefore, ices forming in regions with higher past temperatures should have a lower D/H ratio. Measurements of D/H in Jupiter and Saturn find D/H $\sim 2 \times 10^{-5}$ (Lellouch et al. 2001), the value also found in the ISM hydrogen gas. This value is usually interpreted as the D/H ratio in the protosolar nebula's H₂. For the rest of this work we

follow Drouart et al. (1999) and others in defining f as the D/H enrichment factor in water:

$$f = \frac{[\text{HDO}]/[\text{H}_2\text{O}]}{[\text{HD}]/[\text{H}_2]}. \quad (2)$$

Thus, for the nebular H₂ gas, by definition, f is equal to unity.

1.1. D/H ratio observations in the solar system

The water D/H ratio of small bodies in the solar system has been measured for a large number of comets (Mumma & Charnley 2011), meteorites (Robert 2006), and in the plumes of Saturn's moon Enceladus (Waite et al. 2009; Spencer et al. 2009). In meteorites, organic materials and water both contribute to the bulk D/H value. Therefore, separating the two components is crucial to understanding the contribution from water. This was done by Alexander et al. (2012), who found f values ranging from 3 to 5 in carbonaceous CI chondrites, and ~ 15 in ordinary chondrites (OCs). More recently, a higher value reaching $f \sim 100$ has been also inferred for OCs (Piani et al. 2015). This implies that either low D/H minerals still coexist in the matrix mixed with deuterium-rich organics, or an unknown process has fractionated water and organics differently from an initial low D/H reservoir before their incorporation in the matrix. In neither case have the low values for the D/H ratio obtained from this method ever existed in chondrites. Taken at face value, these results contradict

Table 1: The measured water D/H fractionation and abundance in small bodies in the solar system.

Source	f	% Water Abundance
Ordinary Chondrites (OCs)		
LL3	29 – 44	-
Semarkona (LL3)	~100	-
H and L	≤ 15	1
Carbonaceous Chondrites		
CI	3-5	20
CM	~ 4.5	13
CR	~ 8	6
CO	4 – 7	1
CV	1 – 4	1
Comets		
103P/Hartley	~ 7.4	-
67P	~ 21	-
Oort Cloud Comets (OCCs)	10 – 25	-
Moons		
Enceladus	~ 15	40-50

the predictions from the expected formation locations, since CIs are usually associated with C-complex asteroids that formed between the giant planets, and OCs are associated with S-complex asteroids that formed in situ sunward of Jupiter’s orbit (Chapman 1996; Mothé-Diniz et al. 2003; Walsh et al. 2011). Alexander et al. (2010) noted, however, that due to hydrogen escape via Fe oxidation, the D/H ratio in OCs should be treated as an upper value and could originally have been much lower. This effect was found to be limited to OCs, allowing us to use the values measured in other chondritic families to understand the processes at play.

The carbonaceous CR chondrites are thought to have a high D/H value (Robert & Epstein 1982). The value measured by Alexander et al. (2012) of $f \sim 8$ is very surprising, since this is almost twice the value in CIs, and is actually higher than that found in the comet 103P/Hartley. The D/H ratio was also measured in the ordinary chondrites of type LL3 and found to be even higher than that in L- and H-type ordinary chondrites (Robert 2006; Alexander et al. 2010). Measurements of the D/H ratio in the carbonaceous chondrite types CO, CM, and CV were also found to be low providing further evidence for this discrepancy in the carbonaceous and ordinary chondrite D/H ratios (Robert 2006; Alexander et al. 2012).

In Oort cloud comets (OCCs), classically thought to have formed between the giant planets, f was found to range between 10 and 25. On the other hand, the D/H ratio was measured for the first time in the Jupiter family comet (JFC) 103P/Hartley, a family classically thought to have formed in the Kuiper belt beyond Neptune, and was found to be ~ 7.4 , the value also found in the Earth’s oceans (Hartogh et al. 2011). This was surprising since JFCs are thought to have formed in an area farther out than the OCCs (Morbidelli 2008) (although compare the model of Brassier & Morbidelli 2013, where all comets form beyond the orbital radius of Neptune); it was predicted that their D/H ratio should be higher than or at least equal to that of the OCCs (Mousis et al. 2000; Kavelaars et al. 2011). What made the situation even murkier is the recent measurement of the D/H ratio in the JFC 67P/Churyumov–Gerasimenko by Rosetta where

the value found lies well within the OCC range (Altwegg et al. 2015). A summary of all of the D/H ratio observations discussed here, and the water abundances in chondrites, can be found in Table 1.

1.2. D/H ratio connection to protoplanetary disc models

Classical disk models with a standard monotonically decreasing temperature profile (Lynden-Bell & Pringle 1974; Pringle 1981) all predict that the D/H ratio should similarly follow a monotonic profile, increasing with the icy body’s formation distance from the Sun (Drouart et al. 1999; Mousis et al. 2000; Hersant et al. 2001). An alternative model is that of Yang et al. (2013) who use a new D/H 2D model including the infalling material from the cloud, giving a non-monotonic D/H ratio profile in the nebula due to constant influx of unequilibrated water. However, they did not discuss the D/H ratio in chondrites, and their monotonic temperature profile out to a radius of 10 AU cannot explain the diversity of D/H ratios found in the inner solar system. Another model is that of Jacquet & Robert (2013), who tried to explain the chondritic diversity with a classical disc model that includes an interplay of inward advection and outward diffusion in the nebula. This model, however, also predicted a monotonic D/H profile, and although it can broadly explain the chondrite D/H range, it does not explain, for example, why CRs, which formed closer to the Sun than CIs (Wood 2005), have a higher D/H ratio.

The observed D/H fractionation variations found in chondrites are a challenge to classical disk models since the parent bodies of most chondrites should have formed in the same general region, except those of CIs that probably formed a few AU farther out in the disk. All these results indicate that either the D/H evolution models used are incomplete or that the thermal profile in the protosolar nebula was not monotonic, the hypothesis we are going to explore in this work.

Turbulence within protoplanetary disks drives outward angular momentum transport that allows material to spiral in and be accreted onto the forming star (e.g., Pringle 1981). This turbulence is thought to be driven by the magneto-rotational instabil-

ity (MRI) (Balbus & Hawley 1991). However, it is now generally accepted that the midplanes of protoplanetary disks have a region of zero or weak turbulence known as a “dead zone” (e.g., Gammie 1996; Fromang et al. 2002; Martin et al. 2012a; Dzyurkevich et al. 2013; Turner et al. 2014; Cleeves et al. 2015). This leads to a gradual accumulation of gas in the dead zone region, resulting in an increase in the temperature and pressure (Armitage et al. 2001; Zhu et al. 2010; Martin & Lubow 2011, 2013). The increased surface density of the disc can lead to a second type of turbulence, driven by gravitational instability (Paczynski 1978; Lodato & Rice 2004) and this results in an increase in the temperature locally in that region. The question we are going to tackle in this work is: What effect does a local peak in the temperature have on the D/H ratio in protoplanetary disks, and can it resolve the discrepancies in the observations of the D/H ratio in small bodies in our solar system? In section 2 we discuss the model we use to simulate the processes involved. In section 3 we discuss the results and implications. We draw our conclusions in section 4.

2. The numerical model

2.1. The protoplanetary disk model

We follow Martin & Lubow (2011) and model the protoplanetary disc as a layered accretion disc (see their equations 1-16). The surface density evolves according to conservation of mass and angular momentum (Pringle 1981). The temperature structure is governed by a simplified energy equation that balances viscous heating with blackbody cooling (see, e.g., Pringle et al. (1986); Canizzo (1993)). There are two types of turbulence in protoplanetary discs, magnetic turbulence driven by the MRI and gravitational turbulence (Paczynski 1978).

The MRI requires a critical level of ionization to operate so that the gas is closely coupled to the magnetic field. This can be achieved if the temperature of the disc is higher than the critical $T > T_{\text{crit}} = 800 \text{ K}$ (Umebayashi 1983). In this case, the MRI operates at all disc heights. However, the temperature in the outer parts of the disc is lower than this. In this region, the disc surface layers may be ionized by external sources of ionization such as cosmic rays or X-rays from the central star to a maximum surface density depth of $\Sigma_{\text{crit}} = 200 \text{ g cm}^{-2}$ (e.g., Gammie (1996); Glassgold, Najita & Igea (2004)). If the total surface density of the disc is higher than this, $\Sigma > \Sigma_{\text{crit}}$, then there is a dead zone at the midplane with surface density $\Sigma_{\text{d}} = \Sigma - \Sigma_{\text{crit}}$ and the active layers have $\Sigma_{\text{a}} = \Sigma_{\text{crit}}$. Otherwise, if $\Sigma < \Sigma_{\text{crit}}$, then there is no dead zone layer so that $\Sigma_{\text{d}} = 0$ and $\Sigma_{\text{a}} = \Sigma$.

The MRI active layers have a Shakura & Sunyaev (1973) viscosity α parameter of 0.01 (e.g., Hartmann et al. (1998)). In our model, the dead zone has zero turbulence, unless it becomes self-gravitating. Turbulence in the dead zone could be driven by other sources such as hydrodynamic instabilities (including the baroclinic instability, Klahr & Bodenheimer (2003); Petersen, Julien & Stewart (2007); Lesur & Ogilvie (2010)) or be induced from the magnetohydrodynamic instability in the active surface layers (Fleming & Stone 2003; Simon, Armitage & Beckwith 2011; Gressel, Nelson & Turner 2012). However, we note that a small amount of turbulence within the dead zone does not significantly alter the qualitative disk structure and behavior (Martin & Lubow 2014). The conclusions of our work are not significantly affected by an additional source of turbulence within the dead zone, unless the source is strong enough to be able to produce a steady state disk. This would require a level of turbulence comparable to that produced by MRI (Martin & Lubow 2014).

We discuss the uncertainties associated with the α parameter in Section 3.5.

Gravitational turbulence requires the Toomre (1964) parameter to be less than the critical, $Q < Q_{\text{crit}} = 2$. While a dead zone is present in a protoplanetary disc, the flow through the disc is not steady because material accumulates in the dead zone. With sufficient material in the dead zone, it may become self gravitating, thus a small amount of turbulence may be driven. We include an additional viscous term in the surface density evolution equation and a heating term in the temperature equation. This extra heating in the massive dead zone can eventually cause the disc to reach the critical temperature required for the MRI. Once this is reached, there is a snow plough effect through the disc and the whole disc becomes MRI active in an outburst phase (Martin & Lubow 2013). As material drains on the star, the disc cools and the dead zone can re-form causing repeating outburst and quiescent cycles. Once the infall accretion rate onto the disc drops off, there may not be sufficient inflow through the disc for another outburst to occur, but there can still be a dead zone within the disc.

The infall accretion rate onto a forming star varies over time, although the details of the evolution depends on the specific disc model (e.g., Shu 1977; Basu 1998; Bate 2011; Kratter, Matzner & Krumholz 2008). However, it is thought that at early times the infall accretion rate is approximately $\dot{M}_{\text{infall}} = c_s^3/G$. Thus, assuming a cloud temperature $T \sim 10 \text{ K}$, the initial infall accretion rate is $\sim 10^{-5} M_{\odot} \text{ yr}^{-1}$. In this work, we consider several constant infall rates and thus analyze the disc structure at different evolutionary times. We choose three infall accretion rates onto the disc of $\dot{M}_{\text{infall}} = 2 \times 10^{-5}$, 1×10^{-6} , and $1 \times 10^{-8} M_{\odot} \text{ yr}^{-1}$.

We solve the accretion disc equations with 200 grid points spaced equally in $\log R$. For each infall accretion rate, we run the model until the disc reaches either a steady outburst cycle (for the two highest accretion rates), or a steady state (fully MRI active) disc solution (for the lowest accretion rate). These models represent different stages of the disc evolution. In Fig. 1 we show the surface density and temperature profiles for the disc as a function of radius at three different times for $\dot{M}_{\text{infall}} = 2 \times 10^{-5} M_{\odot} \text{ yr}^{-1}$. The first is a time immediately before an outburst, the second is during the outburst, and the third is immediately after the outburst. During this early phase of the disc evolution, the timescale between the outbursts is only $3 \times 10^3 \text{ yr}$. As we expect the accretion rate on to the disc to decrease exponentially over time, the timescale between the outbursts increases during the disc lifetime (see, e.g., Martin et al. 2012b). Furthermore, the radius of the temperature peak (the radius at which the disc becomes self-gravitating) moves inward over time (Martin & Lubow 2013). In Fig. 2 we show the surface density and temperature profiles corresponding to the different disk stages and infall accretion rates. For high accretion rates, the local thermal peak is present in the disk, and disappears for $\dot{M}_{\text{infall}} \sim 1 \times 10^{-8} M_{\odot} \text{ yr}^{-1}$ because there is no dead zone at this low accretion rate. The model behaves as a classical accretion disk without a dead zone (for a comparison see, e.g., Baillié et al. 2015, who found temperature and surface density profiles comparable to the model we use for a similar accretion rate value). The position of the thermal peak is also sensitive to the infall accretion rate. The model with $\dot{M}_{\text{infall}} = 1 \times 10^{-6} M_{\odot} \text{ yr}^{-1}$ is used as the nominal disk model in this work, and this corresponds to the model used in Martin & Lubow (2013). We note that there is some uncertainty in the value of Σ_{crit} such that it could be much smaller, which would mean that the temperature peak would exist for even lower accretion rates (see section 3.5 for more on this point).

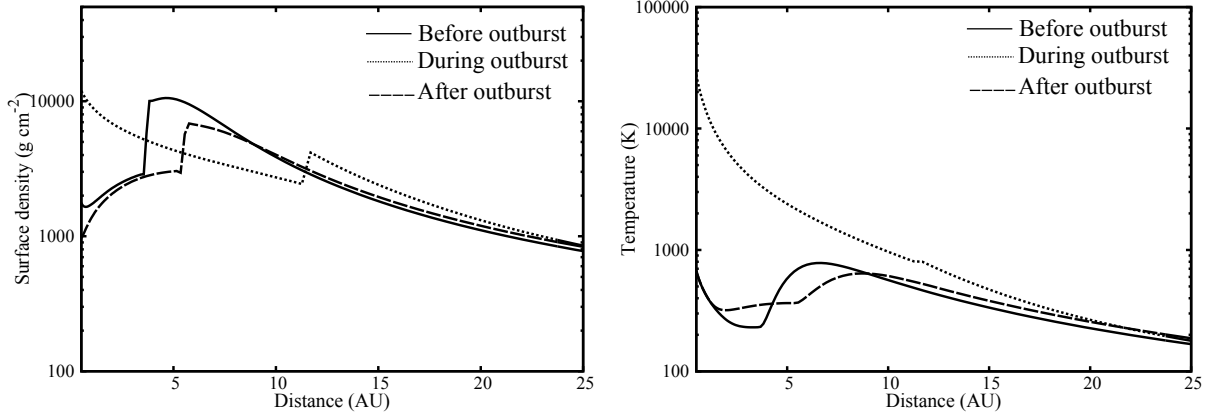


Fig. 1: Disk surface density (left panel) and temperature (right panel) structure for the high infall accretion rate $\dot{M}_{\text{infall}} = 2 \times 10^{-5} M_{\odot} \text{yr}^{-1}$. The profiles are shown just before, during, and just after an accretion outburst. The “during outburst” profile is used in the calculations corresponding to Fig. 4.

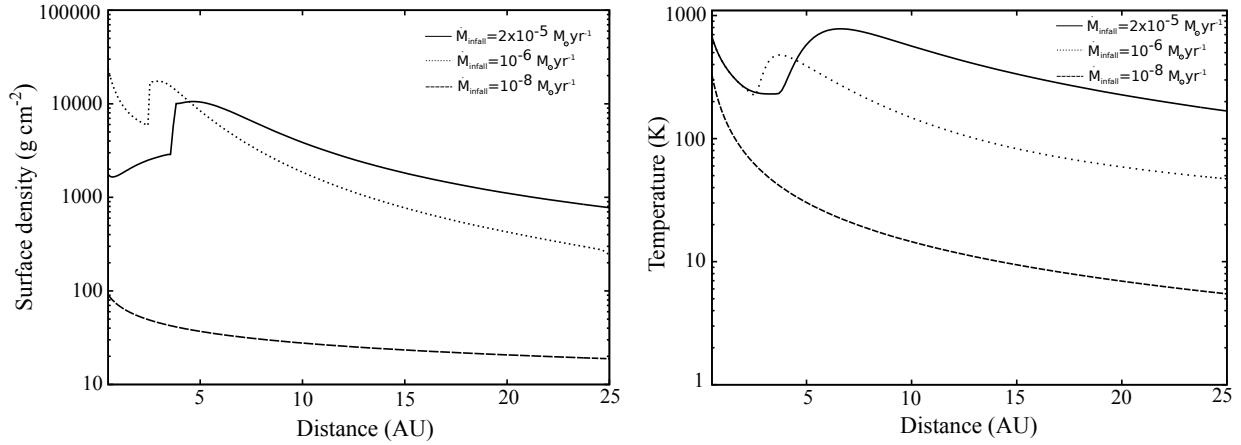


Fig. 2: Disk surface density (left panel) and temperature (right panel) for $\dot{M}_{\text{infall}} = 2 \times 10^{-5} M_{\odot} \text{yr}^{-1}$ (at a time just before an outburst), $10^{-6} M_{\odot} \text{yr}^{-1}$ (at a time between outbursts), and $M_{\text{infall}} = 10^{-8} M_{\odot} \text{yr}^{-1}$ (in steady state). The thermal gradient reversal observable in the right panel is the main element of the disk model. We use $\dot{M}_{\text{infall}} = 1 \times 10^{-6} M_{\odot} \text{yr}^{-1}$ as our nominal disk model.

2.2. The D/H evolution model

Dust and grains in the protoplanetary disk settle to the disc mid-plane within the dead zone layer as there is little or no turbulence there. Thus, we expect that the solar systems bodies formed in the dead zone layer. We couple the protoplanetary disk profiles to a classical 1-D D/H ratio evolution model. The D/H ratio in the dead zone layer is assumed to follow

$$\frac{\partial f}{\partial t} = kP(A - f) + \frac{1}{\Sigma_d R} \frac{\partial}{\partial R} \left(\kappa R \Sigma_d \frac{\partial f}{\partial R} \right) + \left(\frac{2\kappa}{\Sigma_d} \frac{\partial \Sigma_d}{\partial R} - V_R \right) \frac{\partial f}{\partial R} \quad (3)$$

(Drouart et al. 1999), where $k(T)$ is the rate of isotopic exchange, P is the gas pressure, $A(T)$ is the fractionation at equilibrium, and Σ_d is the gas surface density in the dead zone layer. The turbulent

diffusivity is

$$\kappa = \frac{\nu_d}{P_r}, \quad (4)$$

where ν_d is gas viscosity in the dead zone layer and P_r the Prandtl number. The parameter V_R is the radial gas velocity:

$$V_R = -\frac{3}{\Sigma_d R^{1/2}} \frac{\partial}{\partial R} (\nu_d \Sigma_d R^{1/2}) \quad (5)$$

(Pringle 1981). This equation is valid in the midplane dead zone layer assuming that $\Sigma_d \gg \Sigma_a$, which is satisfied in the disk profiles that we use (see section 3.5 for caveats). The viscosity due

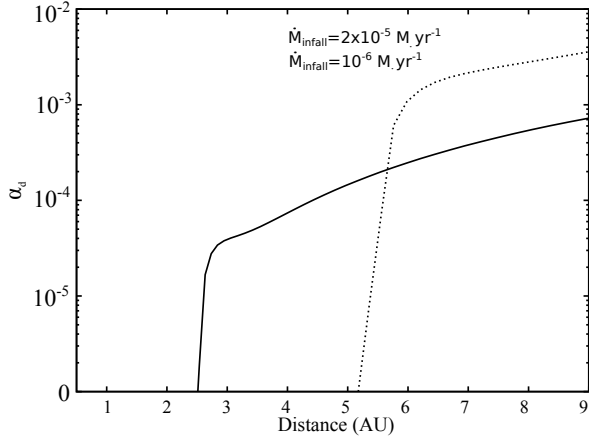


Fig. 3: Dead zone midplane turbulent viscosity parameter α_d . If the disc is not self-gravitating (i.e., $Q > Q_{\text{crit}}$), then $\alpha_d = 0$. Otherwise, its value is depicted by equation (7). We note that we manually smooth the viscosity variation (hence α_d) over five grid points to avoid code divergence. For $\dot{M}_{\text{infall}} = 10^{-6} M_{\odot} \text{yr}^{-1}$ the smoothing is between 2.2 and 2.5 AU and for $\dot{M}_{\text{infall}} = 2 \times 10^{-5} M_{\odot} \text{yr}^{-1}$ between 5.2 and 5.5 AU.

to the self-gravity in the dead zone layer is given by

$$v_d = \alpha_d \frac{C_s^2}{\Omega}, \quad (6)$$

where α_d is the turbulence parameter. Throughout this work α_d , Σ_d , and v_d are the parameters in the midplane (MRI inactive dead zone), and not the value in the MRI active disk surface. The parameter C_s is the speed of sound and Ω the gas Keplerian velocity. The sound speed is calculated with the midplane disc temperature profile. In this disk model, α_d is zero unless the disc locally satisfies $Q < Q_{\text{crit}}$, and then we have

$$\alpha_d = \begin{cases} \alpha \left[\left(\frac{Q_{\text{crit}}}{Q} \right)^2 - 1 \right] & \text{if } Q < Q_{\text{crit}} \\ 0 & \text{otherwise} \end{cases} \quad (7)$$

(Martin & Lubow 2011). We note that if we were to include an additional source of viscosity within the dead zone other than self-gravity, then we would add an additional term to this equation (see Martin & Lubow 2014). Figure 3 shows the viscosity parameter in the dead zone for the two highest disk infall accretion rates that we consider. This viscosity in the dead zone is much smaller than that in the active layers.

The first term on the right side of eq. 3 describes the chemical isotopic exchange between HDO and H_2 , and takes the pressure and temperature of the disk as the input. The second term describes the gas diffusion due to turbulence that depends on α and Σ . The third term describes the gas advection that is dependent on α , Σ , and V_R . In contrast with previous models, we do not neglect this term and we solve the entire equation. The effect of a temperature peak in the nebula in our model is thus controlled by the interplay of these terms. In the absence of turbulence, the first term dominates and the effect of the temperature peak is to decrease the local D/H ratio. However, if the turbulence is strong enough, the diffusion and advection terms erase this gradient. We run all simulations with $k(T)$ and $A(T)$ from (Lécluse & Robert

1994), and set P_r to 0.5 (Prinn 1990; Dubrulle & Frisch 1991) (although we note that any value of order unity will lead to qualitatively similar results).

An explicit forward-time centered-space (FTCS) scheme was first used to solve this equation. During tests in the case of a regular monotonic thermal profile, the code converged if a sufficiently small time step was used. When the new thermal profiles (with temperature gradient reversals) were used the code diverged even for very small time steps, except for almost vanishing turbulence. Thus, we employ semi-implicit (Crank-Nicholson) and fully implicit schemes to solve the equation over the same grid used in the disk model, but we take the water snow line (the radial location in the disc inside of which water is gaseous and outside is solid) that occurs at a temperature of around $T_{\text{snow}} = 170 \text{ K}$ (Lecar 2006) as the outer boundary, since the deuterium exchange can occur only in the vapor phase.

3. Results and discussions

Most simulations in the literature begin with a spatially constant $f = 25$, which is close to the highest value observed today in the solar system of 29–44 in LL3 meteorites (except Semarkona where a possible value of up to 100 was recently inferred (Piani et al. 2015)). However, since we are interested in the D/H ratio difference between two bodies rather than the absolute values, we begin our standard simulations with $f_0 = 15$, which is the average value found in comets. The model evolves from this value and we check the effect of the thermal gradient reversal on the D/H ratio profile. We are therefore implicitly assuming that another transient heating process decreases the initially very high (LL3 or even interstellar) D/H ratios to the lower values we are using as the initial condition. A possible process for this is the gravo-magneto disc instability (Martin & Lubow 2011) and its associated accretion outburst that we first test here (see also Owen & Jacquet 2015). The accretion outburst occurs when the local peak in the temperature profile becomes high enough and reaches the critical temperature, T_{crit} , required to trigger the MRI in the dead zone. During the outburst the disc becomes MRI active throughout and a large amount of material is accreted onto the Sun in a short time. After the outburst, the disk cools, the dead zone re-forms and – providing that there is sufficient accretion inflow – the cycle repeats.

We first run a test simulation with a disk profile representative of the conditions during an accretion outburst (for $\dot{M}_{\text{infall}} \sim 2 \times 10^{-5} M_{\odot} \text{yr}^{-1}$, see Fig. 1). We begin with an enrichment factor of $f_0 = 35$ (representing the very high D/H enrichment that can be found in LL3 or certain ISM environments). The viscosity parameter is $\alpha = 10^{-2}$ everywhere. Furthermore, this leads to the fast transport of material. Thus, there is very fast D/H ratio evolution as shown in Fig. 4, where cometary values are reached in the inner 10 AU over the timescale of an outburst. The outburst period lasts a few hundred to a few thousand years and during this time the D/H enrichment decreases to cometary or lower values in the inner disk, but remains high in the outer disk. These outbursts can happen multiple times during the disk phase and they alter the D/H ratio inhomogeneities that may have existed prior to the instability. For any process to have measurable effects on the D/H ratio today it has to happen after the last accretion outburst, when the disk infall rate from the cloud has dropped to values below certain threshold point. Thus, in the next section and for our standard model we consider the evolution at lower infall accretion rates.

3.1. Standard model

We now describe our standard model with an infall accretion rate of $\dot{M}_{\text{infall}} = 10^{-6} M_{\odot} \text{ yr}^{-1}$. We consider a time between outbursts as shown in Fig. 2. We assume that the last accretion outburst happened at an infall accretion rate of around $\dot{M}_{\text{infall}} \sim 1 \times 10^{-6} M_{\odot} \text{ yr}^{-1}$. Thus, the disk structure does not change rapidly after this. The dead zone accumulates material and heats up in the outer parts by self-gravity leading to the thermal gradient reversal, but without reaching a sufficiently high temperature (~ 800 K) to trigger a further outburst. Results for this model are shown in Fig. 5. We note that the D/H ratio decreases in mainly two locations: in the inner hot disk, and around the thermal peak centered at 3.5 AU. The width and limits of the D/H ratio dip around this region are controlled by the turbulence strength. We also note that in the inner disk, equilibrium is reached in less than 10^4 yr, faster than the evolution time of the disk, thus justifying the use of a snapshot disk model in this region. We discuss this further in Section 3.5. Finally, it should be noted that Fig. 5 shows f decreasing to values lower than the average cometary D/H in the outer disk at late times, but this is an artifact of our disk cooling handling as discussed in the next section.

3.2. Disk cooling and photoevaporation

As long as there is a hot region (T higher than ~ 400 K) along with turbulence within the disk, the global D/H ratio will continue to evolve until it reaches $A(T)$ ($f \sim 1$) throughout the disk (all water equilibrated to nebular gas D/H ratio). Such values of f for the entire disk are contradictory to observations. There are two possible explanations for this.

First, the disk could have cooled down sufficiently quickly for the D/H ratio profile to become frozen, as considered in the classical models (Mousis et al. 2000; Hersant et al. 2001). For low enough temperatures, the chemical exchange (through $k(T)$) becomes very slow and inefficient. The gas-gas reaction then stops completely once water condenses into ice. This needs to happen before the value of f in the chondrite region becomes too low. This is equivalent to the water snow line radius moving quickly inside the chondrite formation region. The snow line is the radial location in the disk inside of which water is gaseous, and outside of which solid, that occurs at a temperature of around $T_{\text{snow}} = 170$ K (Lecar 2006). For our standard model with an accretion rate of $\dot{M}_{\text{infall}} = 1 \times 10^{-6} M_{\odot} \text{ yr}^{-1}$, the snow line is at a radius of around 9 AU. The disk will remain in this state while \dot{M}_{infall} decreases over time and the snow line moves slowly inward (Martin & Livio (2012) and see equation 19 in Martin & Livio (2013)). For the disk parameters we have chosen, our model shows that when \dot{M}_{infall} reaches $\sim 10^{-8} M_{\odot} \text{ yr}^{-1}$, the disk will quickly become cool with a classical monotonic thermal profile with a snow line radius of around 1 AU (see Fig. 2, bottom panel). The infall accretion rate is given by

$$\dot{M}_{\text{infall}} = \dot{M}_i \exp\left(-\frac{t}{t_{\text{ff}}}\right) \quad (8)$$

(equation 19 in Martin et al. 2012b), where \dot{M}_i is the initial infall accretion rate (in this case we take $\dot{M}_i = 10^{-6} M_{\odot} \text{ yr}^{-1}$), t is time, t_{ff} is the free-fall timescale (we take $t_{\text{ff}} = 10^5 \text{ yr}$, e.g., Armitage et al. 2001). This equation shows that \dot{M}_{infall} will reach $\sim 10^{-8} M_{\odot} \text{ yr}^{-1}$ in about $5 \times 10^5 \text{ yr}$. We therefore stop our simulations at this time, and use the end state results to fit the measurements. We are therefore implicitly assuming that the transition to a cold classical MRI active disk happens quickly, with the snow-line moving in from the giant planet region to around 1 AU, thus

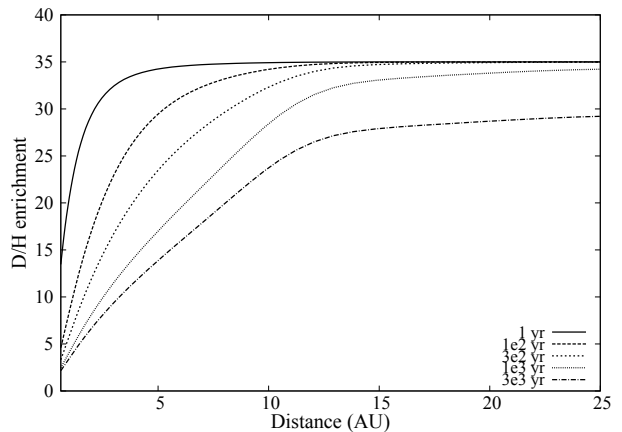


Fig. 4: Evolution of D/H ratio during an accretion outburst. This simulation starts with $f = 35$ as the initial condition to reflect the very high enrichment values often found in LL3 and certain ISM regions.

freezing the D/H ratio in the chondrite regions. The final D/H profile in Fig. 5 is thus in the solid phase.

The second explanation for how the D/H ratio profile became frozen is that the disk was completely photoevaporated on a similar timescale to the evolution of f . During the photoevaporation process at the end of the disk lifetime, the disk is dispersed on a short timescale of around 10^5 yr (Clarke et al. 2001; Alexander et al. 2006; Owen et al. 2010). Thus, the profile for the ratio of D/H would become fixed in the chondrites at this time and similarly, the shape of the profile shown in Fig. 2 would become fixed at this time.

3.3. Implications for chondrites

Now we discuss the implications of our model for chondrites. Figure 5 shows our nominal D/H profile obtained for our nominal model, with some known chondritic D/H ratio ranges. The profile shows a clear peak reaching $f \sim 15$ around 2 AU, followed by a dip reaching $f \sim 4$ around 3.5 AU. The curve then increases all the way to the cometary values. The absolute peak and dip positions with respect to the Sun in this plot are not very important, since they are sensitive to \dot{M}_{infall} , and thus can be varied (since the chondrite parent bodies probably formed slightly outward of these positions, to allow for S-type asteroids to form around 2.2 AU). We chose a single model for simplicity, and this particular value to remain consistent with Martin & Lubow (2013) to allow for comparison. As seen in Figure 5, this profile can fit the D/H values found in most chondrites, and explain their diversity from their formation location. Thus, this explains why CRs have a higher D/H value than other type of chondrites. The relative formation locations in this plot are also compatible with their water abundances (Wood 2005; Brearley 2006), although this abundance alone has its limitations due to the very nature of chondrites as an association of different components. Other indicators such as chondrule abundance should be taken into account. The CI and CM chondrites are more aqueously altered than CRs and OCs, which are more reduced. Assuming naively that water abundance increases with heliocentric distance (although see the dynamical water distribution models of e.g., Ciesla & Cuzzi (2006); Ali-Dib et al. (2014)), this implies

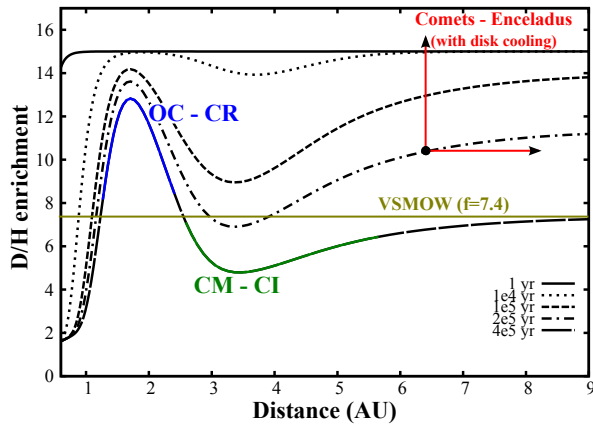


Fig. 5: Evolution of D/H ratio enrichment for our nominal disk. These profiles allow an important D/H ratio diversity in the chondrite formation region. They explain the values measured in the different chondrite families from their formation location. These inferred formation locations are also compatible with the water abundances of chondrites, with OCs and CRs containing less water (hence probably forming closer to the Sun) than CMs and CIs. The exact distance relative to the Sun is not important since the model is scalable with \dot{M}_{infall} . The D/H ratios in comets, Enceladus, and VSMOW (Earth) are shown for reference. Having f decreasing to low values in the cometary region at late times is an artifact of our disk cooling treatment and should be higher with a consistent treatment. Indeed, when the temperature drops below the water condensation point, we keep evolving f , letting it continue to drop, while it should be fixed at the value reached when the water became isolated from gas by freezing.

that CIs and CMs formed farther out than CRs and OCs, which is compatible with this profile, and was proposed by Wood (2005). We can also tentatively try to fit the remaining chondrite families (COs and CVs) that are more reduced than CMs but less than OCs. The D/H profile does contain regions that fit their values; however, we note that there are many uncertainties present in the model since it is only a proof of concept. A caveat in this model is that CIs form too close to CMs, although a distance of several AU might be needed between the formation locations of the two to allow the formation of chondrules.

3.4. Implications for comets

The next step is to check if such model can explain the D/H ratio diversity in comets. Naively one can expect that earlier in the disk lifetime, when \dot{M}_{infall} was higher, the thermal peak could have existed farther out in the disk, maybe in the comet region. This can lead to a D/H profile analogous to Fig. 5, but farther out in disk, with its own peak and dip. This dip can give a neat explanation for the relatively low D/H value in 103P/Hartley, with the other comets forming in other locations. Assuming a classical comet formation model with the JFCs forming farther out than OCCs, 103P/Hartley could have formed on the D/H dip, while 67P/C-G formed slightly farther out, outside of the dip, and the OCCs inside of it. To test this hypothesis we used a profile de-

rived from our disk simulation with $\dot{M}_{\text{infall}} = 2 \times 10^{-5} M_{\odot} \text{ yr}^{-1}$ corresponding to the time just before an outburst. The results are shown in Fig. 2 (top panel). At this stage of the disk evolution, the thermal reversal (and the corresponding D/H enrichment dip) are around 8 AU, farther out than in our canonical case, and as expected from an early disk. The thermal reversal's position, even for such a young disk, is still too close in to be relevant for comet formation. Another problem posed by this profile is that it almost certainly leads to an outburst, homogenizing the D/H ratio across the disk. Within the model and parameters that we use, we are unable to explain the low D/H ratio in 67P/C-G. The possibility that there is another set of parameters and/or assumptions within the same framework that can lead to a thermal reversal in the comet region is not excluded, however, and is left to future work. We note that all cometary D/H models assume that the value measured in the comet's ejecta reflect its bulk value, although Podolak et al. (2002) showed that the nuclei D/H ratio might be different than on the surface. Additionally, experiments by Brown et al. (2012) showed that the measured value might also change a function of the instrument-target distance.

Another seemingly unrelated problem that can be addressed using such models is the origin of crystal silicates and Calcium-Aluminum inclusions (CAIs) in comets. These minerals can form only at temperatures on the order of thousands of kelvins, but they are found in comets (Campins & Ryan 1989; Wooden et al. 2005; Chi et al. 2009; Kelley & Wooden 2009). How the high temperature minerals got to the cold region where comets form is a classic problem. Some of the proposed solutions are outward turbulent diffusion of particles (Bockelée-Morvan et al. 2002) and photophoresis (Mousis et al. 2007). The recent observation of narrow crystal silicates features in the spectra of a young solar-like star during an accretion outburst indicated that these outbursts might be the formation mechanism of high temperature minerals (Ábrahám et al. 2009). For the accretion outburst for $\dot{M}_{\text{infall}} \sim 2 \times 10^{-5} M_{\odot} \text{ yr}^{-1}$, the outburst trigger radius (the radius of the temperature peak) in our model is around 7 AU (see Fig. 1), considerably widening the high temperature mineral formation region. It should be mentioned that most materials inside the trigger radius get accreted onto the Sun during the accretion outburst, so only elements forming beyond this radius remain in the disk. Quantifying any of these possible solutions is beyond the scope of this work.

3.5. Caveats

Since this work was only intended to be a proof of principle highlighting the concept and quantifying the relative strengths of diffusion and chemistry in a non-monotonic nebula, numerous assumptions and simplifications were made in this model:

- Ideally, one should use a time evolving disk model coupled dynamically with the D/H module, to track the simultaneous evolution of both components. However, for simplicity we used a static (snapshot) disk profile with the time dependent D/H module. Hence, we are making the implicit assumption that the D/H ratio evolves on a shorter timescale than the disk. This assumption is justified by the short timescale of the D/H evolution ($10^4 - 10^5$ yr) compared to the disk evolution timescale ($\sim 10^6$ yr).
- Our disk profiles are derived from a layered (active and dead zones) disk. In this work, we only track the D/H ratio in the midplane (dead zone) and ignore any effect the active layer

might have, including the sedimentation of equilibrated water. Our work is thus valid only if the dead zone surface density is much higher than the active layer surface density. Since our domain starts beyond the dead zone inner boundary at 0.5 AU and extends out to the snow line radius at 9 AU (for the particular choice of the infall rate and thus disk age), much closer than the dead zone outer boundary at 23 AU. This validity condition for our model is thus applicable throughout the entire domain.

- We note that there are several unknown parameters in the layered disc model. For example, the critical surface density that is ionized by external sources is not well determined. Dead zone models that include more physics generally find active layer surface densities that may be very small (e.g., Bai (2011)). However, such small active layers cannot explain accretion rates observed in T Tauri stars (e.g., Perez-Becker & Chiang (2011); Martin et al. (2012b)). Thus we fold all of the uncertainty into the parameter Σ_{crit} . The value of α in the active layers is also not well determined. However, these parameters do not affect the qualitative behavior of the disc.
- In this work we started our main simulation (Fig. 5) from a constant D/H value throughout the disk. Realistically, however, the preceding outburst may lead to a heterogeneous D/H distribution. Quantifying this effect needs a fully time dependent coupled disk-D/H evolution, for a smooth temperature variation to occur. This is left for future work.
- Recently, 2D (r-z) steady-state models of protoplanetary discs have been constructed with an α -variation over the disc height to mimic the effects of a reduced (but non-zero) α in a dead zone (Bitsch et al. 2014). These disc models do not find the increase in temperature in the dead zone region present in our disc models because self-gravity does not operate. There is not a sufficient buildup of material in their disc models to cause the disc to become self-gravitating because the chosen values for α are high enough for a steady state disc to be found. Martin & Lubow (2014) showed that even with some turbulence in the dead zone, the qualitative disc behavior is as we have described in this paper, unless the turbulence in the dead zone is comparable to that in the active layer where a steady state may be found. Previous 2D (r-z) simulations that are time-dependent and included a dead zone with a smaller viscosity agree with the numerical models used in this work (Zhu et al. 2009). Additional detailed magnetohydrodynamic time-dependent numerical simulations are required in order to determine the correct value of α in the dead zone (see, e.g., Simon et al. 2013).
- In our simplified model, we set the viscosity in the dead zone to zero, except where it is generated by self-gravity. It is possible for other hydrodynamical instabilities to operate in the dead zone (for example the baroclinic instability and vertical shear instability (Turner et al. 2014)). However, as discussed by Martin & Lubow (2014), the qualitative disc behavior is the same even if there is a small amount of turbulence in the dead zone. The temperature peak is still there, and the outbursts still occur.

4. Conclusions

We have coupled a D/H enrichment code including diffusion, advection, and chemical exchange to snapshots from a protoplanetary disk model that includes a dead zone. The disk model contains a local temperature peak at a radius of around 3 AU due to the heating by self-gravity in the outer parts of the dead zone.

We found that this leads to a dip in the D/H profile around the same region, in contrast with the classical monotonic D/H models. The new profile can explain the origin of the D/H ratio variations between the different chondrite families. We propose that CI chondrites (which have a relatively low D/H ratio) formed in the region of the thermal gradient reversal, but CRs (which have a high D/H ratio) formed just inside this region. The new D/H profile also accommodates the formation of COs, CVs, and CMs. However, even with a younger disk profile the model is unable to explain the D/H ratio in 67P/C-G. The thermal gradient reversal is too close to the Sun to be relevant. Finally, we proposed that the accretion outbursts associated with these models can explain the presence of high temperature minerals across the disk.

This work shows that detailed temperature profiles from time-dependent layered disk models provide a potential explanation for the rich variation of D/H ratios found in the solar system. A more detailed understanding of the role the thermal inversions in dead zones and outbursts plays in shaping the chemistry of the nebula necessitate a more elaborate exploration of the parameter space, and should be the subject of future works.

Acknowledgements. Special thanks go to D. Bockelée-Morvan and E. Lellouh for useful discussions on comets. We thank the two anonymous referees for useful comments. M.A.-D was supported by a grant from the city of Besançon. O.M. acknowledges support from CNES. This work has been partly carried out thanks to the support of the A*MIDEX project (n° ANR-11-IDEX-0001-02) funded by the “Investissements d’Avenir” French Government program, managed by the French National Research Agency (ANR). JIL acknowledges support from the JWST program through a grant from NASA Goddard.

References

- Ábrahám, P., Juhász, A., Dullemond, C. P., et al. 2009, *Nature*, 459, 224
 Alexander, R. D., Clarke, C. J., & Pringle, J. E. 2006, *MNRAS*, 369, 229
 Alexander, C. M. O. ’., Newsome, S. D., Fogel, M. L., et al. 2010, *Geochim. Cosmochim. Acta*, 74, 4417
 Alexander, C. M. O. ’., Bowden, R., Fogel, M. L., et al. 2012, *Science*, 337, 721
 Ali-Dib, M., Mousis, O., Petit, J.-M., & Lunine, J. I. 2014, *ApJ*, 785, 125
 Altwegg, K., Balsiger, H., Bar-Nun, A., et al. 2015, *Science*, 347, A1261952
 Armitage, P. J., Livio, M., & Pringle, J. E. 2001, *MNRAS*, 324, 705
 Bai, X.-N. 2011, *ApJ*, 739, 50
 Baillié, K., Charnoz, S., & Pantin, E. 2015, *A&A*, 577, A65
 Balbus, S. A., & Hawley, J. F. 1991, *ApJ*, 376, 214
 Basu S., 1998, *ApJ*, 509, 229
 Bate M. R., 2011, *MNRAS*, 417, 2036
 Bockelée-Morvan, D., Gautier, D., Hersant, F., Huré, J.-M., & Robert, F. 2002, *A&A*, 384, 1107
 Bitsch, B., Morbidelli, A., Lega, E., Kretke, K., & Crida, A. 2014, *A&A*, 570, A75
 Brasser, R., & Morbidelli, A. 2013, *Icarus*, 225, 40
 Brearley, A. J. 2006, *Meteorites and the Early Solar System II*, 584
 Brown, P. D., & Millar, T. J. 1989, *MNRAS*, 237, 661
 Brown, R. H., Lauretta, D. S., Schmidt, B., & Moores, J. 2012, *Planet. Space Sci.*, 60, 166
 Campins, H., & Ryan, E. V. 1989, *ApJ*, 341, 1059
 Cannizzo, J. K. 1993, *ApJ*, 419, 318
 Ceccarelli, C., Caselli, P., Bockelée-Morvan, D., et al. 2014, *Protostars and Planets VI*, 859
 Chapman, C. R. 1996, *Meteoritics and Planetary Science*, 31, 699
 Chi, M., Ishii, H. A., Simon, S. B., et al. 2009, *Geochim. Cosmochim. Acta*, 73, 7150
 Ciesla, F. J., & Cuzzi, J. N. 2006, *Icarus*, 181, 178
 Clarke, C. J., Gendrin, A., & Sotomayor, M. 2001, *MNRAS*, 328, 485
 Cleaves, L. I., Bergin, E. A., Qi, C., Adams, F. C., Öberg, K. I. 2015, *ApJ*, 799, 204
 Dartois, E., Thi, W.-F., Geballe, T. R., et al. 2003, *A&A*, 399, 1009
 Drouart, A., Dubrulle, B., Gautier, D., & Robert, F. 1999, *Icarus*, 140, 129
 Dubrulle, B., & Frisch, U. 1991, *Phys. Rev. A*, 43, 5355
 Dzyurkevich, N., Turner, N. J., Henning, T., & Kley, W. 2013, *ApJ*, 765, 114
 Fleming T., Stone J. M., 2003, *ApJ*, 585, 908
 Fromang, S., Terquem, C., & Balbus, S. A. 2002, *MNRAS*, 329, 18

- Gammie, C. F. 1996, *ApJ*, 457, 355
- Glassgold, A. E., Najita, J., Igea, J. 2004, *ApJ*, 615, 972
- Gressel O., Nelson R. P., Turner N. J., 2012, *MNRAS*, 422, 1140
- Gressel, O., Turner, N. J., Nelson, R. P., & McNally, C. P. 2015, *ApJ*, 801, 84
- Hartmann, L., Calvet, N., Gullbring, E., & D'Alessio, P. 1998, *ApJ*, 495, 385
- Hartogh, P., Lis, D. C., Bockelée-Morvan, D., et al. 2011, *Nature*, 478, 218
- Hersant, F., Gautier, D., & Huré, J.-M. 2001, *ApJ*, 554, 391
- Jacquet, E., & Robert, F. 2013, *Icarus*, 223, 722
- Kavelaars, J. J., Mousis, O., Petit, J.-M., & Weaver, H. A. 2011, *ApJ*, 734, LL30
- Kelley, M. S., & Wooden, D. H. 2009, *Planet. Space Sci.*, 57, 1133
- Klahr H. H., Bodenheimer P., 2003, *ApJ*, 582, 869
- Kratter K. M., Matzner C. D., Krumholz M. R., 2008, *ApJ*, 681, 375
- Lecar M., Podolak M., Sasselov D., Chiang E., 2006, *ApJ*, 640, 1115
- Lécluse, C., & Robert, F. 1994, *Geochim. Cosmochim. Acta*, 58, 2927
- Lellouch, E., Bézard, B., Fouchet, T., et al. 2001, *A&A*, 370, 610
- Lesur G., Ogilvie G. L., 2010, *MNRAS*, 404, L64
- Lodato, G., Rice, W. K. M. 2004, *MNRAS*, 351, 630
- Lynden-Bell D., Pringle J. E., 1974, *MNRAS*, 168, 603
- Martin, R. G., & Lubow, S. H. 2011, *ApJ*, 740, LL6
- Martin R. G., Livio M., 2012, *MNRAS*, 425, L6
- Martin, R. G., Lubow, S. H., Livio, M., & Pringle, J. E. 2012a, *MNRAS*, 420, 3139
- Martin, R. G., Lubow, S. H., Livio, M., & Pringle, J. E. 2012b, *MNRAS*, 423, 2718
- Martin, R. G., & Lubow, S. H. 2013, *MNRAS*, 432, 1616
- Martin, R. G., & Livio, M. 2013, *MNRAS*, 434, 633
- Martin R. G., Lubow S. H., 2014, *MNRAS*, 437, 682
- Morbidelli, A. 2008, *Saas-Fee Advanced Course 35: Trans-Neptunian Objects and Comets*, 79
- Mousis, O., Gautier, D., Bockelée-Morvan, D., et al. 2000, *Icarus*, 148, 513
- Mousis, O., Petit, J.-M., Wurm, G., et al. 2007, *A&A*, 466, L9
- Mothé-Diniz, T., Carvano, J. M. á., & Lazzaro, D. 2003, *Icarus*, 162, 10
- Mumma, M. J., & Charnley, S. B. 2011, *ARA&A*, 49, 471
- Owen, J. E., Ercolano, B., Clarke, C. J., & Alexander, R. D. 2010, *MNRAS*, 401, 1415
- Owen, J. E., & Jacquet, E. 2015, *MNRAS*, 446, 3285
- Paczynski, B. 1978, *Acta Astron.*, 28, 91
- Parise, B., Du, F., Liu, F.-C., et al. 2012, *A&A*, 542, L5
- Perez-Becker, D., & Chiang, E. 2011, *ApJ*, 727, 2
- Petersen M. R., Julien K., Stewart G. R., 2007, *ApJ*, 658, 1236
- Piani, L., Robert, F., & Remusat, L. 2015, *Earth and Planetary Science Letters*, 415, 154
- Podolak, M., Mekler, Y., & Prialnik, D. 2002, *Icarus*, 160, 208
- Pringle, J. E. 1981, *ARA&A*, 19, 137
- Pringle, J. E., Verbunt, F., & Wade, R. A. 1986, *MNRAS*, 221, 169
- Prinn, R. G. 1990, *ApJ*, 348, 725
- Robert, F., & Epstein, S. 1982, *Geochim. Cosmochim. Acta*, 46, 81
- Robert, F. 2006, *Meteorites and the Early Solar System II*, 341
- Shakura, N. I., & Sunyaev, R. A. 1973, *A&A*, 24, 337
- Shu F. H., 1977, *ApJ*, 214, 488
- Simon J. B., Armitage P. J., Beckwith K., 2011, *ApJ*, 743, 17
- Simon J. B., Bai X.-N., Stone J. M., Armitage P. J., Beckwith K., 2013, *ApJ*, 764, 66
- Spencer, J. R., Barr, A. C., Esposito, L. W., et al. 2009, *Saturn from Cassini-Huygens*, 683
- Toomre, A. 1964, *ApJ*, 139, 1217
- Turner, N. J., Fromang, S., Gammie, C., et al. 2014, *arXiv:1401.7306*
- Umebayashi, T. 1983, *Progress of Theoretical Physics*, 69, 480
- Walsh, K. J., Morbidelli, A., Raymond, S. N., O'Brien, D. P., & Mandell, A. M. 2011, *Nature*, 475, 206
- Waite, J. H., Jr., Lewis, W. S., Magee, B. A., et al. 2009, *Nature*, 460, 487
- Wood, J. A. 2005, *Chondrites and the Protoplanetary Disk*, 341, 953
- Wooden, D. H., Harker, D. E., & Brearley, A. J. 2005, *Chondrites and the Protoplanetary Disk*, 341, 774
- Yang, L., Ciesla, F. J., & Alexander, C. M. O. . 2013, *Icarus*, 226, 256
- Zhu, Z., Hartmann, L., & Gammie, C. 2009, *ApJ*, 694, 1045
- Zhu Z., Hartmann L., Gammie C. F., Book L. G., Simon J. B., Engelhard E., 2010, *ApJ*, 713, 1134

4.6 Perspectives: Dead zones and the formation of Jupiter

As discussed in chapter 1, the origin of the volatiles enrichment mechanism in Jupiter is still an open question, along with the corresponding formation location of the giant planet. Here I propose a possible solution in the framework of the dead zone disk model discussed above and based on the original idea of Lodders (2004). I advance a mechanism capable of transforming the water snowline (or any other sharp viscosity transition region) into a “tar line”. The formation of Jupiter on this new tar line, along with the hydrogen depletion in the envelope discussed by Lodders (2004) can explain the observed chemical composition of Jupiter, and is compatible with its dynamical evolution and our current understanding of disks.

4.6.1 A pressure trap on the snowline ?

Condensation fronts have always been associated with planetary formation and composition. The diffusion and subsequent condensation of water vapor across its snowline has been proposed as a mechanism for solids enrichment at this region (the cold finger effect) (Stevenson and Lunine, 1988). Furthermore, the formation of Uranus and Neptune on the CO iceline has been invoked as an explanation for their elemental and isotopic compositions (Ali-Dib et al. (2014b), cf. chapter 3 of this manuscript) . A newly studied aspect of the water snowline though is the possible presence of a gas pressure trap (gas positive pressure maxima) at its location (Kretke and Lin, 2007; Brauer et al., 2008), assuming the disk’s midplane is in a dead zone state. The effects of this pressure bump on the chemical properties of planets have not been studied. In this section, I investigate if this pressure trap present at the water snowline can act as a tar line by trapping the inward drifting refractory solids, turning this location into a “tar line”. This would lead to a solids density increase in this location, augmented further by cold finger effect (Ali-Dib et al., 2014a). I want to check if a planet forming in this region will have a chemical composition similar to Jupiter.

I discussed in section 4.2 the layered accretion model Gammie (1996) and many others, where the disk surface is MRI active with the turbulent $\alpha \sim 10^{-2}$ and the midplane is a region of weaker turbulence ‘dead’ zone with α usually taken to be $\sim 10^{-4}$. MRI suppression in disks is caused mainly by dust that serves as the main recombination source by removing the free electrons from the gas (Turner et al., 2007). Dust density however is location dependent, since it increases by a factor 4 beyond the snowline due to water condensation. Assuming a vertically isothermal disk, the ionization fraction should get lower once we cross the snowline, decreasing the surface density of the active layer, while increasing that of the dead zone. In this case, the midplane pressure is given by:

$$P = \Sigma_g c_s^2 / (2\pi H) \quad (4.1)$$

where Σ_g is the dead zone surface density, c_s the speed of sound, and H is the scale height. In this model, Σ_g will increase suddenly outside of the snowline, reversing the pressure

gradient over a narrow region and leading to a local pressure maxima. This maxima will stop the particles inward drift via gas drag. Let $\tau_s \equiv t_{stop}\Omega$ be the dimensionless stopping time, where t_{stop} is the damping timescale for particles motion relative to the gas. Particles with $\tau_s \approx 1$ (centimetric to decimetric pebbles at 3-5 AU) will feel strong gas drag and drift following the gas pressure gradient (Weidenschilling, 1977; Youdin, 2010) :

$$v_r = \frac{1}{2\rho} \frac{\partial P}{\partial r} \Omega_k^{-1} \quad (4.2)$$

where v_r is the radial velocity of the drifting particles relative to the gas. In a classical monotonic pressure gradient, particles will drift inward toward to sun. In the presence of a pressure maxima, as the one we assumed exists on the snowline, their drift will be reversed and they will get trapped around this narrow region leading to a local increase in solids density.

4.6.2 Jupiter's formation region initial chemical composition

With temperatures in the order of 150 K, no major volatile other than water can condense in the region around the water snowline (Fray and Schmitt, 2009). This implies that the material concentrating on the pressure trap is mostly of refractory nature. Two types of bodies containing refractory materials are thought to have formed in the giant planets region: C-type asteroids and Oort cloud comets (OCC). C-type asteroids are thought to be the parent bodies of CI chondrites, and thus the composition of these meteorites is used as a proxy to understand C-type asteroids. To date, 1P/Halley is the only comet studied in situ, and thus is our only proxy to the refractory composition of comets. The following is a summary of current knowledge about the chemistry of the giant planets region.

Carbon

CI chondrites, on average, are depleted in carbon by an order of magnitude with respect to the solar value (Lodders, 2003). One can assume that the remaining carbon was in volatiles (CO and CO₂), but comets (from all dynamical families) observations show that these volatiles can only account for up to 50% in molar abundance with respect to the solar value (in terms of C/O ratio), although the value varies from a comet to another and can be an order of magnitude lower (Mumma and Charnley, 2011). This implies That the remaining carbon (at least $\sim 50\%$ of solar molar abundance) must be in the cometary carbonaceous refractories. In Halley, when normalized to Mg, 80% of carbon is in the refractory dust (Jessberger et al., 1988; Encrenaz and Knacke, 1991). For this reason, I will assume that an individual refractory solid particle drifting inward and then trapped in the pressure maxima contains 0.5 to $0.8 \times$ solar carbon abundance. The gaseous carbon component will thus contain 0.2 to $0.5 \times$ solar carbon abundance.

Sulfur

On the other hand, sulfur is much trickier. Refractory sulfur in CI chondrites has an almost solar abundance (Lodders, 2003), implying a low fraction in volatiles. In comets, the volatile phase of sulfur (H_2S) represent at most up to 2/3 the solar abundance, although (as in the case of volatile carbons) can be much lower. In Halley though, all sulfur is in refractories at almost $1.5\times$ solar abundance. This anomalous value is usually attributed to ion yielding issues in the data analysis, making these results less than fully reliable. Sulfur was also detected in the dust samples returned from Wild 2 by Stardust. The CI normalized value was found to be ~ 0.17 (Flynn et al., 2006), much lower than in Halley and too low to account for the remaining sulfur along with volatiles. Whether this value is real or caused by capture heating is not settled (Zolensky et al., 2006; Bockelée-Morvan, 2011). With all this uncertainty, I am going to assume that the particles captures in the pressure trap have a 0.5 to $1\times$ solar value, which is needed to obtain the Jovian abundances. The gaseous sulfur component will thus contain 0 to $0.5\times$ solar sulfur abundance. These values are compatible with the model of Pasek et al. (2005).

Nitrogen

The origin of nitrogen in the solar system bodies is very controversial. In CI chondrites, nitrogen (in its refractory phases) is depleted by 2 orders of magnitude with respect to the solar value. One would then expect the very volatile N_2 to be the major nitrogen bearing specie in the nebula. However, nitrogen is also very depleted in comets (Rubin et al., 2015), although N_2 has the same volatility as the much more abundant CO (Fray and Schmitt, 2009). For these reasons, I will assume that nitrogen in the nebula is only under gaseous N_2 form, and that its depletion in comets is related to their formation processes (Mousis et al., 2012).

Phosphorus

As discussed in section 1.3.1, Phosphorus is present in an almost solar abundance in chondrites, but not definitively detected through its volatile phase PH_3 in comets. I hence assume that trapped particles have a solar abundance of phosphorus.

Other elements

Since most other volatile elements (H, He, Ne, Ar, Kr and Xe) are extremely depleted with respect to solar value in both comets and CI chondrites, I assume that they are absent from the trapped solids and present only in gaseous form in solar abundance throughout the giant planets region. All of these species will initially be present in solar molar abundances (with respect to H_2) in the planet's envelope.

Table 4.1: The chemical composition of the snowline region in this model, normalized to the solar abundances, and relative to solar and depleted hydrogen abundances. Carbon and sulfur model predictions were obtained by adding the solids enriched value to the calculated volatiles component. Jupiter’s measured composition is also included for comparison.

Element	X/H ₂	0.5 × H ₂	Measurements
H ₂	≡ 1.0	≡ 0.5	≡ 1.0
He	1	2	0.72
Ne	1	2	0.12
Ar	1	2	1.8 - 3.4
Kr	1	2	1.6 - 2.8
Xe	1	2	1.6 - 2.8
C	1.5 - 1.8	3 - 3.6	3.2 - 5.5
N	1	2	2 - 6
P	2	4	3.0 - 3.7
S	1.5 - 2	3 - 4	2.2 - 3.6

The snowline’s region final composition

To estimate the final chemical composition of the snowline pressure trap region we need to assess the amount of solids present in the pressure trap. In this model, we need an increase by a factor of ~ 2 in refractory carbons. This is the same order of magnitude found by Ida and Lin (2008) for the increase in the solids surface density due to the pressure trap. I hence assume that the solid phase beyond the snowline is twice above the solar value. The final chemical composition of this region is shown in Table 4.1 along with the measured Jovian composition.

4.6.3 The role of water

Water is the biggest question mark related to Jupiter. Although it is probably the most important element for giant planets formation, its abundance in Jupiter is currently unknown. In the model I presented, water should be among the solids concentrating on the snowline and later accreted by the planet. This should lead, assuming a solar water abundance in solids, to a final factor 4 enrichment in Jupiter (after hydrogen depletion). However, this is far from being the only source of water in Jupiter, where the cold finger effect can play a significant role increasing further the water (and total solids) abundance in this region. However, we need to first understand how do pressure traps affect this effect.

The basic physical mechanism behind the cold finger effect is the vapor’s turbulence driven diffusion across the snowline following its concentration gradient. This basic effect is robust and should take place as long as turbulence and the snowline are present in the disk. Quantitatively, diffusion is governed by:

$$\frac{\partial c}{\partial t} - \frac{2D}{r} \frac{\partial c}{\partial r} - D \frac{\partial^2 c}{\partial r^2} + S(r, t) = 0 \quad (4.3)$$

where c is the vapor normalized concentration, S a source function and D the diffusion coefficient. Turbulence is introduced to this system via D , usually taken to be equal to the disk's turbulent viscosity ν :

$$D \sim \nu \quad (4.4)$$

where:

$$\nu = \alpha c_s H \quad (4.5)$$

with α the free dimensionless turbulence parameter. Any effect the pressure trap will have on vapor diffusion will be via ν . The pressure trap fundamentally is caused by the change in α just outside of the snowline. In a naive and simple picture of a nebula with a very sharp snowline transition and razor thin pressure trap, the dust density increase just outside of the snowline will decrease α in this region, but won't affect the turbulence just inside of the snowline. Vapor in this case will thus diffuse across the snowline and condensate, then encounter the lower turbulence region. The pressure trap is thus not expected to affect the vapor diffusion. However, its effect on the newly condensed dust is more interesting. Once vapor has crossed the snowline, it will condense on the already present solids in this region increasing their size, possibly all the way to centimetric pebbles (Ros & Johansen, 2013). These pebbles however are outward of the pressure trap, and thus can't drift inward to sublimate. The pressure trap will indirectly act as a sink for the vapor inside of the snowline since once they have condensed into large particles, their inward drift is inhibited. This "diode-like" effect allowing one-way transport of material should increase further the total solids density just outside of the snowline, assisting in the planet's core formation, and lead to a very oxygen rich giant planet.

If for any reason this effect is muted, the planet will anyhow have the \sim factor 4 oxygen enrichment discussed above, and should not in any case be bulk depleted below the solar value.

4.6.4 Caveats & Discussions

Summary

The Jupiter formation model I presented in this section can be summarized as follows:

1. The formation of a pressure trap on the water snowline due to the turbulence strength variation.
2. This pressure trap will increase (double) the amount of solids in this region by capturing inward drifting pebbles.
3. The enhanced solids abundance will stimulate the formation of planetesimals leading to Jupiter's core.
4. The core will then proceed to accrete its envelope via standard core accretion mechanisms.

5. Once formed, the hydrogen in the envelope will get locked up in the interior forming the metallic hydrogen layer, what increases the relative abundance with respect to hydrogen of all elements in the envelope.

We finally end up with an atmosphere with the chemical composition showed in Table 4.1. Jupiter's noble gases, in addition to carbon, sulfur and phosphorus are well accounted. Nitrogen on the other hand lays just within the measured lower value. If the measured mean nitrogen abundance is indeed the average bulk planetary value, this implies a shortcoming for this model. However, the large uncertainty on the value however precludes me from any interpretations.

Caveats

This work is still in its preliminary phases. More efforts and detailed quantitative modeling are needed in order to strengthen the presented case. In its current form, two main caveats can be identified:

- The presence of a pressure trap on the snowline: recent work by Bitsch et al. (2014) and others show that a very sharp viscosity transition is needed for the pressure trap to form. Whatever such transition is present at the water snowline is still an open question with further work needed in order to verify and quantify this issue. However, This scenario does not need to take place at the water snowline, since any pressure trap can do. Recent works show for example how sharp viscosity transitions can result in a Rossby wave instability leading to an anticyclonic vortices that can trap present and drifting pebbles (Lyra et al., 2008, 2009). These viscosity transitions can be found for example on the inner and outer edges of dead zones.
- The differential hydrogen locking in the metallic interior: as stated by Lodders (2004), a first order molecular to metallic transition is needed to allow for a preferential filtration of elements. It is not proved however that such a transition exists, although it is not excluded (Hubbard et al., 2002),

Perspectives

This model's main predictions, Jupiter's water and nitrogen abundances, are to be verified by *Juno* (Bolton, 2010) or more refined indirect observations (Wang et al., 2015). A bulk water abundance of more than $10 \times$ solar can result from the discussed one way water transport effect, while my inferred bulk nitrogen abundance is $2 \times$ solar only. N_2 trapping in clathrate-hydrates however can increase the nitrogen abundance further, if for some reason the temperature became low enough (~ 45 K) in this area to allow clathration to take place (although cf. Rubin et al. (2015)).

This model assumes that Jupiter's chemical composition is dominated by the solid core's. This however contradicts the scenario of Ali-Dib et al. (2014a) explaining the composition of carbon rich Jupiters through gaseous envelope dominated composition, and that

assumes the core to be decoupled from the envelope. It is possible that several formation channels for Jupiters exists, leading to different compositional outcomes. More precise spectroscopic data on exo-Jupiters is necessary for models refinements, as those we expect to get with the E-ELT and the JWST. My model can also be investigated further in the future for predictions related to the Jovian satellites.

Bibliography

- Agúndez, M., Biver, N., Santos-Sanz, P., Bockelée-Morvan, D., Moreno, R. 2014. Molecular observations of comets C/2012 S1 (ISON) and C/2013 R1 (Lovejoy): HNC/HCN ratios and upper limits to PH₃. *Astronomy and Astrophysics* 564, LL2.
- Agúndez, M., Cernicharo, J., Decin, L., Encrenaz, P., Teyssier, D. 2014. Confirmation of Circumstellar Phosphine. *The Astrophysical Journal* 790, LL27.
- Alexander, C. M. O. '., Bowden, R., Fogel, M. L., Howard, K. T., Herd, C. D. K., Nittler, L. R. 2012. The Provenances of Asteroids, and Their Contributions to the Volatile Inventories of the Terrestrial Planets. *Science* 337, 721.
- Ali-Dib, M., Mousis, O., Petit, J.-M., Lunine, J. I. 2014. Carbon-rich Planet Formation in a Solar Composition Disk. *The Astrophysical Journal* 785, 125.
- Ali-Dib, M., Mousis, O., Petit, J.-M., Lunine, J. I. 2014. The Measured Compositions of Uranus and Neptune from their Formation on the CO Ice Line. *The Astrophysical Journal* 793, 9.
- Alibert, Y., Mousis, O., Mordasini, C., Benz, W. 2005. New Jupiter and Saturn Formation Models Meet Observations. *The Astrophysical Journal* 626, L57-L60.
- Altwegg, K., and 31 colleagues 2015. 67P/Churyumov-Gerasimenko, a Jupiter family comet with a high D/H ratio. *Science* 347, 1261952.
- Armitage, P. J. 2011. Dynamics of Protoplanetary Disks. *Annual Review of Astronomy and Astrophysics* 49, 195-236.
- Asplund, M., Grevesse, N., Sauval, A. J., Scott, P. 2009. The Chemical Composition of the Sun. *Annual Review of Astronomy and Astrophysics* 47, 481-522.
- Atreya, S. K., Mahaffy, P. R., Niemann, H. B., Wong, M. H., Owen, T. C. 2003. Composition and origin of the atmosphere of Jupiter - an update, and implications for the extrasolar giant planets. *Planetary and Space Science* 51, 105-112.
- Balbus, S. A., Hawley, J. F. 1991. A powerful local shear instability in weakly magnetized disks. I - Linear analysis. II - Nonlinear evolution. *The Astrophysical Journal* 376, 214-233.

- Bitsch, B., Morbidelli, A., Lega, E., Kretke, K., Crida, A. 2014. Stellar irradiated discs and implications on migration of embedded planets. III. Viscosity transitions. *Astronomy and Astrophysics* 570, A75.
- Bockelée-Morvan, D. 2011. An Overview of Comet Composition. *IAU Symposium* 280, 261-274.
- Bolton, S. J. The Juno Mission. *IAU Symposium* 269, 92-100.
- Brasser, R., Morbidelli, A. 2013. Oort cloud and Scattered Disc formation during a late dynamical instability in the Solar System. *Icarus* 225, 40-49.
- Brauer, F., Henning, T., Dullemond, C. P. 2008. Planetesimal formation near the snow line in MRI-driven turbulent protoplanetary disks. *Astronomy and Astrophysics* 487, L1-L4.
- Brearley, A. J. 2006. The Action of Water. *Meteorites and the Early Solar System II* 584-624.
- Brown, R. H., Lauretta, D. S., Schmidt, B., Moores, J. 2012. Experimental and theoretical simulations of ice sublimation with implications for the chemical, isotopic, and physical evolution of icy objects. *Planetary and Space Science* 60, 166-180.
- Ciesla, F. J. 2015. Sulfidization of Iron in the Dynamic Solar Nebula and Implications for Planetary Compositions. *The Astrophysical Journal* 800, LL6.
- Duncan, M., Quinn, T., Tremaine, S. 1987. The formation and extent of the solar system comet cloud. *The Astronomical Journal* 94, 1330-1338.
- Encrenaz, T., Knacke, R. 1991. Carbonaceous compounds in comets - Infrared observations. *IAU Colloq. 116: Comets in the post-Halley era* 167, 107-137.
- Feuchtgruber, H., and 11 colleagues 2013. The D/H ratio in the atmospheres of Uranus and Neptune from Herschel-PACS observations. *Astronomy and Astrophysics* 551, AA126.
- Flynn, G. J., and 79 colleagues 2006. Elemental Compositions of Comet 81P/Wild 2 Samples Collected by Stardust. *Science* 314, 1731.
- Fray, N., Schmitt, B. 2009. Sublimation of ices of astrophysical interest: A bibliographic review. *Planetary and Space Science* 57, 2053-2080.
- Gammie, C. F. 1996. Layered Accretion in T Tauri Disks. *The Astrophysical Journal* 457, 355.
- Gautier, D., Hersant, F., Mousis, O., Lunine, J. I. 2001. Enrichments in Volatiles in Jupiter: A New Interpretation of the Galileo Measurements. *The Astrophysical Journal* 550, L227-L230.

- Gounelle, M., Spurný, P., Bland, P. A. 2006. The orbit and atmospheric trajectory of the Orgueil meteorite from historical records. *Meteoritics and Planetary Science* 41, 135-150.
- Guillot, T., Hueso, R. 2006. The composition of Jupiter: sign of a (relatively) late formation in a chemically evolved protosolar disc. *Monthly Notices of the Royal Astronomical Society* 367, L47-L51.
- Hartogh, P., and 12 colleagues 2011. Ocean-like water in the Jupiter-family comet 103P/Hartley 2. *Nature* 478, 218-220.
- Hersant, F., Gautier, D., Lunine, J. I. 2004. Enrichment in volatiles in the giant planets of the Solar System. *Planetary and Space Science* 52, 623-641.
- Hubbard, W. B., Burrows, A., Lunine, J. I. 2002. Theory of Giant Planets. *Annual Review of Astronomy and Astrophysics* 40, 103-136.
- Ida, S., Lin, D. N. C. 2008. Toward a Deterministic Model of Planetary Formation. V. Accumulation Near the Ice Line and Super-Earths. *The Astrophysical Journal* 685, 584-595.
- Jessberger, E. K., Christoforidis, A., Kissel, J. 1988. Aspects of the major element composition of Halley's dust. *Nature* 332, 691-695.
- Kley, W., Nelson, R. P. 2012. Planet-Disk Interaction and Orbital Evolution. *Annual Review of Astronomy and Astrophysics* 50, 211-249.
- Kretke, K. A., Lin, D. N. C. 2007. Grain Retention and Formation of Planetesimals near the Snow Line in MRI-driven Turbulent Protoplanetary Disks. *The Astrophysical Journal* 664, L55-L58.
- Krot, A. N., and 15 colleagues 2009. Origin and chronology of chondritic components: A review. *Geochimica et Cosmochimica Acta* 73, 4963-4997.
- Lodders, K. 2003. Solar System Abundances and Condensation Temperatures of the Elements. *The Astrophysical Journal* 591, 1220-1247.
- Lodders, K. 2004. Jupiter Formed with More Tar than Ice. *The Astrophysical Journal* 611, 587-597.
- Lyra, W., Johansen, A., Klahr, H., Piskunov, N. 2008. Embryos grown in the dead zone. Assembling the first protoplanetary cores in low mass self-gravitating circumstellar disks of gas and solids. *Astronomy and Astrophysics* 491, L41-L44.
- Lyra, W., Johansen, A., Zsom, A., Klahr, H., Piskunov, N. 2009. Planet formation bursts at the borders of the dead zone in 2D numerical simulations of circumstellar disks. *Astronomy and Astrophysics* 497, 869-888.

- Martin, R. G., Lubow, S. H. 2013. Propagation of the gravo-magneto disc instability. *Monthly Notices of the Royal Astronomical Society* 432, 1616-1622.
- Martin, R. G., Livio, M. 2014. On the Evolution of the CO Snow Line in Protoplanetary Disks. *The Astrophysical Journal* 783, LL28.
- Monga, N., Desch, S. 2015. External Photoevaporation of the Solar Nebula: Jupiter's Noble Gas Enrichments. *The Astrophysical Journal* 798, 9.
- Morbidelli, A. 2008. Comets and Their Reservoirs: Current Dynamics and Primordial Evolution. *Saas-Fee Advanced Course 35: Trans-Neptunian Objects and Comets* 79-164.
- Morbidelli, A., Levison, H. F., Gomes, R. 2008. The Dynamical Structure of the Kuiper Belt and Its Primordial Origin. *The Solar System Beyond Neptune* 275-292.
- Mousis, O., Guilbert-Lepoutre, A., Lunine, J. I., Cochran, A. L., Waite, J. H., Petit, J.-M., Rousselot, P. 2012. The Dual Origin of the Nitrogen Deficiency in Comets: Selective Volatile Trapping in the Nebula and Postaccretion Radiogenic Heating. *The Astrophysical Journal* 757, 146.
- Mousis, O., Lunine, J. I., Madhusudhan, N., Johnson, T. V. 2012. Nebular Water Depletion as the Cause of Jupiter's Low Oxygen Abundance. *The Astrophysical Journal* 751, L7.
- Mousis, O., and 50 colleagues 2014. Scientific rationale for Saturn's in situ exploration. *Planetary and Space Science* 104, 29-47.
- Mumma, M. J., Charnley, S. B. 2011. The Chemical Composition of Comets—Emerging Taxonomies and Natal Heritage. *Annual Review of Astronomy and Astrophysics* 49, 471-524.
- Owen, T., Mahaffy, P., Niemann, H. B., Atreya, S., Donahue, T., Bar-Nun, A., de Pater, I. 1999. A low-temperature origin for the planetesimals that formed Jupiter. *Nature* 402, 269-270.
- Pasek, M. A., Milsom, J. A., Ciesla, F. J., Lauretta, D. S., Sharp, C. M., Lunine, J. I. 2005. Sulfur chemistry with time-varying oxygen abundance during Solar System formation. *Icarus* 175, 1-14.
- Qi, C., Öberg, K. I., Wilner, D. J., D'Alessio, P., Bergin, E., Andrews, S. M., Blake, G. A., Hogerheijde, M. R., van Dishoeck, E. F. 2013. Imaging of the CO Snow Line in a Solar Nebula Analog. *Science* 341, 630-632.
- Ros, K., & Johansen, A. 2013, *A&A*, 552, A137
- Rubin et al. 2015. *Science* DOI: 10.1126/science.aaa6100

- Scott, E. R. D. 2007. Chondrites and the Protoplanetary Disk. *Annual Review of Earth and Planetary Sciences* 35, 577-620.
- Stevenson, D. J., Lunine, J. I. 1988. Rapid formation of Jupiter by diffuse redistribution of water vapor in the solar nebula. *Icarus* 75, 146-155.
- Turner, N. J., Sano, T., Dziourkevitch, N. 2007. Turbulent Mixing and the Dead Zone in Protostellar Disks. *The Astrophysical Journal* 659, 729-737.
- Turner, N. J., Fromang, S., Gammie, C., Klahr, H., Lesur, G., Wardle, M., Bai, X.-N. 2014. Transport and Accretion in Planet-Forming Disks. *Protostars and Planets VI* 411-432.
- Walsh, K. J., Morbidelli, A., Raymond, S. N., O'Brien, D. P., Mandell, A. M. 2011. A low mass for Mars from Jupiter's early gas-driven migration. *Nature* 475, 206-209.
- Wang, D., Gierasch, P. J., Lunine, J. I., Mousis, O. 2015. New insights on Jupiter's deep water abundance from disequilibrium species. *Icarus* 250, 154-164.
- Wasson, J. T., Kallemeyn, G. W. 1988. Compositions of chondrites. *Royal Society of London Philosophical Transactions Series A* 325, 535-544.
- Weidenschilling, S. J. 1977. Aerodynamics of solid bodies in the solar nebula. *Monthly Notices of the Royal Astronomical Society* 180, 57-70.
- Weiss, B. P., Elkins-Tanton, L. T. 2013. Differentiated Planetesimals and the Parent Bodies of Chondrites. *Annual Review of Earth and Planetary Sciences* 41, 529-560.
- Wood, J. A. 2005. The Chondrite Types and Their Origins. *Chondrites and the Protoplanetary Disk* 341, 953.
- Wooden, D. H., Harker, D. E., Brearley, A. J. 2005. Thermal Processing and Radial Mixing of Dust: Evidence from Comets and Primitive Chondrites. *Chondrites and the Protoplanetary Disk* 341, 774.
- Youdin, A. N. 2010. From Grains to Planetesimals. *EAS Publications Series* 41, 187-207.
- Zolensky, M. E., and 74 colleagues 2006. Mineralogy and Petrology of Comet 81P/Wild 2 Nucleus Samples. *Science* 314, 1735.

Conclusions & perspectives

Summary

Several subjects have been addressed in this manuscript. The central common idea is that the chemical composition of both small and large bodies depend on the physical properties of disks such as their density and temperature profiles, particles growth rates, and turbulence. We saw in chapters 2-3 that for standard turbulence strengths, the outward diffusion of vapors following their concentration gradients across their iceline will overcome the inward replenishment of these vapors through pebbles drift and sublimation. Vapors are thus depleted inside of their icelines on a timescale proportional to the sun-iceline distance squared. This implies that water will be depleted much faster than CO inside the water snowline, increasing the gas phase C/O ratio in this region to near unity and allowing giant planets accreting their envelopes here through migration to have a near unity C/O ratio and subsolar C/H ratio regardless of the disk's initial values, assuming no core-envelope mixing.

Another implication of this vapor depletion is an increase of the corresponding ices densities in the regions just beyond the icelines. My calculations showed that on a timescale of 10^5 yr (or 10^6 yr for a dead zone), the CO ices density will increase by a factor around 40 times nominal value in the 0.5 AU just beyond the CO iceline. I proposed hence that Uranus and Neptune formed in this region, allowing these planets to obtain their carbon rich atmospheres. Since the N_2 is few AU further out from the CO iceline, Uranus and Neptune formation region will be poor in nitrogen as measured in their atmospheres. Finally, Assuming most of the water in their interior originated as dissolved CO, I retrieved the D/H ratios measured in these planets.

In chapter 4 I showed how the non monotonic thermal profile in layered disk models caused by the residual turbulence in the autogravitating part of the dead zone can lead to a non monotonic D/H profile in the chondrites regions and potentially explain the values diversity observed between the different families.

Chapters 2-4 showed that parameters directly controlling physical (in contrast with chemical) properties of the disk can have far reaching and measurable consequences on its chemical composition. The total amount of turbulence in the midplane for example can control the C/O ratio in the gas to be accreted by the giant planets. The effect of turbulence in this case be negated only by a very low pebbles formation timescale, allowing them to replenish the vapor fast enough. The turbulence's profile and radial dependency

on the other hand can lead to measurable variations in the D/H ratio of water to be accreted by the chondritic parent bodies. Finally, As discussed at the end of chapter 4, the pressure profile can allow the formation of solids pressure traps increasing the local metallicity of the region and any planet forming on it.

The take-away message of this thesis, if any, hence is:

The static and dynamical physical properties of disks can affect seemingly unrelated aspects of their chemical properties, and lead to a diversity in the planets and small bodies composition.

Perspectives

Future work: Toward a global picture

A major methodological difference between the models presented in chapters 2-3 and chapter 4 is the used protoplanetary disk model, where we assumed a classical fully turbulent 1+1D disk with an outward advective nebula in the first, and a layered disk with a dead zone in the second. Of course any given disk can only be in one of these two states at a time. Since both Uranus & Neptune and chondrites are components of our own solar system, a more consistent approach should be considered. I showed in Fig. 5 of the published paper in chapter 3 that the vapor depletion inside of the CO iceline persist even if we consider low turbulence amount such as these found in the a dead zone, since both particles growth and vapor diffusion will take longer times. What was not considered however is the possibility of strong spatial variations in the amount of turbulence in the disk, such as the case presented in chapter 4. This is left for future work. It will be also interesting to check the effect of the resulting non monotonic thermal profile on the cold finger effect along with the possibility it entails of the presence of multiple icelines for the same chemical specie in the disk. The time dependency of the presence and position of these icelines and the influence it has on the chemical composition of the disk is also worth investigating. Another point of comparison is the accretion details in chapters 2 and 3. Both models (in addition to the Jupiter formation model in chapter 4), allow the planets to accrete their cores in situ, and then their envelopes during their inward migration. A difference between the two cases was the consideration that WASP 12b's measured composition depend solely on its accreted gaseous envelope, whereas Uranus and Neptune's depend on their core's composition. This difference can be partly justified by the nature of these planets. WASP 12b is a massive Jovian planet who's mass is dominated by its envelope and so can be its composition. Uranus and Neptune on the other hand are dominated in both mass and composition by their cores. Future studies taking into account the interior structure of these planets is necessary to validate these assumptions. Finally, In chapter 4 I assumed the disk to be in the post-outbursts phase. These accretional outbursts should remove an very important fraction of the disk's mass into the star. The effect of these outbursts on the planets formation has not been studied

yet, and the study of their chemical effects on the disk are still preliminary. Further work in this direction is also needed.

Another future direction worth pursuing is in the field of astrobiology. In this thesis I discussed the distribution of volatiles and their influence of the planets formations. Volatile elements however can have other crucial roles, since most major elements necessary for life as we know it such as carbon, hydrogen, nitrogen, oxygen and sulfur (with the notable exception of phosphorus) exist in the disk mainly as volatiles. The amount and form of these elements delivered to terrestrial planets depend strongly on their form and distribution in the disk. The classical definition of a planetary habitable zone is the region around the star where the temperature allows the existence of stable liquid water on a planet's surface, assuming sufficient atmospheric pressure. However, we know that this is not the only important factor. On earth, the presence of sufficient amounts of C, H, O, N, P and S elements in accessible reservoirs was crucial to allow life to evolve. Studying volatiles delivery and evolution on terrestrial planets is also a research direction I would like to take in the future.

Open questions

Lots of work remain to be done in this still young but very promising field. A plethora of data is expected soon from the upcoming space missions such as *Juno* currently en route to Jupiter, and the next generation telescopes such as the *E-ELT* and the *JWST*. These new instruments will give much more detailed informations on the chemical compositions of exoplanets and our own solar system, allowing us for the first time to perform statistical analysis to find general trends. The following is a list of related questions I would love to see settled in the next couple of decades:

1. What is the bulk water abundance in Jupiter? Is it supersolar as expected from models or subsolar as indicated by some exoplanets observations and recent tropospheric CO interpretations? This will probably be answered by *Juno* in 2016. *Juno* is equipped with a microwave radiometer designed in order to measure Jupiter's emission in wavelengths ranging from 1.3 to 50 cm. This will allow an estimation of the bulk water abundance of the planet's interior, showing at least if it's depleted or enriched with respect to the solar value. An enrichment will be a triumph for formation models, while a depletion will send us back to the drawing boards. *Juno* might also measure the deep nitrogen abundance, also very useful to constraint models. The Gravity Science instrument on the other hand might allow us a better characterization of Jupiter's core. This will constraint the formation models relying on the interior processes/differentiation of Jupiter to explain its composition. The lunch of the *HST* successor *JWST* is planned for 2018, six years before the *E-ELT* sees first light. These two instruments will cover wavelengths ranging from the optical to the mid-IR range with unprecedented sensitivity. I hope that these instruments will allow a much more precise determination of the water abundance in hot Jupiters. These results can then be compared with *Juno*'s. A similarity (in terms of depletion

vs enrichment) would entail a universal Jupiter-like planets formation scenario, but a difference would indicate several formation/evolution channels for these planets.

2. Where was all of the nitrogen present during the planetary formation phase and why none of it is conserved in today's comets or asteroids ? If it was present only as gas how did it get enriched in Jupiter ? I discussed in this manuscript how nitrogen is absent from CI chondrites and comets under all forms, but might be enriched in Jupiter. If Jupiter's core accreted from a 67P/CG like building blocks, then it should have been also depleted in nitrogen. A first step toward understanding the nitrogen chemistry of the nebula will lay again in *Juno*. If it does confirm the nitrogen enrichment found using *Galileo* and *Cassini*, then this problem will become much more pressing. A more robust determination of the nitrogen abundance in Uranus and Neptune can also reveal an important piece of the puzzle. If Jupiter turns indeed to be enriched in nitrogen while Uranus and Neptune are truly depleted, this hints strongly to the model I proposed in chapter 3. If however these measurements turn out to be imprecise, then a revision of the models is necessary.
3. Why still haven't we found any comet with D/H lower than Earth's VSMOW ? The D/H ratio was measured in the last two decades in a plethora of comets from different dynamical families. However, 103P/Hartley is the only one found with a VSMOW value, all of the other comets are at least factor 2 above it. Is there any physical or chemical reason stopping comets from having low D/H values ? and on a more speculative tone is there a reason why the lowest cometary D/H value found is precisely the Earth's VSMOW value or is it a mere coincidence/bias ? Moreover, why is this seemingly random value found at the same time in a large number of CI chondrites in addition to comet 103P/Hartley ? Answering these questions necessitate first insuring that no bias is present in our cometary sample. More precise observations are needed for a more detailed D/H picture, particularly for JFCs. If this turns out to be real, then a lot of information on the thermal profile in the comets region of the protosolar nebula, in addition to early solar system dynamics, can be inferred.
4. How do super-Earths and mini-Neptunes form and why are they totally absent from our solar system although being the most abundant planetary type in our part of the galaxy ? Is it a stochastic event or more related to the properties of our protosolar nebula ? Our sun is a very typical star and was probably surrounded by a very typical disk. Following this logic, then a super-Earth should have been formed in our solar system, so why it didn't ? Or was it ejected later as predicted by some dynamical models ?
5. On a more speculative note, do massive planets (super-Earths and larger) form randomly in the disk or with higher probability in special locations (snowlines, deadzones edges ..) as I propose in chapters 3 and 4 ? If this is the case, can this lead to a statistical composition trend to be seen in exoplanets ? How does this relate

to the absence of a super-Earth from our solar system ? If super-Earths do form on the inner edge of the deadzone (at several tenths of an AU) as many proposed, and our Uranus & Neptune on the CO iceline, does not this imply universal processes at play ? Lots of new data on this subject are expected soon, again with the *E-ELT* and the *JWST*, but also with the next phase ALMA. ALMA already hinted into enhanced solids growth near the main icelines, this is crucial and need to be verified with future high angular resolution observations. I suggest either CO abundance measurement in HL Tau, or multi wavelengths continuum emission very high angular resolution observations in TW Hya to start with, in order to verify the hypothesis we I proposed at the end of chapter 2.

A lot will happen in the next couple of decades in this thriving and fast moving field of science. While I certainly hope for the mysteries enshrouding planets formation theory to unravel, the curious child inside of me certainly only wish for more puzzles.

Other peer reviewed contributions

- **Ali-Dib, M.**, Mousis, O., Pekmezci, G. S., Lunine, J. I., Madhusudhan, N., Petit, J.-M. 2014. Influence of the C/O ratio on titanium and vanadium oxides in protoplanetary disks. *Astronomy and Astrophysics* 561, A60.
- Ellinger, Y., Pauzat, F., Mousis, O., Guilbert-Lepoutre, A., Leblanc, F., **Ali-Dib, M.**, Doronin, M., Zicler, E., Doressoundiram, A. 2015. Neutral Na in Cometary Tails as a Remnant of Early Aqueous Alteration. *The Astrophysical Journal* 801, L30.
- Guilbert-Lepoutre, A., Besse, S., Mousis, O., **Ali-Dib, M.**, Höfner, S., Koschny, D., Hager, P. 2015. On the Evolution of Comets. *Space Science Reviews* 23.
- Lellouch, E., **Ali-Dib, M.**, Jessup, K.-L., Smette, A., Käufel, H.-U., Marchis, F. 2015. Detection and characterization of Io's atmosphere from high-resolution 4- μ m spectroscopy. *Icarus* 253, 99-114.
- Mousis, O., and 50 colleagues 2014. Scientific rationale for Saturn's in situ exploration. *Planetary and Space Science* 104, 29-47.
- Mousis, O., Lunine, J. I., Fletcher, L. N., Mandt, K. E., **Ali-Dib, M.**, Gautier, D., Atreya, S. 2014. New Insights on Saturn's Formation from its Nitrogen Isotopic Composition. *The Astrophysical Journal* 796, L28.
- Mousis, O., and 59 colleagues 2014. Instrumental methods for professional and amateur collaborations in planetary astronomy. *Experimental Astronomy* 38, 91-191.
- Mousis, O., and 10 colleagues 2015. Methane Clathrates in the Solar System. *Astrobiology* 15, 308-326.
- Pauzat, F., Ellinger, Y., Mousis, O., **Ali-Dib, M.**, Ozgurel, O. 2013. Gas-phase Sequestration of Noble Gases in the Protosolar Nebula: Possible Consequences on the Outer Solar System Composition. *The Astrophysical Journal* 777, 29.
- Willacy, K., and 14 colleagues 2015. The Composition of the Protosolar Disk and the Formation Conditions for Comets. *Space Science Reviews* 49.

Appendices

Appendix A

Chapter 2: numerical methods

A.1 Vapor diffusion

Let's consider the vapor diffusion equation

$$\frac{\delta c}{\delta t} - \frac{2D}{r} \frac{\delta c}{\delta r} - D \frac{\delta^2 c}{\delta r^2} + S(r, t) = 0 \quad (\text{A.1})$$

The forward difference of the left part gives:

$$\frac{\partial c}{\partial t} = \frac{c_i^{n+1} - c_i^n}{\Delta t} \quad (\text{A.2})$$

where Δt is the time step. A centered differentiation of the first order spatial component can be expressed by:

$$\frac{\partial c}{\partial r} = \lambda \frac{(c_{i+1}^{n+1} - c_{i-1}^{n+1})}{2\Delta x} + (1 - \lambda) \frac{(c_{i+1}^n - c_{i-1}^n)}{2\Delta x} \quad (\text{A.3})$$

where Δx is the spatial step between two grid points and:

$$\lambda = \begin{cases} 0.5 & \text{for a semi implicit (Crank-Nicolson) scheme} \\ 0 & \text{for a fully explicit (FTCS) scheme} \\ 1 & \text{for a fully implicit scheme} \end{cases}$$

we can similarly center differentiate the second order spatial component into:

$$\frac{\partial^2 c}{\partial r^2} = \lambda \frac{(c_{i+1}^{n+1} - 2c_i^{n+1} + c_{i-1}^{n+1})}{\Delta x^2} + (1 - \lambda) \frac{(c_{i+1}^n - 2c_i^n + c_{i-1}^n)}{\Delta x^2} \quad (\text{A.4})$$

we now define:

$$a = \frac{2D}{R} \frac{1}{2} \frac{\Delta t}{\Delta x} \quad (\text{A.5})$$

with $a_1 = \lambda a$ and $a_2 = (1 - \lambda)a$, and similarly:

$$b = D \frac{\Delta t}{\Delta x^2} \quad (\text{A.6})$$

with $b_1 = \lambda b$ and $b_2 = (1 - \lambda)b$.

Equation A.1 translates as:

$$c_i^{n+1} - c_i^n = a_1(c_{i+1}^{n+1} - c_{i-1}^{n+1}) + a_2(c_{i+1}^n - c_{i-1}^n) + b_1(c_{i+1}^{n+1} - 2c_i^{n+1} + c_{i-1}^{n+1}) + b_2(c_{i+1}^n - 2c_i^n + c_{i-1}^n) \quad (\text{A.7})$$

which we factorize into:

$$\begin{aligned} & c_{i+1}^{n+1}(-a_1 - b_1) + c_i^{n+1}(1 + 2b_1) + c_{i-1}^{n+1}(+a_1 - b_1) \\ &= c_{i+1}^n(a_2 + b_2) + c_i^n(1 - 2b_2) + c_{i-1}^n(-a_2 + b_2) + S(r, t)\Delta t \end{aligned} \quad (\text{A.8})$$

we now define $A = (-a_1 - b_1)$, $B = (1 + 2b_1)$, $C = (+a_1 - b_1)$, and D as the entire term to the right of the equal sign. A , B , C , and D are all function of r . This equation can be written in the tridiagonal matrix form:

$$\begin{bmatrix} B_1 & C_1 & 0 & 0 & \dots & 0 \\ A_2 & B_2 & C_2 & 0 & \dots & 0 \\ 0 & A_3 & B_3 & C_3 & 0 & \\ \vdots & \vdots & \vdots & \vdots & \vdots & \vdots \\ 0 & \dots & 0 & A_{SL} & B_{SL} \end{bmatrix} \begin{bmatrix} c_{1,n+1} \\ c_{2,n+1} \\ \vdots \\ c_{SL,n+1} \end{bmatrix} = \begin{bmatrix} D_1 \\ D_2 \\ \vdots \\ D_{SL} \end{bmatrix}$$

where $A_1, B_1..$ are the values at the inner border, and $A_{SL}, B_{SL}..$ are the values at the snowline (SL). The values at both ends (boundary conditions) should be taken in advance, either through an assumption or precise knowledge. At the inner border the matrix gives:

$$B_1 c_1^{n+1} + C_1 c_2^{n+1} = D_1 \quad (\text{A.9})$$

Let's define the flux at the inner border as:

$$F = \frac{c_2^{n+1} - c_1^{n+1}}{r_2 - r_1} \quad (\text{A.10})$$

and take for this particular case a null flux condition at the inner border. This implies:

$$c_1^{n+1} = c_2^{n+1} \quad (\text{A.11})$$

leading to the inner border limit condition:

$$B_1 = 1, C_1 = -1, D_1 = 0 \quad (\text{A.12})$$

At the outer border we have:

$$A_{SL} c_{SL-1}^{n+1} + B_{SL} c_{SL}^{n+1} = D_{SL} \quad (\text{A.13})$$

where vapor will cross the snowline and get removed. This implies an outer boundary condition of $c_{SL}^{n+1} = 0$, giving:

$$A_{SL} = 0, B_{SL} = 1, D_{SL} = 0 \quad (\text{A.14})$$

Equation A.1 can now be solved efficiently using a Thomas matrix reversal algorithm.

A.2 Gas drag

Let's consider the set of equations governing gas drag in a turbulent nebula:

$$2\overline{v_\phi} - \frac{\overline{v_r}}{\Omega_k t_{s*}} = -\frac{1}{\overline{\rho}} \frac{\partial \overline{P}}{\partial r} \frac{1}{\Omega_k} \quad (\text{A.15})$$

$$2\overline{v_r} + \frac{\overline{v_\phi}}{\Omega_k t_{s*}} = -\overline{V_r} - 3r^{-1/2} \frac{\partial}{\partial r} \left(r^{1/2} \frac{\nu}{Sc} \right) + \frac{(D - 3\nu)}{Sc} \frac{1}{\overline{\rho_d}} \frac{\partial \overline{\rho_d}}{\partial r} \quad (\text{A.16})$$

These are a set of 2 coupled non linear equations with v_r and v_ϕ as unknowns. To solve these equations we first assumed $D = 3\nu$, thus nullifying the last term of the second equation. The non linearity of these equations reside in the stopping time t_{s*} and the Schmidt number Sc .

In the case of the Epstein regime (Fig. A.1), we have:

$$t_s = \frac{s\rho_s}{\rho_g C_s} \quad (\text{A.17})$$

where s is the particle's radius and ρ_s its density, ρ_g the gas density and C_s the speed of sound. The only non linear dependency in this case is thus in Schmidt number defined as:

$$Sc = (1 + \Omega_k t_s) \sqrt{1 + v_{drift}^2 / V_t^2} \quad (\text{A.18})$$

where $v_{drift} = \sqrt{v_r^2 + v_\phi^2}$ and V_t is the gas turbulent velocity. Assuming $v_{drift} \ll V_t$, Sc dependency on the system's variables is removed. This is justified by the high turbulent velocities we get from our disk model ($\sim 10^4$ cm/s), much higher than any expected drift velocity. We get finally in the case of Epstein regime a system of coupled linear equations that can be solved simply with a Gauss-Johnson algorithm.

In the case of the Stokes regime on the other hand, t_s is always dependent on the problem's variables and the system is non linear. We hence use a globally convergent Newton method to solve this system of equations, while maintaining the full non approximated Schmidt number equation.

Reynolds number $Re = 2s\rho v/\eta$	Stokes law $\lambda < 4s/9$	Epstein law $\lambda > 4s/9$
$Re < 1$	$F_D = 24Re^{-1}F$	$F_D = \frac{4\pi}{3}\rho s^2 v C_s$
$1 < Re < 800$	$F_D = 24Re^{-0.6}F$	
$Re > 800$	$F_D = 0.44F$	
$F = \pi s^2 \rho \frac{v^2}{2}$		

Figure A.1: The different drag laws as a function of the particle's radius and gas mean free path.

A.3 Pebbles sublimation

Let's consider the sublimation law:

$$\frac{\partial R}{\partial t} = \frac{-0.63 \times v_s P_p}{\sqrt{2\pi m k T}} \quad (\text{A.19})$$

This equation need to be solved in order to obtain the time needed for the initial particle radius to decrease to zero. Initially, a typical Euler scheme was used, where we quantified the equation into:

$$\frac{\Delta R}{\Delta t} = \frac{-0.63 \times v_s P_p}{\sqrt{2\pi m k T}} \quad (\text{A.20})$$

giving finally:

$$R_{t+1} = \frac{-0.63 \times v_s P_p}{\sqrt{2\pi m k T}} \times \Delta t + R_t \quad (\text{A.21})$$

where R_t is the particle's radius at time t . Equation A.21 is then evolved by replacing R_t with R_{t+1} (starting with $R_{t=0}$ as the pebble's initial radius) at each iteration till it reaches zero. The (number of iterations) $\times \Delta t$ will then be the time required for the particle to sublimate. The Euler method is a first order scheme, and its global truncation error is proportional to the step size to the power one. Therefore, small step sizes are needed for accurate results. However, due to the simplicity of the used sublimation law with its very slow (relative to the time step) dependency on the temperature (that evolves following the particle's position, hence on gas drag timescale), the Euler method should be accurate enough.

A.4 Putting the pieces together

A.4.1 The model's flowchart

The algorithm will first take the particle's size, chemical identity and gas advective law (inward or outward) as input. It will then calculate the particle's relative (drift)

and total speeds. In the particle's total speed is inward, these informations are then inputted into the sublimation module that will calculate the time this drifting particle needs to completely sublimate (t_{sub}), in addition to the sublimation distance (r_{sub}). If the particle's total speed is outward, then the coagulation module is invoked, where it will calculate the time this particle needs in order to grow into an inward drifting pebble (t_{coag}), supposing a constant dust surface density. The total replenishment time is then defined as $t_{tot}^{rep} = t_{coag} + t_{sub} + t_{drift}$, and is taken as input along with r_{sub} for the vapor diffusion module's source function defined as:

$$S(t) = \frac{c_{SL}^s}{t_{tot}} \quad (\text{A.22})$$

where c_{SL}^s is the total solids concentration on the snowline, calculated as the total removed vapor due to diffusion. This module is then evolved till a steady state is reached or for a defined timelimit.

To test the diffusion formalism behavior, we conduct two tests: one with a null source function, expecting the initial concentration to drop to zero due to the absence of replenishment, and a second with a very quick replenishment rate (100 yr), where we expect to maintain the initial bulk matter distribution. Results are shown in Fig. A.2. In both cases the code behave as expected, where the vapor is totally removed in the first case, and the total vapor quantity remain constant in the second (although the vapor's spatial distribution changes).

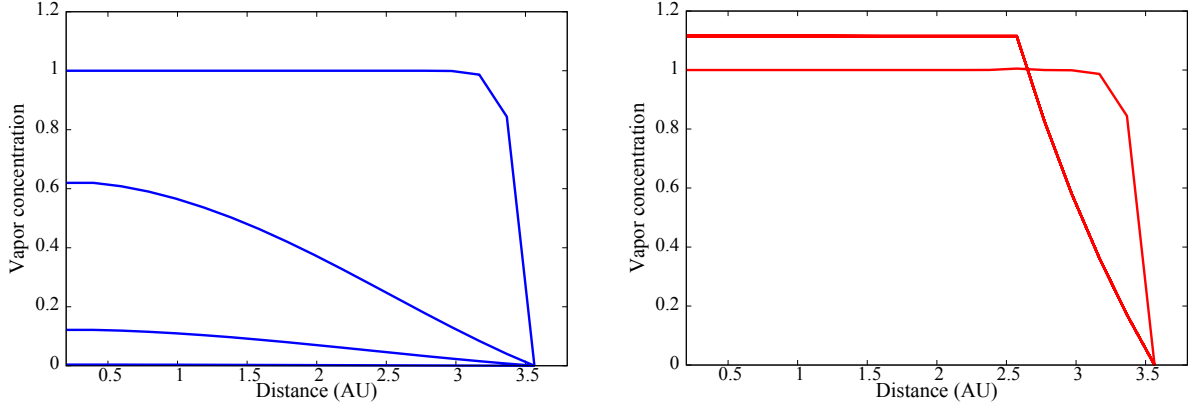


Figure A.2: The vapor concentration evolution for $S(r, t) = 0$ (left) and $t_{tot}^{rep} = 100$ yr (right). Both simulations start with a uniform $c = 1$ vapor distribution. The final states are steady states.

A.4.2 On the diffusion timescale

The fundamental reason behind the depletion inside of the snowlines in this model is t_{tot}^{rep} being much larger than $t_{diff} \propto r_{diff}^2 / \alpha_{turb}$ where r_{diff} is the vapor's diffusion length

scale and α_{turb} the amount of turbulence in the disk. It is important to mention here that if we take r_{diff} to be the sun-iceline distance, t_{diff} will be the total time all of the vapor needs to diffuse all the way to the iceline. This can be thought of as the time needed for a test vapor particle placed near the sun to get to the iceline. This value can be calculated to be equal to or even larger than the replenishment timescale t_{tot}^{rep} . In the case of a non null source term $S(r, t)$ however (as in the case of this model, where the source term originates from the sublimating ices), the replenishment timescale should be compared with the diffusive timescale obtained by taking r_{diff} to be the distance between the iceline and the pebbles sublimation point. Pebbles sublimate well before reaching the sun, and thus their resulting vapor needs to diffuse a shorter distance before reaching the iceline and in a shorter t_{diff} . This will significantly decrease the time the volatile spends as a vapor, and hence explain the replenishments found in my models. It is important to emphasize that this interpretation is in posteriori to the results, and not a hypothesis underlying them.

Appendix B

Chapter 4: numerical methods

B.1 Solving the global equation

Let's consider the main equation governing the D/H evolution in the nebula:

$$\frac{\partial f}{\partial t} = kP(A - f) + \frac{1}{\Sigma_d R} \frac{\partial}{\partial R} \left(\kappa R \Sigma_d \frac{\partial f}{\partial R} \right) + \left(\frac{2\kappa}{\Sigma_d} \frac{\partial \Sigma_d}{\partial R} - V_R \right) \frac{\partial f}{\partial R} \quad (\text{B.1})$$

that we develop into:

$$\frac{\partial f}{\partial t} = kPA - kPf + \frac{1}{\Sigma R} \partial_R f \times (\partial_R(\kappa \Sigma R)) + \kappa \partial_R^2 f + \left(\frac{2\kappa}{\Sigma_d} \frac{\partial \Sigma_d}{\partial R} - V_R \right) \frac{\partial f}{\partial R} \quad (\text{B.2})$$

we take a forward differentiation for the time dependent component:

$$\frac{\partial f}{\partial t} = \frac{f_i^{n+1} - f_i^n}{\Delta t} \quad (\text{B.3})$$

and centered differentiations for the spatial dependent components:

$$\frac{\partial f}{\partial r} = \lambda \frac{(f_{i+1}^{n+1} - f_{i-1}^{n+1})}{\Delta x_p + \Delta x_m} + (1 - \lambda) \frac{(f_{i+1}^n - f_{i-1}^n)}{\Delta x_p + \Delta x_m} \quad (\text{B.4})$$

$$\frac{\partial^2 f}{\partial r^2} = \lambda \frac{(f_{i+1}^{n+1} - 2f_i^{n+1} + f_{i-1}^{n+1})}{\left(\frac{1}{2}(\Delta x_p + \Delta x_m)\right)^2} + (1 - \lambda) \frac{(f_{i+1}^n - 2f_i^n + f_{i-1}^n)}{\left(\frac{1}{2}(\Delta x_p + \Delta x_m)\right)^2} \quad (\text{B.5})$$

with $\Delta x_p = R_{i+1} - R_i$, $\Delta x_m = R_i - R_{i-1}$, and:

$$\lambda = \begin{cases} 0.5 & \text{for a semi implicit (Crank-Nicolson) scheme} \\ 0 & \text{for a fully explicit (FTCS) scheme} \\ 1 & \text{for a fully implicit scheme} \end{cases}$$

Now we define the following variables:

$$a = \left(\frac{\kappa \Delta t}{\frac{1}{4}(\Delta x_p + \Delta x_m)^2} \right) \quad (\text{B.6})$$

$$b = \frac{\partial_R(\kappa R \Sigma)}{\Sigma R} \Delta t \times \frac{1}{(\Delta x_p + \Delta x_m)} \quad (\text{B.7})$$

$$c = kPA \times \Delta t \quad (\text{B.8})$$

$$d = -kP\Delta t \quad (\text{B.9})$$

$$g = \left(\frac{2\kappa}{\Sigma_d} \frac{\partial \Sigma_d}{\partial R} - V_R \right) \frac{\partial f}{\partial R} \quad (\text{B.10})$$

and set $a_1 = \lambda a$, $a_2 = (1 - \lambda)a$, $b_1 = \lambda b$, $b_2 = (1 - \lambda)b$, $d_1 = \lambda d$, $d_2 = (1 - \lambda)d$, $g_1 = \lambda \Delta t g$, and $g_2 = (1 - \lambda) \Delta t g$.

We finally write:

$$\begin{aligned} & f_{i+1}^{n+1}(-a_1 - b_1 + g_1) + f_i^{n+1}(1 - d_1 + 2a_1) + f_{i-1}^{n+1}(b_1 - a_1 - g_1) \\ &= f_{i+1}^n(a_2 + b_2 - g_2) + f_i^n(1 + d_2 - 2a_2) + f_{i-1}^n(-b_2 + a_2 + g_2) + c \end{aligned} \quad (\text{B.11})$$

We define $A = (-a_1 - b_1 + g_1)$, $B = (1 - d_1 + 2a_1)$, $C = (b_1 - a_1 - g_1)$, and D as the entire term right to the equal sign. We translate B.11 to the tridiagonal matrix form:

$$\begin{bmatrix} B_1 & C_1 & 0 & 0 & \dots & 0 \\ A_2 & B_2 & C_2 & 0 & \dots & 0 \\ 0 & A_3 & B_3 & C_3 & 0 & \\ & & & & & \\ 0 & \dots & & 0 & A_{SL} & B_{SL} \end{bmatrix} \begin{bmatrix} f_{1,n+1} \\ f_{2,n+1} \\ \\ \\ f_{SL,n+1} \end{bmatrix} = \begin{bmatrix} D_1 \\ D_2 \\ \\ \\ D_{SL} \end{bmatrix}$$

where $A_1, B_1..$ are the values at the inner border, and $A_{SL}, B_{SL}..$ are the values at the snowline (SL).

with the first row corresponding to the inner limit:

$$B_1 f_1^{n+1} C_1 f_2^{n+1} = D_1 \quad (\text{B.12})$$

and the last row corresponding the the outer limit:

$$A_{SL} f_{SL-1}^{n+1} + B_{SL} f_{SL}^{n+1} = D_{SL} \quad (\text{B.13})$$

Now we set the boundary conditions. Let's define the flux at the outer border as:

$$F_{out} = \frac{f_{SL}^{n+1} - f_{SL-1}^{n+1}}{\Delta x_m} \quad (\text{B.14})$$

giving:

$$f_{SL}^{n+1} = F_{out} \times \Delta x_m + f_{SL-1}^{n+1} \quad (\text{B.15})$$

for a null outer flux condition ($F_{out} = 0$) we get $f_{SL}^{n+1} = f_{SL-1}^{n+1}$. This finally translates to the outer boundary condition:

$$A_{SL} = 1, B_{SL} = -1, D_{SL} = 0 \quad (\text{B.16})$$

On the other hand, the inner boundary flux is defined as:

$$F = \frac{f_2^{n+1} - f_1^{n+1}}{\Delta x_p} \quad (\text{B.17})$$

We set this flux to null, giving us the inner boundary condition:

$$B_1 = 1, C_1 = -1, D_1 = 0 \quad (\text{B.18})$$

Allowing us then to solve the problem iteratively in time.

B.2 Numerical convergence

Three parts of equation B.2 need to be checked for numerical convergence: on diffusive and two advective terms.

The only explicitly diffusive term in the equation is $\kappa \partial_R^2 f$. Lets consider:

$$\frac{\partial f}{\partial t} = \kappa \partial_R^2 f$$

and perform a Von Neumann stability analysis by decomposing our field into its Fourier components: $f_j^n = \epsilon^n e^{ikjh}$ where n is the time index, j the spatial index, k the wave number, h the spatial step, and ϵ is the complex amplification factor for a mode of a wavenumber (beware the convention change from above). After quantification (equations B.3 and B.5), developing the resulting terms and factorizing ϵ we get:

$$\epsilon = \frac{1 - 2D(\cos kh - 1)}{1 + 2D(\cos kh - 1)} \quad (\text{B.19})$$

with

$$D = \frac{\kappa \Delta t}{\Delta x^2}$$

In this case, $|\epsilon| < 1$, meaning that the diffusive term is unconditionally stable in an implicit scheme. We similarly consider the first advective term:

$$\frac{\partial f}{\partial t} = a \partial_R f$$

with $a = \frac{1}{\Sigma R} \partial_R(\kappa R \Sigma)$. We conduct an analogues Von Neumann stability analysis to finally obtain:

$$\epsilon = \frac{1 + \frac{a\Delta t}{4\Delta x}(2i \sin(kh))}{1 - \frac{a\Delta t}{4\Delta x}(2i \sin(kh))} \quad (\text{B.20})$$

In this case, $|\epsilon| = 1$, also indicating that this advective term is unconditionally stable in an implicit scheme. The second advective term

$$\frac{\partial f}{\partial t} = b \partial_R f$$

with $b = \left(\frac{\partial \Sigma}{\partial R} - V_R\right)$ can also be shown to be unconditionally stable by similar reasoning.